DOCUMENT OFFICE DOCUMENT ROOM 36-412
RESEARCH LABORATORY OF ELECTRONICS
MASSACHUSETTS INSTITUTE OF TECHNOLOGY

Loan Copy #2

FUSION REACTOR BLANKET EXPERIMENT

PATRICK S. SPANGLER

TECHNICAL REPORT 437

JULY 13, 1965

MASSACHUSETTS INSTITUTE OF TECHNOLOGY
RESEARCH LABORATORY OF ELECTRONICS
CAMBRIDGE, MASSACHUSETTS

The Research Laboratory of Electronics is an interdepartmental laboratory in which faculty members and graduate students from numerous academic departments conduct research.

The research reported in this document was made possible in part by support extended the Massachusetts Institute of Technology, Research Laboratory of Electronics, by the JOINT SERVICES ELECTRONICS PROGRAMS (U.S. Army, U.S. Navy, and U.S. Air Force) under Contract No. DA36-039-AMC-03200(E); additional support was received from the National Science Foundation (Grant GK-57).

Reproduction in whole or in part is permitted for any purpose of the United States Government.

MASSACHUSETTS INSTITUTE OF TECHNOLOGY

RESEARCH LABORATORY OF ELECTRONICS

Technical Report 437 July 13, 1965

FUSION REACTOR BLANKET EXPERIMENT

Patrick S. Spangler

This report is based on a thesis submitted to the Department of Nuclear Engineering, M. I. T., September 21, 1964, in partial fulfillment of the requirements for the degree of Doctor of Science.

(Manuscript received March 31, 1965)

Abstract

The behavior of 1-14 Mev neutrons has been measured in cylinders, 46 cm in diameter and 38 cm thick, to evaluate previous theoretical calculations on neutron economy and tritium production in proposed fusion reactor blankets. The cylinders were constructed from 0.5-inch graphite slabs and 1-inch layers of solid lithium-beryllium fluoride salt encased in aluminum pans. To approximate first-wall materials, 0-3 cm molybdenum plates were placed at the base of the cylinder.

A point source of 14-Mev neutrons on the center line of the cylinder, 14 cm below its base, was produced by bombarding an adsorbed tritium target with the deuteron beam from a 150-kev Cockcroft-Walton accelerator. The design and operation of a tritium gas target for a 1-3 Mev Van de Graaff accelerator is also described.

The neutron spectrum $\phi(E)$ was measured with a series of threshold detectors: U-238(n, f), P-31(n, p), Fe-56(n, p), I-127(n, 2n), and F-19(n, 2n). The spectrum is determined from the threshold detector data by the method of W. D. Lanning and K. W. Brown, in which $\phi(E)$ is expanded as the product of a weight function w(E) and a weighted sum of polynomials which are orthogonal with respect to w(E).

The spectra in the graphite assemblies are characterized by a sharp peak near 14 Mev, with a smaller, broader peak at 3 Mev. Farther from the source, the 14-Mev peak is attenuated more than the 3-Mev peak. Adding 3-cm Mo to the base of the assembly shifts the 3-Mev peak to lower energies and increases its size at the expense of the 14-Mev peak, because of the Mo-92(n, 2n) reaction. Addition of the lithium-beryllium fluoride has no effect, because of the similarity in the scattering properties of the salt and the graphite. The removal of neutrons through the Li-6(n, t) reaction was not observed, because of the small size of the assembly and the low (1-3%) isotopic content of Li-6 in the salt.

The measurements are in semiquantitative agreement with the results of previous theoretical calculations. Preliminary measurements indicate the feasibility of directly measuring the tritium produced in the assemblies by the Li-6(n, t) and Li-7(n, tn) reactions.

PREFACE

This is the fourth in a series of five reports on Fusion Blanket research.

In this report computer listings of Threshold Activation Data, SAMTAPE Source Programs, and SPECTRUM Source Programs, which constituted Appendices E, F, and G of the author's doctoral thesis, have been omitted. This material is available by application to the Research Laboratory of Electronics, Massachusetts Institute of Technology, Cambridge, Massachusetts, 02139.

A list of the authors and titles of the other four reports in this series follows.

Technical Report 434	Albert J. Impink, Jr., "Neutron Economy in Fusion Reactor Blanket Assemblies"
Technical Report 435	William G. Homeyer, "Thermal and Chemical Properties of the Thermonuclear Blanket Problem"
Technical Report 436	Laszlo N. Lontai, "Study of a Thermonuclear Reactor Blanket with Fissile Nuclides"
Technical Report 438	Lester M. Petrie, Jr., "Gamma-Ray Spectra in Fusion Blanket Mock-ups"

TABLE OF CONTENTS

CONTENTS

CONTENTS

I. INTRODUCTION

The controlled fusion of the heavy isotopes of hydrogen (deuterium and tritium) offers a virtually inexhaustible source of energy, and has been the subject of extensive research for more than ten years. The primary goal of this research has been to create and maintain a plasma at a sufficient temperature and density to sustain a continuous or quasi-continuous fusion reaction. In the past few years our knowledge of plasma physics has increased, and various stumbling blocks, principally those of plasma instabilities, are gradually being overcome – making it not unreasonable to hope for the attainment of a thermonuclear plasma.

Since the primary goal – the attainment of the fusion plasma – has not been accomplished, relatively little thought has been given to the problems of converting the energy of the fusion reaction into a useful form, presumably into electricity. Studies[1-4] made on possible fusion machines indicate that there are problems outside the plasma itself which must be solved before a useful energy-producing device can be built, even if a controlled fusion plasma is attained. One such problem is the design of a blanket which would remove the fusion energy from the enclosed plasma as high-temperature heat, and regenerate the tritium that is burned in the plasma.

Computer codes that had been written for fission reactors were extended to higher energies for early fusion-blanket neutronics calculations. These codes were inadequate because of the differences in the behavior of the fission neutrons, and those produced by the $H^3(d,n)He^4$ reaction (or DT reaction). Impink[3] made a study, using codes in which the conditions peculiar to the fusion reactor blanket were considered. He used multigroup diffusion and integral transport codes for an infinite-slab blanket with an infinite-slab source. From his calculations it is possible to obtain an idea of the most promising blanket configurations from the point of view of neutron economy and tritium production. These calculations were limited by the absence of much microscopic data (cross sections, emission spectra of inelastically scattered neutrons, etc.), as well as the lack of suitable macroscopic experiments to check the validity of simplifications, which he had to make in the scattering models to hold the computer codes to a reasonable size.

The purpose of the work reported here is to develop experimental techniques that can be used with present materials and equipment to evaluate the macroscopic neutronic properties of proposed fusion blanket materials and designs. These experiments were limited to a finite blanket assembly with a point source of neutrons. We planned to check the general predictions that Impink made about various blanket configurations with respect to high-energy neutron spectra (>3 Mev) and tritium production rates. Only the spectral measurements were successful.

At first, it appeared that a quantitative comparison of our experimental data with Impink's results could be made by integrating the point-source results to the plane source that was used by Impink. Later, we found that this simple comparison would not work, because of the high neutron leakage from the small experimental blanket

assemblies. Lontai[5] has begun writing a Monte Carlo code to describe the point-source experiments. The extension of these codes to geometries that are practical for a fusion machine will remain a problem for future investigators.

In a study that paralleled Impink's, Homeyer[4] considered matters related to gamma heating and materials problems in the blanket. Petrie[6] is conducting experiments to obtain data for comparison with Homeyer's calculations.

The rest of this work will be organized in the following manner. Consideration will first be given to outlining the general characteristics of a fusion reactor as conceived by earlier studies, delineating the requirements and limitations imposed on the blanket, and summarizing the conclusions of Impink's calculations. Then, we shall be concerned with the experimental equipment and techniques, including the blanket mock-ups themselves, the neutron sources that were developed, the physical properties of the threshold detectors that were used to map the flux in the mock-ups, the methods of analyzing the threshold detector data to determine the neutron energy spectrum, and the attempts to measure tritium production in the mock-ups. The results of the threshold detector measurements in a variety of experimental assemblies will be summarized and compared, appropriate conclusions will be drawn, and recommendations concerning the future course of these studies will be made. Finally, the details of the digital computer codes used to reduce the data, and the threshold cross sections which were used in the spectral analyses will be presented in appendices.

Every effort has been made to preserve a consistent scheme of notation throughout. In those cases in which usage dictates inconsistencies in the notation employed in treating unrelated problems, the generally accepted notation has been given preference.

1.1 FUSION PLASMAS

From earlier work[1,3,4,7] the general characteristics of a useful thermonuclear plasma can be outlined, and the values of various parameters can be estimated (although with some uncertainty). The plasma for a hypothetical 1,000,000 kw (thermal) machine might be a cylinder, 75-100 meters long and ~1 meter in diameter. The ends of the cylinder may be closed by some arrangement of magnetic mirrors, or the cylinder may be closed to form a torus, as in the stellarator concept. The plasma will contain approximately equal amounts of deuterium and tritium with a total ion density of approximately 10^{14} ions/cm^3 at a temperature of approximately 10^9°K. The plasma boundaries are kept away from the material walls by a magnetic field of approximately 50,000 gauss, which is supplied by a superconducting solenoid.

The primary fusion reaction will be the DT reaction:

$$H^2 + H^3 \longrightarrow (He^4 + 3.67\ \text{Mev}) + (n + 14.06\ \text{Mev}). \qquad (1)$$

The DD reaction

$$H^2 + H^2 \begin{cases} \nearrow (He^3 + 0.82\ \text{Mev}) + (n + 2.45\ \text{Mev}) \\ \searrow (H^3 + 1.01\ \text{Mev}) + (p + 3.03\ \text{Mev}), \end{cases} \tag{2}$$

in which each branch of Eq. 2 occurs with almost equal probability, would be more convenient from the standpoint of blanket design. Since the density and temperature of the plasma for sustained DD fusion must be 10-50 times higher than the still unattainable numbers stated above, it does not appear that a device based on the DD reaction can soon be built, unless some outstanding breakthroughs occur in plasma physics.

A DT plasma operating under these conditions would generate a neutron current density of 5×10^{13} n/cm^2 sec at the vacuum wall (a cylinder 2.0 m in diameter). The power density at the inside diameter of the vacuum wall would be 1.9 Mw/m^2.

1.2 REQUIREMENTS FOR THE FUSION REACTOR BLANKET

The blanket for this hypothetical fusion reactor is shown schematically in Fig. 1. The blanket consists of a vacuum wall, a first-wall coolant channel, a primary attenuator where the bulk of the neutron moderation and tritium production take place, a coil-shield region, the superconducting coil windings, and the biological shielding.

a. Tritium Production and Neutron Economy

Since tritium, which constitutes half of the plasma ions, does not occur in nature, at least one triton must be generated in the blanket for every triton that is consumed by a fusion reaction in the plasma itself. Also, an allowance must be made for the inevitable losses caused by recycling, chemical recovery, and radioactive decay. These losses may be as high as 15 per cent.

The only potential source of tritium through nuclear reactions is the 14-Mev neutrons emitted in the fusion reaction (Eq. 1). Of the large number of neutron-induced reactions that yield tritium as a reaction product, the only reactions that appear to offer any real hope of tritium regeneration are

$$Li^6 + n \longrightarrow H^3 + He^4 \tag{3}$$

and

$$Li^7 + n \longrightarrow H^3 + He^4 + n'. \tag{4}$$

The cross sections for these reactions for natural lithium are shown in Fig. 2 for neutron energies above 0.1 Mev. The $Li^6(n,t)$ cross section gradually assumes a 1/v dependence at lower energies, and reaches a value of 71 barns at 0.025 Mev.

The reaction $Li^7(n,tn)$ is particularly advantageous, since it produces a second neutron that can be used in the $Li^6(n,t)$ reaction to produce a second triton; however, the contribution of the $Li^7(n,tn)$ reaction is limited by competitive downscattering. Since the cross section for the $Li^6(n,t)$ reaction, from which the bulk of the tritium will have

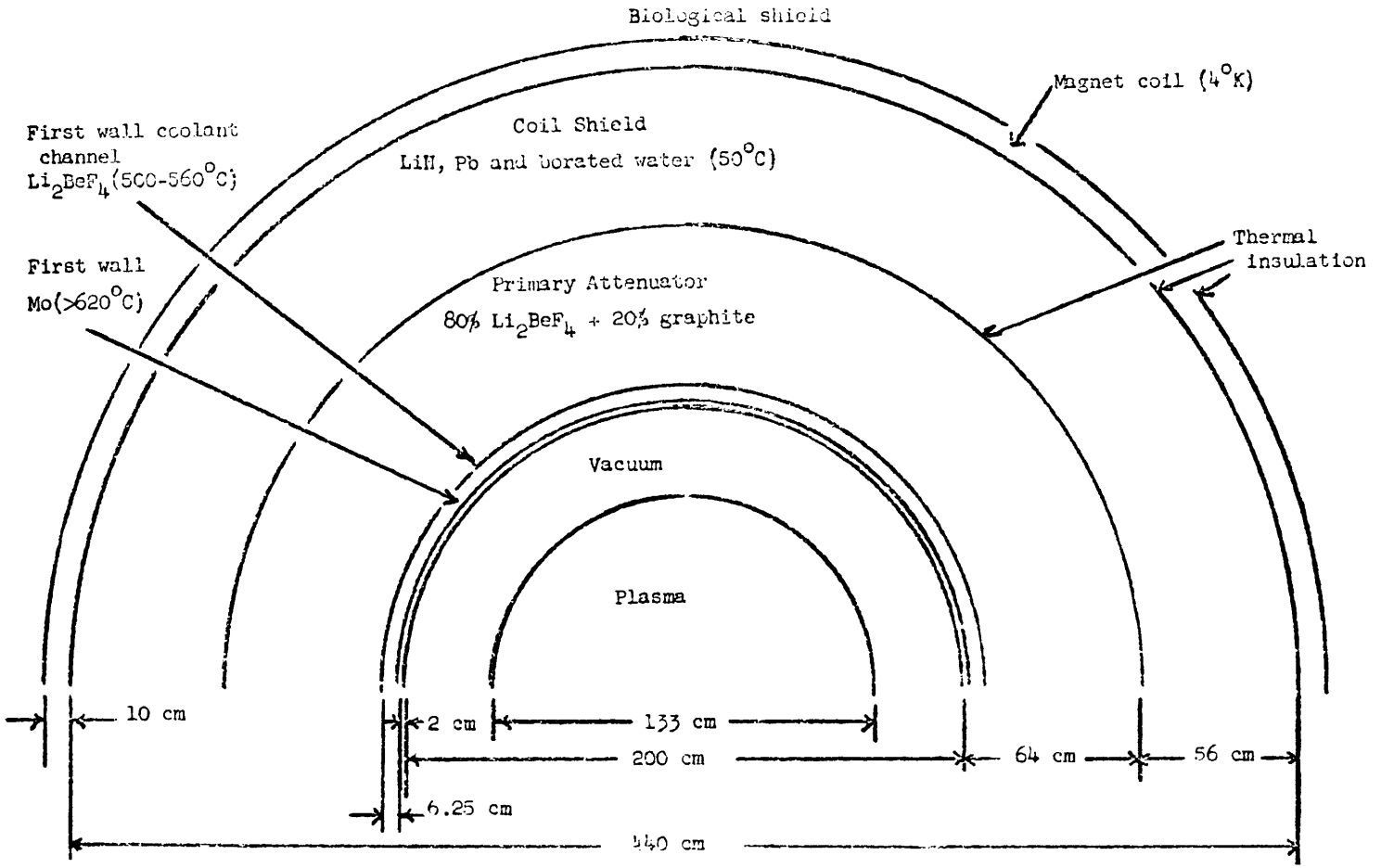

Fig. 1. Schematic diagram for a thermonuclear reactor blanket.

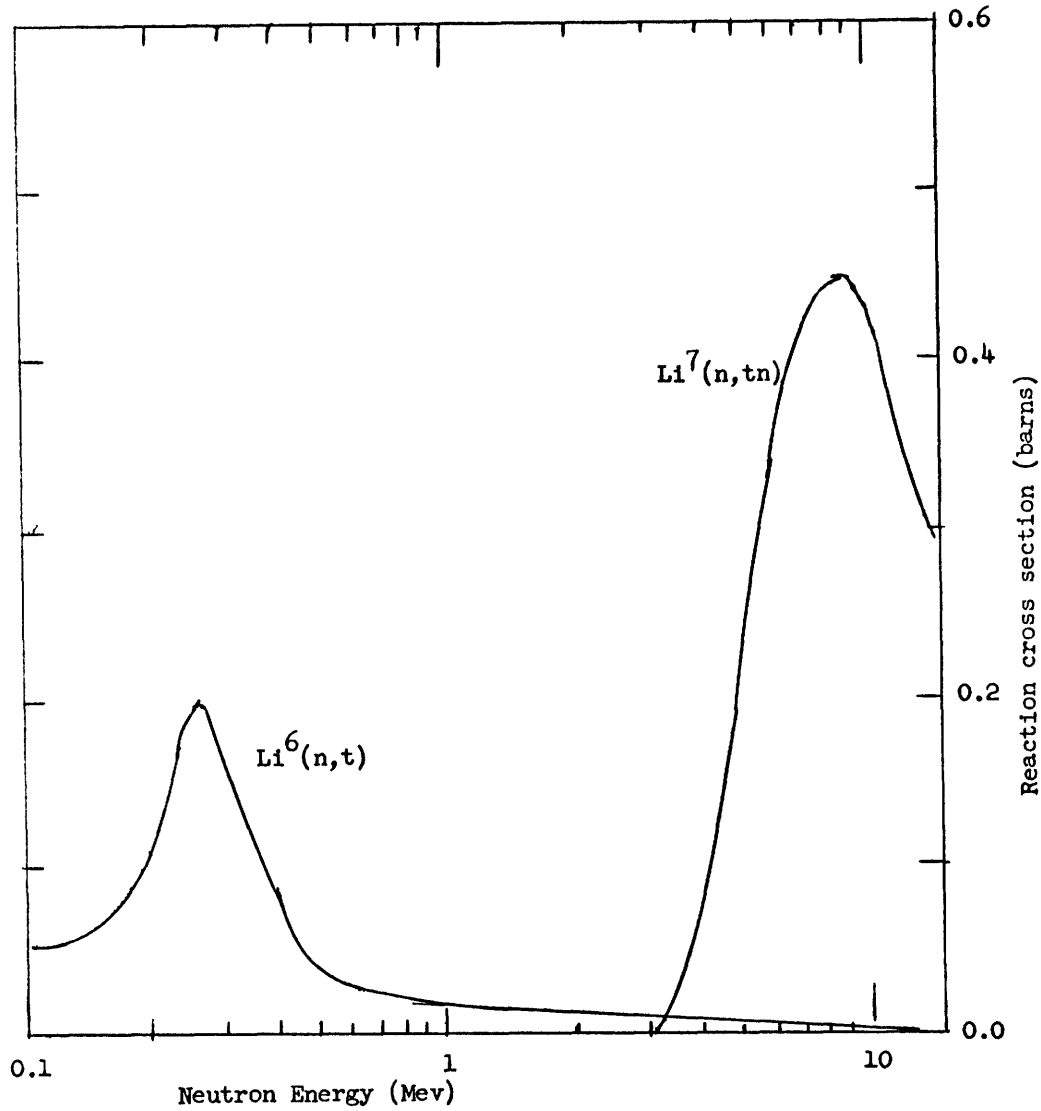

Fig. 2. Tritium-yielding cross sections in natural lithium.

to come, is appreciable only below 0.5 Mev, the neutrons must be moderated to this energy from 14 Mev. Problems of neutron economy, similar to those for a fission reactor, thus arise.

The first consequence of neutron economy is that materials with high parasitic neutron reaction cross sections must be avoided whenever possible. Since the neutron energies under consideration extend to 14 Mev, the important parasitic reactions include the (n, p) and (n, α) reactions, as well as the (n, γ) reaction which is of concern in fission technology. For example, oxygen, which has a low (n, γ) cross section, and is therefore perfectly well behaved for thermal neutrons, has large (n, p) and (n, α) cross sections. Thus coolants containing oxygen are unsuitable for fusion blankets.

Some parasitic neutron capture will occur, so some provision must be made for creating additional neutrons. Advantage may be taken of the high energies of the incident

neutrons by using materials with high (n, 2n) cross sections such as beryllium, or the heavy metals such as molybdenum, near the vacuum before any appreciable neutron moderation has taken place. The fast fission of U^{238} or Th^{232} also appears to offer good neutron multiplication; however, the high resonance absorption of these materials consumes many of the additional neutrons from the (n, f) reactions, and use of these materials introduces problems of fission product waste – problems which a fusion reactor can basically avoid.

b. Power Generation and Material Compatability

Besides satisfying the neutron economy requirements listed above, the blanket must be able to convert the kinetic energy of the neutrons into high-temperature heat, and must remove this heat to presumably conventional heat exchangers and turbines. The materials used in the blanket must be stable at the high temperatures to be encountered (500°-600°C), and must be mutually compatible at these temperatures.

High-temperature operation imposes restrictions on the choice of coolants. Organics are too unstable, water contains to much oxygen and would have too high a vapor pressure, and gases have such poor heat-transfer characteristics that excessive volumes of gas would be required. Liquid metals, particularly liquid lithium, which would provide tritium regeneration, have been proposed.[8] Pumping a liquid metal across the magnetic field lines, however, entails prohibitive power costs because of ohmic heating. Molten salts with strong ionic bonding minimize the ohmic heating problem. Lithium nitrite and lithium nitrate have been suggested. They may or may not have the required stability; but they are both eliminated because of the presence of oxygen. A salt that appears to satisfy all requirements is a mixture of 66 mole-% LiF and 34 mole-% BeF_2. The addition of the BeF_2 decreases the melting point of the salt, and also provides for neutron multiplication through the Be^9(n, 2n) reaction.

The materials for the vacuum wall deserve particular attention. The vacuum wall must not only be able to withstand the bombardment by the large flux of 14-Mev neutrons but also to transmit large quantities of heat arising from the deposition within the wall of the electromagnetic radiation (γ- and x-rays, plus Bremsstrahlung and cyclotron radiation) which is generated within the plasma. It is assumed that most of the charged α-particles which are formed in the fusion reaction are kept away from the walls by the magnetic fields, and are deposited in some region removed from the blanket under study. These considerations, plus those of structural integrity and sputtering on the first surface, dictate the use of a refractory material for the first wall, probably one of the refractory metals, but the beryllides of molybdenum, niobium or zirconium may also prove suitable.

Similar considerations must be made for the structural materials elsewhere in the blanket, although the conditions are not as extreme as at the first wall. Compatibility with the coolant salt is a necessary requirement, in addition to those mentioned above. Graphite appears to be the best material at this time, although the beryllides mentioned

above may also prove useful. Surfaces facing the molten salt may have to be clad with the nickel based alloy INOR-8, which was designed especially for compatibility with fused fluorides; however, the presence of large quantities of this alloy in the blanket could ruin the neutron economy.

c. Shielding Requirements

The use of superconducting coils to provide the magnetic fields for the plasma confinement imposes still more restrictions on the blanket. Superconductivity occurs only at temperatures of a few degrees Kelvin. Thus large quantities of electrical work must be expended to pump to room temperature the energy deposited in the coils by neutron scattering and capture, γ-attenuation, and direct leakage. A comfortable upper limit for a heat-removal rate from the coils is ~100 w/m^2 of coil area facing the blanket. Thus the blanket must also serve as a neutron and gamma attenuator, and as a thermal barrier.

Because of the intensity limitations of the neutron source in the present experiments, consideration of the coil shielding, as well as the biological shielding that will be required, is beyond the scope of this work.

II. THEORETICAL STUDIES OF THE FUSION REACTOR BLANKET

A comprehensive study of the neutron economy in the fusion reactor blanket was made by Impink,[3] who used a differential neutron transport code with 50 energy groups and up to 5 spatial regions. A concurrent study of materials questions and the effects of gamma heating was made by Homeyer.[4] The basic differences between the systems that they

Table 1. Comparison of neutron phenomena in the fission reactor and in the fusion reactor blanket.

Phenomenon	Fission Reactor	Fusion Reactor Blanket
Neutron energy degredation.	Mainly by elastic scattering.	Mainly by non-elastic scattering.
Angular coorelation in neutron scattering.	Almost isotropic in laboratory coordinates.	Forward-peaked, even in center-of-mass coordinates.
Parasitic absorption.	Mainly by (n,γ) reactions.	Mainly by (n,p), (n,α), (n,d) reactions.
Nuclear heating.	Mainly from ionization by fission fragments.	Mainly from γ-rays from inelastic scattering.

studied and the thermal fission reactor are summarized in Table 1. The conclusions mentioned above, as well as the blanket design shown in Fig. 1, are the results of their efforts.

2.1 COMPONENT STUDIES

Molybdenum was chosen as the first-wall material; niobium was considered, but important cross section data were not available. The primary attenuator consisted of molten salt flowing in a graphite matrix. The salt and graphite were homogenized in the calculations. Because the salt in the first-wall coolant channel has a higher temperature, it is distinguished from the salt in the rest of the blanket. Neutrons that escaped the outer boundary of the primary attenuator were considered lost, as far as tritium production and useful heat recovery were concerned. Impink showed that a coil-shield region consisting of 30 cm of lead cooled by borated water (80 volume-% lead and 20 volume-% water with a 0.1 molar concentration of boric acid) was sufficient to attenuate the neutron flux to ~0.02% of its original value.

Impink considered many variations of the blanket design shown in Fig. 1, including materials that could not be used in an actual blanket because of poor structural

Table 2. Tritium production rates for various blanket rates (see Impink[3]).

Run No.	First Wall	First-Wall Coolant Channel cm	salt	Primary Attenuator[a] cm	salt	Tritium Production[b] Total	$Li^7(n,tn)$
3-103	3 cm Be	3.75	FS1	35	FS1	1.207	.106
3-104	8 cm Pb	"	"	"	"	1.447	.048
3-105	None	"	"	"	"	0.869	.129
3-110*	3 cm Mo	5.00	"	30	"	1.162	.083
3-111*	1 cm Mo	"	"	48	"	1.141	.116
3-113*	2 cm Mo	"	"	"	"	1.168	.100
3-114*	None	"	"	"	"	1.072	.136
3-115*	1 cm Ni	"	"	"	"	1.004	.111
3-122	2 cm Mo	6.25	"	56	"	1.150	.100
3-128	"	"	FS2	"	"	1.137	.088
3-129	"	"	"	"	FS2	1.123	.070
3-130	"	"	FS3	"	FS3	0.817	.097
3-131	"	"	FS1[c]	"	FS1	1.181	.094
3-132	"	"	FS1[d]	"	FS1[d]	1.216	.054
5-133	"	"	FS1[e]	70	FS1	1.346	.088
5-134	1 cm Ni	"	FS1[f]	"	"	1.371	.087
5-135	2 cm Mo	"	FS1[g]	"	"	1.202	.065
3-501	"	"	FS4	56	"	1.071	.080
3-503	2 cm Th	"	FS1	"	"	1.135	.103
3-504	1.5 cm U	"	"	"	"	1.417	.106

Fused-salt compositions: (mole per cent)

FS1 = 66% LiF + 34% BeF_2 FS3 = 100% $LiNO_2$

FS2 = 50% LiF + 50% BeF_2 FS4 = 60% LiF + 30% BeF_2 + 10% UF_4

Notes:
a. Primary attenuator is 80% salt and 20% graphite (mole per cent).
b. Tritons per incident neutron.
c. 20% of Li is Li-6
d. 50% of Li is Li6
e. 5 cm of Be between first-wall coolant and primary attenuator.
f. 10 cm of Be " " " " " " .
g. 9 cm of BeO " " " " " " .
* Nuclide densities are 25% for the fused salts in these calculations.

properties, incompatibility, and the like, but which served to emphasize certain principles of neutron economy. Table 2 lists the total tritium production, as well as the tritium produced from the $Li^7(n, tn)$ reaction, for various combinations of materials. Impink's run designations are given here to facilitate reference to his work. The runs 3-105 and 3-114 with no first wall were made for comparison purposes. Various aspects of the blanket construction were considered.

a. First-Wall Material

Molybdenum and nickel were the only materials with suitable physical properties for which sufficient neutronics data were available. Runs 3-115 and 3-111 show that molybdenum is superior. Runs were made with beryllium, lead, uranium, and thorium to demonstrate the superior neutronic properties of these materials. Thorium is the only one of the four that might have sufficiently good structural properties for a first wall. From more recent data it appears that beryllium, in the form of the alloys $MoBe_{12}$, $NbBe_{12}$ or $ZrBe_{12}$ might be a possible choice.

b. First-Wall Thickness

Since molybdenum appeared to be the only suitable first-wall material, studies were made (runs 3-111, 3-113, and 3-114) to determine the optimum thickness, which is approximately 2 cm. Continually increasing the thickness of the molybdenum does not lead to continuous increase in tritium production, principally because increased neutron-energy degradation in the first wall precludes $Li^7(n, tn)$ reactions in the attenuator, and leads to more parasitic (n, α) and (n, p) wall reactions.

c. Fused-Salt Constituents

Runs 3-128 and 3-129 show that increasing the LiF content of the salt above the 66% that was chosen because of the superior physical properties causes a net decrease in tritium production. From run 3-130 it can be seen that $LiNO_2$ has a tritium-breeding ratio of less than unity, so it could not be used. Run 3-501 shows that adding U^{238} to the fused salt, where uranium could be handled physically as UF_4, does not lead to an increase in tritium breeding over other systems because the increased resonance absorption overbalances gains from the $U^{238}(n, f)$ and $U^{238}(n, 2n)$ reactions.

d. Isotopic Content of Li^6

Increasing the isotopic content of Li^6 in the salt leads to a modest increase in tritium production (runs 3-131 and 3-132), but also increases the cost of the salt. A comparison of the $Li^6(n, t)$ and $Li^7(n, tn)$ reaction rates shows, however, that the lithium in the make-up salt must contain approximately 95% Li^6.

e. Neutron-Multiplying Back-up Regions

The use of a layer of beryllium or beryllium oxide immediately behind the first-wall coolant channel was investigated (runs 5-133, 5-134, and 5-135). Enough of an increase in tritium production was observed, so that even a nickel first wall might be feasible, although such a wall did not appear to be favorable with the standard blanket (run 3-115).

f. Salt-to-Graphite Ratio

Two preliminary runs were made in which the graphite fraction in the primary attenuator was 0.21 and 0.71. While these runs are not directly comparable with those listed in Table 2, they show that the primary effect of the additional graphite is to dilute the lithium concentration in the blanket. Secondary losses occur because of the $C^{12}(n, \alpha)$ reaction.

Impink concluded from his studies that a sufficiently large tritium-breeding ratio could be achieved in a physically practical blanket configuration, and that there was enough flexibility in the choice of blanket materials, so that some degree of optimization of other aspects such as nuclear heating and coil shielding could be permitted.

2.2 LIMITATIONS OF THE COMPUTATIONAL METHOD

Impink's studies represent the first serious attempt to treat the complexities of the neutron behavior in a fusion blanket. There are some serious limitations to the use of these calculations.

1. Elastic scattering of 14-Mev neutrons is predominantly straight ahead, even in center-of-mass coordinates. As the neutron energies approach 2-3 Mev the scattering is more nearly isotropic in center-of-mass coordinates. To keep the computations within reasonable bounds for the computer, the simplifying assumption is made that scattering is only straight ahead for neutrons above 5 Mev, is isotropic for neutrons <5 Mev with nuclides of mass <20, and is an empirical mixture of isotropic and straight-ahead scattering for neutrons <5 Mev with nuclides of mass >40. The results indicate that this approximation is sufficiently good to calculate critical quantities such as the tritium-breeding ratio, but it introduces serious errors in the calculation of higher energy events.

2. Impink tried to compare calculated results with the results of several experiments that had been conducted to investigate the moderation of 14-Mev neutrons in various media. In only one case (measurements of the Fermi age in graphite) did he have much success. In the other cases agreement was not too good because the scattering-model errors were accentuated in these experiments, and the materials and geometries were not those for which his codes were designed.

3. A limitation of any computational method will be the detailed data required for each nuclide used in the blanket. The cross sections for all energetically possible reactions must be known as a function of energy. Since the energy range in the blanket is

from thermal energies to 14 Mev, the list of possible reactions is large, including such reactions as (n, p), (n, α), (n, np), etc., as well as the (n, γ), (n, n) and (n, n') reactions which are important in fission reactor calculations. If neutrons are emitted, as is the case for the reactions (n, 2n), (n, n'), (n, pn), etc., the energy spectra of the emitted neutrons are needed. Impink found that much of the required experimental data were not available, although some could be estimated from theoretical nuclear models.

4. The calculations were carried out for infinite-plane blankets with an infinite-plane plasma source. The errors thus introduced are only minor because the blankets for the envisioned cylindrical reactor have only small curvature.

Impink felt that more experimental data were needed before further refinement of the calculational models could be justified.

III. EXPERIMENTAL BLANKET ASSEMBLIES

3.1 CONFIGURATIONS SELECTED FOR STUDY

Only three aspects of the component studies mentioned in Section II are amenable to small-scale experiment: the salt-to-graphite ratio, first-wall materials, and first-wall thickness. Materials for the other aspects are unavailable or too expensive.

The ten configurations that were originally selected for investigation are listed in Table 3. The neutron-energy spectrum was to be mapped with threshold detectors in each configuration. Tritium-production measurements were to be made in those configurations containing salt. For reasons that will be described in Section VII, only the spectral measurements were successful.

Only configurations 1-7 in Table 3 were studied experimentally, for three reasons:

1. The results from the first 7 configurations were sufficient to demonstrate the validity of the threshold-detector techniques.

2. The refinement necessary to gain sufficient precision to detect the effects of the component changes indicated for configurations 8-10 is beyond the scope of an exploratory investigation.

3. Configurations 8-10 do not represent practical blanket configurations.

3.2 GEOMETRY OF THE EXPERIMENTAL ASSEMBLIES

Although most of Impink's computer runs were made with an infinite-slab geometry, his codes could also handle a cylindrical blanket with a diffuse-cylinder source, or a spherical blanket with a spherical source. Since the only available source of 14-Mev neutrons is a point source (see Section IV), the plane and cylindrical geometries could not be used. The manufacture of the spherical shells that would be needed to duplicate the spherical geometries would be prohibitively expensive, if not impossible. As a result, the geometry of the experimental blanket assemblies was chosen for convenience in interchanging the components. Some computational scheme is then necessary for a quantitative comparison of the experimental results with those of Impink's codes.

The original scheme was as follows:

1. The blanket assembly would consist of a central core and a graphite reflector to reduce neutron leakage, as shown in Fig. 3. Only the central core would be varied to form the configurations listed in Table 3. The reflector would not drastically alter the spectrum at the center of the core, since the graphite and the salt have similar scattering properties.[3]

2. The results of radial flux traverses within the core could be fitted to the Bessel function $J_o(\alpha r)$, and an extrapolated core boundary could be found.

3. The point-source results for the extrapolated core could be integrated to duplicate Impink's infinite-plane results.

This scheme was not usable because a $J_o(\alpha r)$-distribution implies isotropic

Table 3. Suggested experimental blanket configurations. (Configurations 1-7 were actually investigated.)

No.	First Wall	Percentage[a] Salt	Graphite	Purpose
1	None		100	1. Development of threshold-detector techniques. 2. One-region assembly for future Monte Carlo codes.
2	9/8"Mo		100	Effect of molybdenum wall (compared with no. 1).
3	None		100[b]	Effect of aluminum used to encase salt (compared with no. 1).
4	3/8"Mo	67	33	Effect of first-wall thickness
5	3/4"Mo	67	33	
6	9/8"Mo	67	33	
7	3/4"Mo	50	50	Effect of salt-to-graphite ratio (compared with no. 5).
8	3/4"Mo	80	20	
9	1" Pb	67	33	Effect of different first-wall materials (compared with no. 5).
10	1" U	67	33	

Notes: a. Percentage may be either by volume or by weight, since the densities of the salt and the graphite used in the experiments were almost the same. Salt is $2LiF \cdot BeF_2$; isotopic content of lithium is about 1-3% Li^6.

b. Aluminum plates 0.030" thick were inserted between several graphite slabs.

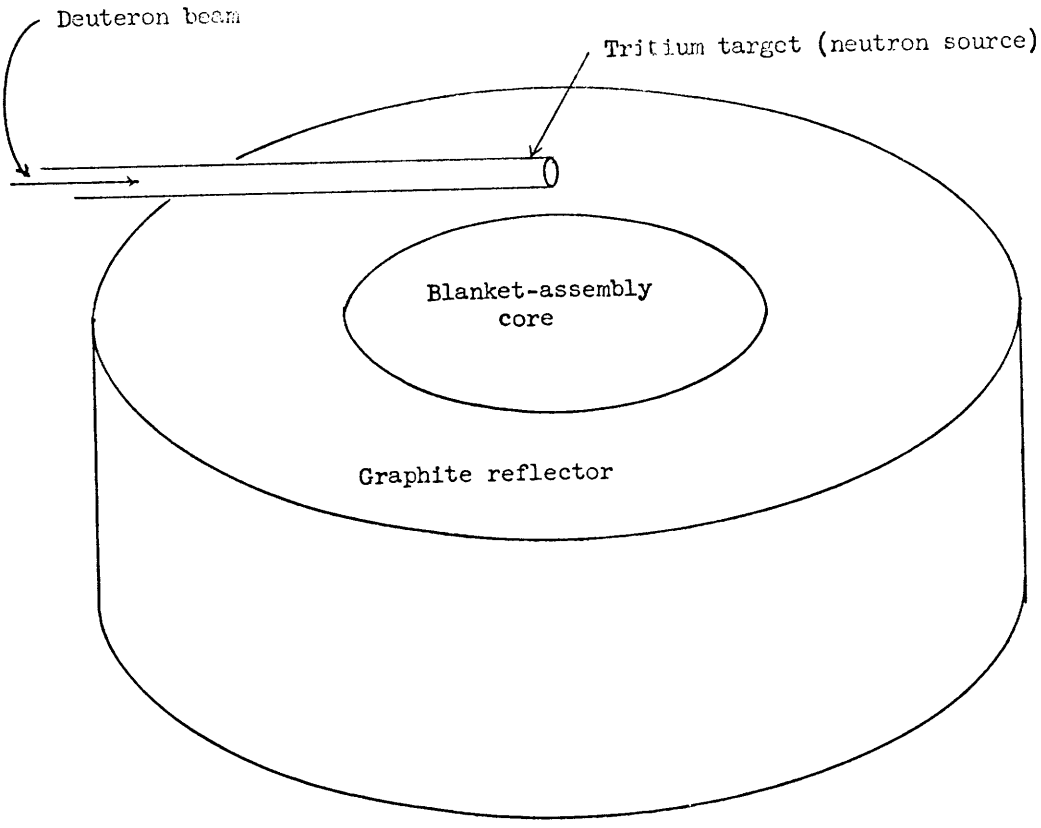

Fig. 3. Schematic diagram of the preliminary blanket assembly.

scattering, but in the assemblies scattering is peaked in the forward direction. A Monte Carlo calculation was indicated. Here the high leakage is an advantage, because the neutrons make only a few collisions before being absorbed or leaking out. If accuracies of 5-10% are sufficient, only a relatively small number of neutron histories are required. In this case the reflector would only complicate the calculations, so it was discarded in favor of a bare core assembly (see Fig. 13).

3.3 MATERIALS FOR THE EXPERIMENTAL ASSEMBLIES

a. Lithium-Beryllium Fluoride Salt

The Reactor Chemistry Division of Oak Ridge National Laboratory supplied approximately 300 lb of lithium-beryllium fluoride salt (composition $2LiF \cdot BeF_2$) cast in the form of 120° wedges, as shown in Fig. 4. The wedges were contained in covered aluminum pans (Fig. 5). The covers were sealed to the pans by rubber gaskets, and held in place by special stainless-steel bands (Fig. 6). The bulk of the salt was used for several experiments. Salt samples which were to be used for tritium measurements in each blanket configuration were placed in the central void formed when three wedges were placed in a pan.

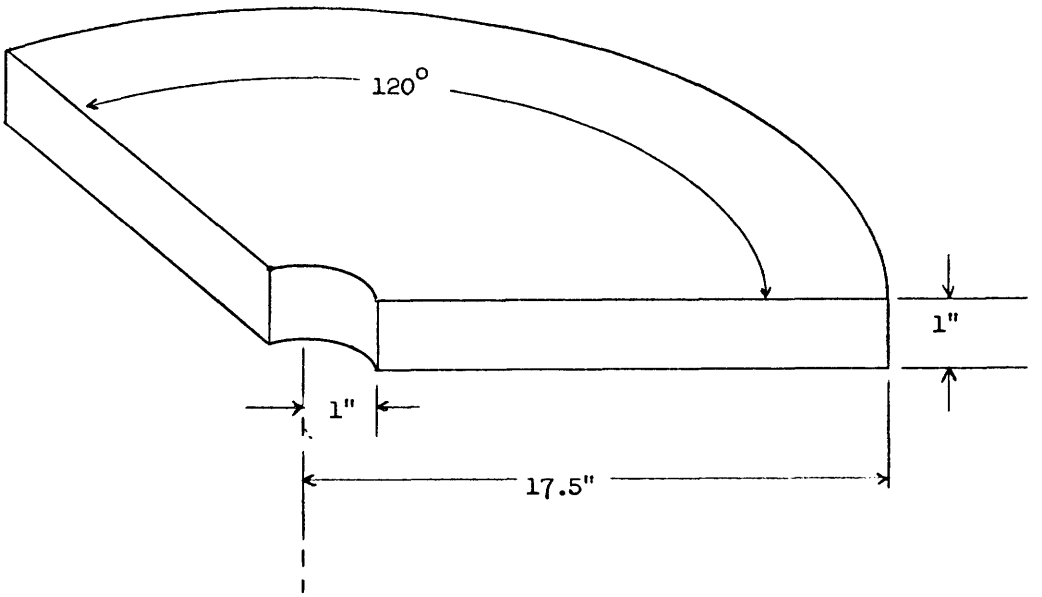

Fig. 4. Sample wedge of lithium-beryllium fluoride.

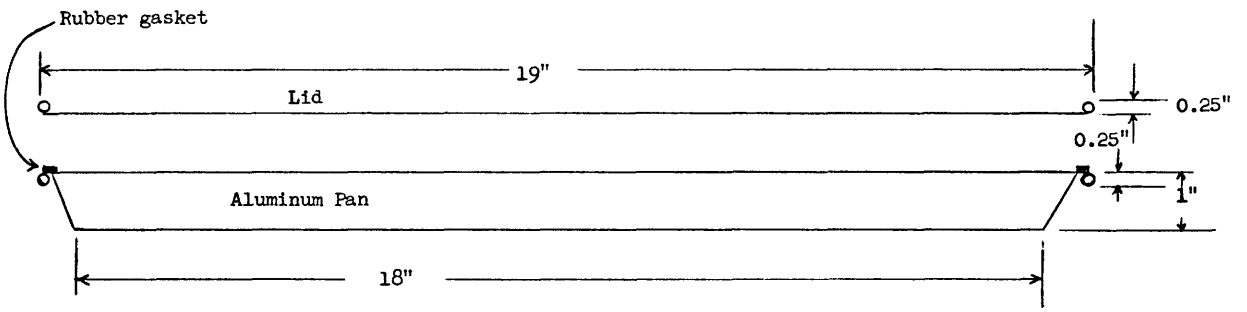

Fig. 5. Pan for lithium-beryllium fluoride.

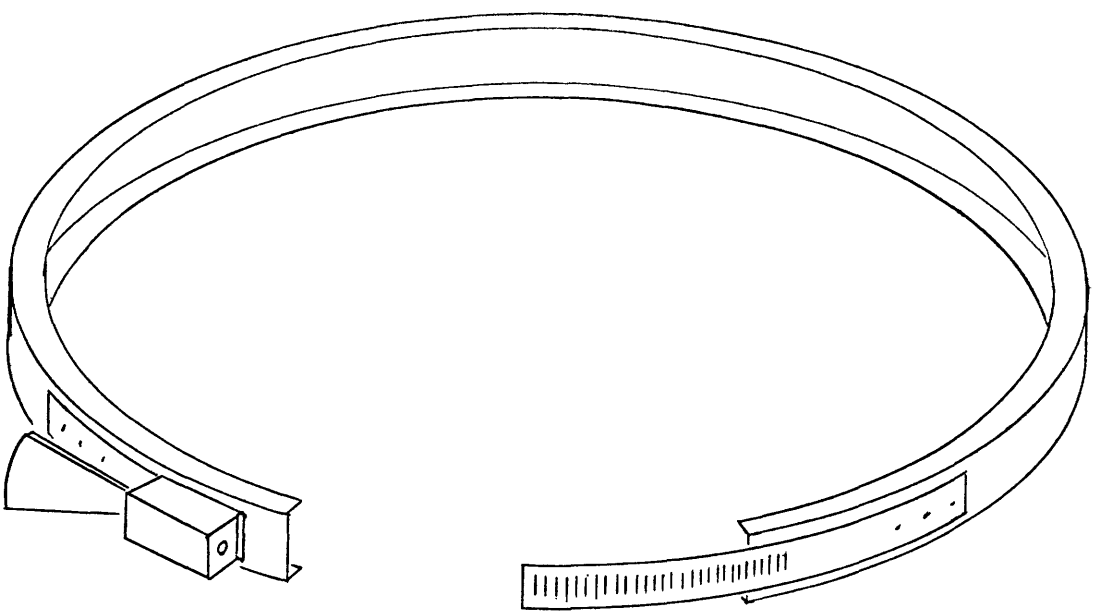

Fig. 6. Stainless-steel band for holding the lid to the aluminum pan.

b. Graphite

The graphite (reactor grade, manufactured by Union Carbide Corporation) is in the form of 26 slabs that are nominally 18 inches in diameter and 0.5 inch thick. The actual thicknesses are listed in Table 4. A cylindrical depression, 0.209 inch deep and 0.875 inch in diameter, was milled in the center of each slab to hold the threshold detectors. Depressions that held no threshold detectors during an irradiation were filled with graphite buttons. Radial depressions were milled in two of the slabs (labeled A and

Table 4. Thicknesses of Graphite Slabs. The slabs were nominally 18 inches in diameter and 0.5 inch thick. Actually, their shape was somewhat irregular. The thicknesses listed below for each slab are the averages of measurements at four points near the perimeter of each slab.

Slab Number	Thickness (centimeters)
100	1.491
200	1.480
300	1.476
400	1.496
500	1.427
600	1.488
700	1.478
800	1.387
900	1.455
1000	1.511
1100	1.458
1200	1.560
1300	1.450
1400	1.453
1500	1.471
1600	1.427
1700	1.471
1800	1.478
1900	1.499
2000	1.466
2100	1.458
2200	1.471
2300	1.496
2400	1.478
A	1.631
B	1.435

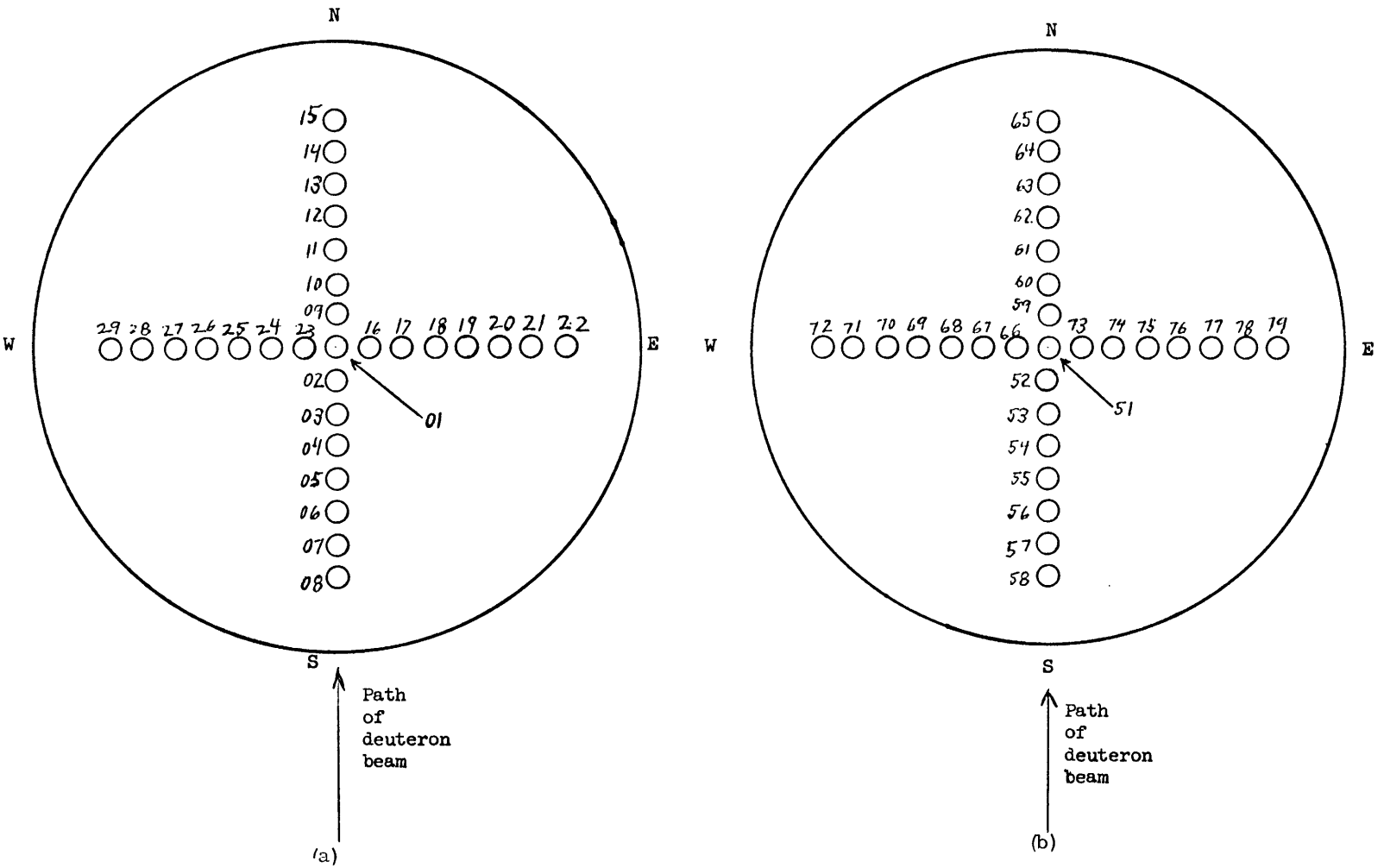

Fig. 7. Position numbers: (a) for graphite slab A; (b) for graphite slab B.

B), as shown in Fig. 7. The slabs with only central depressions are numbered by hundreds from 100 to 2400; during irradiations slab 100 was nearest the neutron source (see Fig. 13).

c. First-Wall Materials

Three plates of molybdenum, 1 ft square and 0.375, 0.500, and 0.750 inch thick, were used to simulate the molybdenum first wall. Lead was available in the form of an irregularly shaped plate, 1 inch thick. Uranium was available in the form of bars 3 ft × 1 inch × 0.25 inch. One deterrent to studying the uranium first wall was that this uranium had been previously irradiated, and it had a flaking oxide coating. Special handling would have been required.

3.4 POSITION NUMBERS FOR THRESHOLD DETECTORS

Each threshold detector position was identified by a number. For the all-graphite configurations (1-3) this number was the slab number if only axial measurements were desired. For radial measurements slab A (or B) was inserted in place of a numbered slab at the desired axial position. Then these position numbers were formed by adding the depression number for slab A (or B, see Fig. 7) to the number of the slab which had been replaced.

The configurations (4-7) with 67% and 50% graphite were constructed by alternating one pan of salt with one and two slabs of graphite, respectively. In these configurations most of the threshold detectors were placed in the graphite slabs; the numbering system is the same as above. One set of threshold detectors was placed directly behind the molybdenum wall (position "1"). The resulting air gap between the molybdenum wall and the first salt pan had no appreciable effect on the neutron flux because, at this area in the blanket, the neutron paths were mainly perpendicular to the first wall.

The salt pans were numbered from 1 to 4 with pan 1 nearest the neutron source. The actual composition of each experimental blanket assembly is shown in the appropriate figure with the threshold-detector results (Figs. 35-40).

IV. THE NEUTRON SOURCE

4.1 INTRODUCTION

A source of 14-Mev neutrons with an intensity of 10^{10} neutrons per second (in 4π-geometry) was found to be necessary to sufficiently activate the threshold detectors and to produce detectable amounts of tritium in the lithium-beryllium fluoride salt. In the actual experiments these neutrons were produced by bombarding a solid tritium target (manufactured by the Texas Nuclear Corporation, Austin, Texas) with 150-kev deuterons from a Cockcroft-Walton accelerator. When work was begun in the summer of 1961, the Cockcroft-Walton machine was not available, so we planned to use the 1-3 Mev Van de Graaff accelerator at the U. S. Air Force Cambridge Research Laboratory (AFCRL) in Bedford, Massachusetts.

With a solid target, in which the tritium is absorbed on a titanium (or other) film that has been deposited on a copper disc, all of the energy of the bombarding deuterons is deposited in the target, and must be dissipated as heat through the water-cooled copper backing. (Only the kinetic energy of the deuterons must be considered. Since less than one deuteron in 1000 undergoes a D-T reaction, the energy of the He^3 ion produced in this reaction may be neglected.) A Cockcroft-Walton machine requires a 200-μa beam (which is 1.3-2.0 cm in diameter) to produce the required neutron intensity; the heat which must be dissipated to the coolant is a comfortable 20 watts/cm^2. On the other hand, the minimum energy at which the Van de Graaff at AFCRL can deliver a stable beam is 1 Mev, and the maximum diameter of the beam is 0.6 cm. At this energy only a 100-μa beam is required, but the temperature at which the resultant 350 watts/cm^2 can be removed by the coolant is so high that the tritium would rapidly boil off the target. Schemes for effectively spreading the beam by rotating the target or oscillating the deuteron beam with an AC magnet were considered to be too expensive. Attempts were made to use "high-temperature" solid targets (manufactured by NRA, Inc., Long Island City, New York) in which the tritium is absorbed on rare earth films, but these targets proved to be no better than the titanium targets.

The only other alternative was a tritium gas target, which has the disadvantage of handling tritium gas, with the associated safety problems. A satisfactory gas target was developed, and would have been used for the experiments had the Cockcroft-Walton accelerator not become available. A description of the gas target is included here, since it does provide a useful neutron source with a Van de Graaff accelerator.

Much of the succeeding material has been published elsewhere.[9-11] Material from these sources will be used without further reference.

4.2 TRITIUM GAS TARGET

a. Construction of the Gas Target

The gas target, shown in Fig. 8, contains the tritium gas in a stainless-steel tube, 0.25 inch ID and 1.3 inches long. The target window, a disc of commercial aluminum

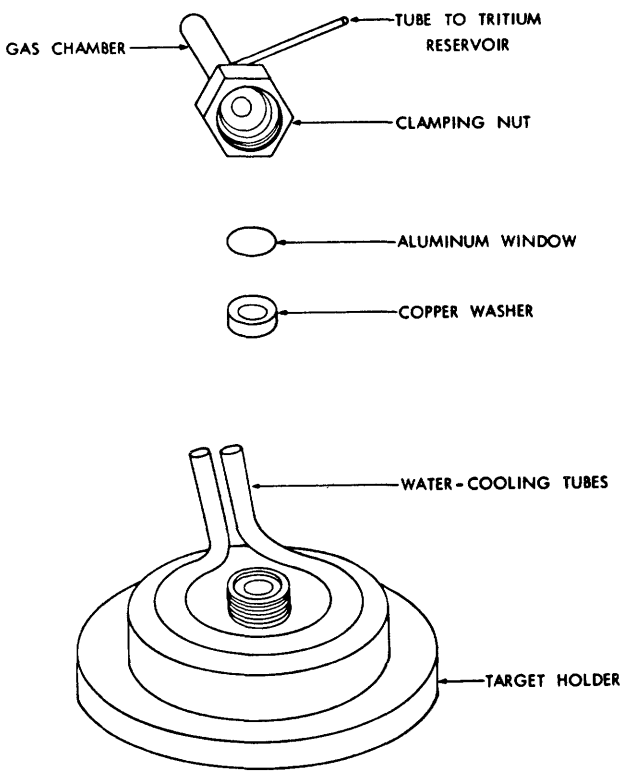

Fig. 8. Gas target.

foil, 33.8 μ thick, is held to the polished surface of a flange on the open end of the cylinder. A copper washer seals the window to the cylinder; the other side of the washer forms a seal with the target holder. The tritium is admitted to the target through a 0.125-inch stainless-steel tube that is hard-soldered to the base of the target chamber. The incident 2.7-Mev beam of deuterons is slowed to 400 kev in the window, whence it enters the gas chamber where it is slowed to 40 kev. The calculated yield is 9×10^8 neutrons per second per microampere, which is higher than the yield of the solid target by a factor of almost ten.

The target window must (a) form a wall between the target chamber and the accelerator drift tube which is able to withstand the pressure difference (0.5-1.0 atm versus 10^{-5} mm Hg); (b) be relatively impervious to hydrogen at the operating temperature; (c) be available in thin enough foils, so that the energy degradation within the window is within reasonable limits; and (d) be able to dissipate the energy lost in the window to the rim. The last requirement eliminates all nonmetallic windows. The distance to produce a given decrement in the deuteron energy is proportional to Z^{-2}, where Z is the atomic number of the window material. Refractory metals have atomic numbers that are too high: the windows would be prohibitively thin. Titanium, iron, and nickel have lower Z, but would allow too much tritium to diffuse through the window into the accelerator because of their high permeability to hydrogen. Aluminum is a satisfactory material, and is readily available. Other metals that are alloyed with the aluminum in the commercial foil did not noticeably affect the energy-degradation characteristics of the windows.

b. Collimation System

The gas target holder is connected to a collimation system (see Fig. 9) which consists of an aperture assembly with a 0.25-inch ID aperture and a 0.5-inch ID baffle to trap the deuterons that are deflected by large angles upon collision with the edge of the aperture, and an electron repeller with a 0.375-inch ID opening that is maintained at -135 volts to prevent secondary electrons, which are emitted when deuterons strike the aperture and the target, from confusing beam-current measurements. The aperture disc and the target holder are water-cooled. The components are positioned by nylon spacing

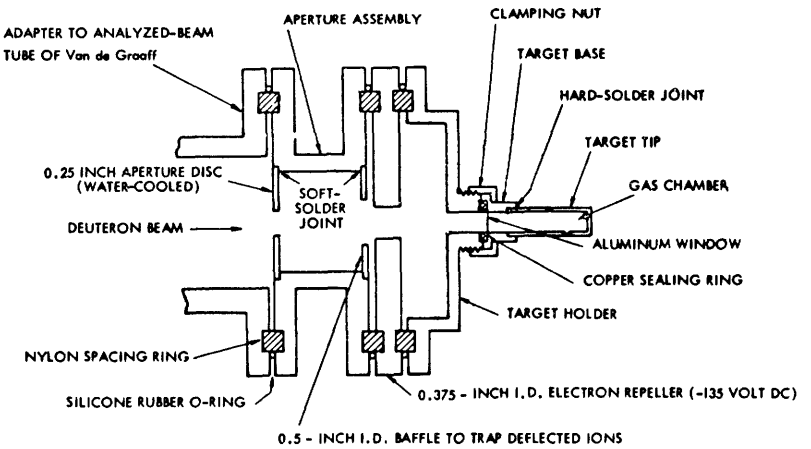

Fig. 9. Collimation system for gas target assembly.

rings, sealed by silicone rubber O-rings, and fastened by screws that are protected with teflon tubing and fiber washers to keep the joints electrically insulating. The assembly was attached to the analyzed-beam tube of the Van de Graaff accelerator. Since the end of the tube was already insulated from ground, the connection between the tube and the aperture assembly was not insulated.

The currents flowing from the aperture assembly, the electron repeller, and the target were monitored during the runs. The current from the electron repeller was zero. The target current measured the intensity of the deuteron beam, and the aperture current measured the focus and alignment of the beam. For a well-focused and correctly aligned beam of 3 μa on the target, the aperture current was less than 0.5 μa.

c. Uranium Reservoirs

The tritium for the gas target was obtained from uranium tritide in stainless-steel reservoirs, one of which is shown in Fig. 10. The system is similar to that described by Johnson and Banta.[12] The tritium was released by heating the reservoir to 410°C. For this purpose, a nichrome heating wire was threaded on a boron nitride cylinder that could slip on the reservoir; a larger boron nitride cylinder covered the assembly. Stainless-steel snap rings held the heater in place. The temperature was measured by an iron-constantan thermocouple that was spot-welded to the bottom of the reservoir. The reservoir was sealed inside a water-cooled protective can to trap any tritium that might diffuse through the walls of the reservoir during the heating cycle.

The reservoir was constructed by welding a plug to the bottom of a stainless-steel tube, 4 inches long, 0.25 inch ID, and 0.375 inch OD. The oxide layer was removed from 5-7 grams of depleted uranium foil scrap by momentarily immersing the foil in concentrated nitric acid, then rinsing, first in distilled water and finally in acetone. The air-dried foil was minced into the reservoir; the volume above the uranium was packed with glass wool, and the tube was welded to the stainless-steel feed tube (0.1875 inch

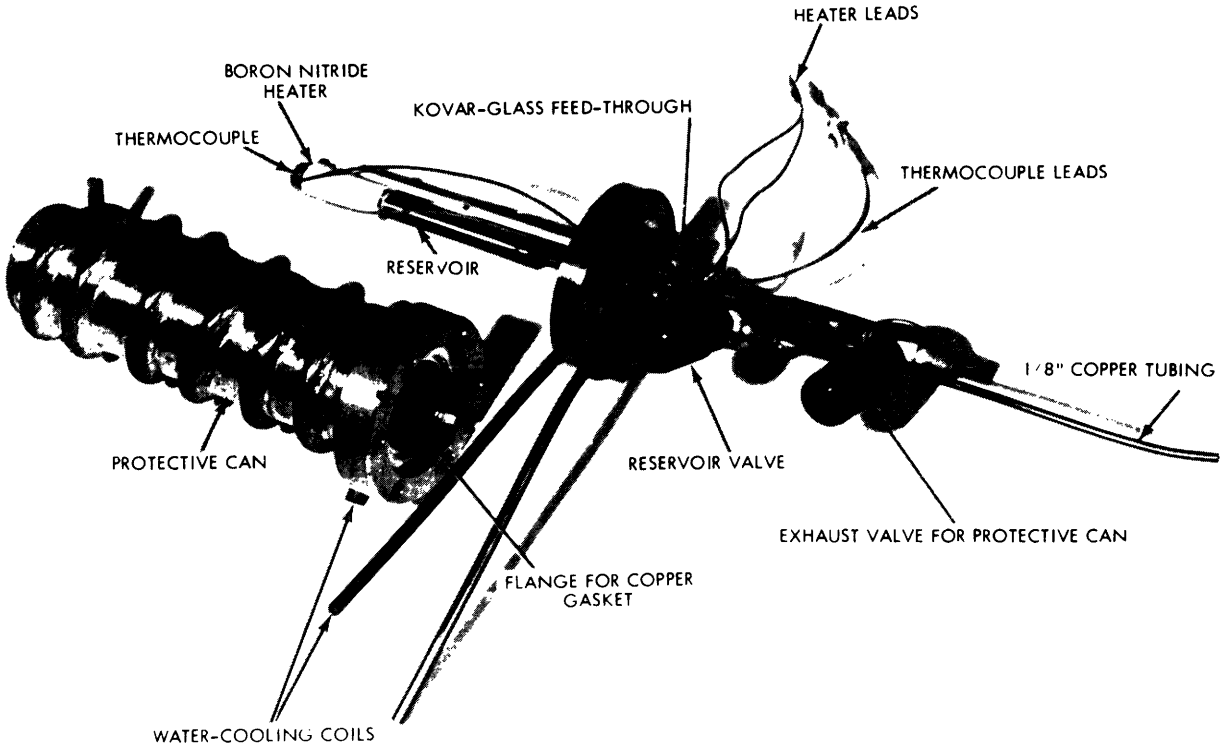

Fig. 10. Uranium tritide reservoir and protective can.

OD, flared to 0.25 inch OD at the point of the weld) which led through the lid of the protective can (where it was fastened by a soft-solder joint). The other end of the feed tube was soft-soldered to a Hoke bellows valve (either No. 482 or A431). Johnson and Banta recommend a 0.125-inch OD feed tube butt-welded to a 0.25-inch OD plug, but we found that the butt weld leaked. Helium was made to flow in through the furnace valve before heliarc welding to avoid igniting the uranium during the welding process. During the weld the reservoir tube was cooled by a wet cloth. Care had to be taken during the final stages of the welding that the heated gases inside the reservoir did not cause a pressure build-up and a blow-through in the weld. After the reservoir had been welded to the lid assembly, the whole assembly was helium-leak tested before the thermocouple and heater connections were spot-welded into place.

The reservoir assembly was then connected to a manifold and pumped to ~1 μ with the reservoir temperature at 410°C. Afterwards the reservoir was cooled to approximately 200°C and hydrogen was let into the system. After a short delay caused by hydrogen diffusion through the surface oxide on the uranium, up to 1 liter-atmosphere of hydrogen was taken up within 30 minutes. After the hydriding reaction had ceased, the furnace was heated to 410°C and the hydrogen was pumped off to approximately 1 μ. This cycle was repeated several times to ensure activation of all of the uranium in the reservoir. If all of the uranium had been packed below the level of the heater, a system volume of hydrogen let in at 1 atm could be driven off at 1 atm by raising the reservoir

temperature to 410°C – even in the presence of excess uranium. The excess uranium was necessary so that small amounts of air, which would inevitably leak into the reservoir through the valve seat during transfer operations, could be combined with the uranium (as a uranium nitride and uranium oxide) without impairing the effectiveness of the reservoir.

For transportation purposes, the uranium reservoir in the protective can was placed in a helium atmosphere in a container whose lid was sealed with an O-ring. This container was, in turn, placed in a "2R" container that consisted of a cast-iron pipe with end caps.

d. Gas-Handling System

After the reservoir had been filled with 30 curies of tritium at the New England Nuclear Corporation, in Boston, Massachusetts, it was transported to AFCRL and connected to the gas-handling system shown schematically in Fig. 11, which consisted of an inner system made of 0.125-inch copper tubing, a Bourdon gauge (0-30 in. Hg), the reservoir, a stand-by reservoir, and the gas target; and an outer system that contained a thermocouple vacuum gauge for routine leak checking and measuring the final take-up of tritium into the reservoir, and connections to a helium line for leak testing and to a forepump. The stand-by reservoir was included in the system in case it became necessary to remove the tritium from the system while the tritium reservoir was still hot.

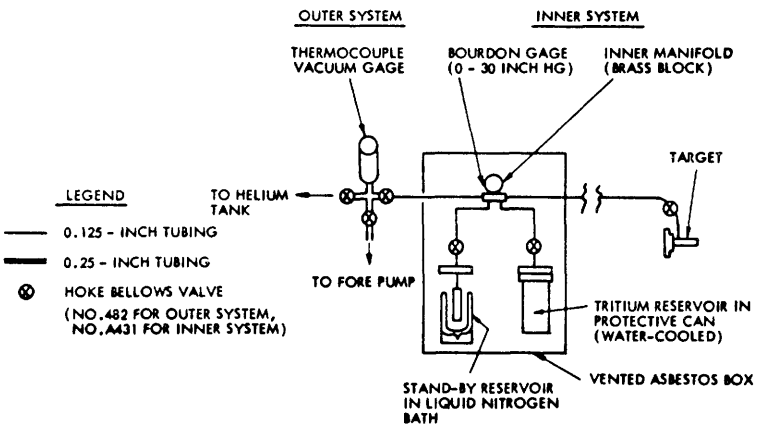

Fig. 11. Gas-handling system at the U. S. Air Force Cambridge Research Laboratories.

To reduce tritium contamination of the air in the target room, the asbestos box that contained the reservoirs and the forepumps for the tritium handling system and the accelerator were exhausted to a point 50 ft above the ground outside the building.

e. Safety Precautions

The work with the tritium required an amendment to the U. S. Atomic Energy Commission by-product material license held by the Massachusetts Institute of Technology.

In order to obtain this amendment a comprehensive study[13] of the hazards involved was made with the cooperation of the Radiation Protection Committee of M. I. T. and the Wing Radiological Hazards Committee at AFCRL, and appropriate safety precautions were developed. Of chief concern were the possible release of all or some of the tritium into the atmosphere, and the contamination of personnel who operated the tritium system or who worked in the building.

A particular source of tritium release was the possible failure of the aluminum target windows. Extensive tests showed that while the window would operate indefinitely (more than 12 hours) with a defocused beam of 6-7 μa, it would break within a minute at approximately 8 μa. Here a defocused beam is defined as one for which the target current and aperture current are equal. To guard against an accidental increase in current on the target window, a gate valve in the beam tube closed automatically when the target current exceeded 7 μa. The gate valve was also closed automatically by a rise in pressure in the beam tube, or could be closed manually from the control room. A drop in the neutron flux, as monitored by a BF_3 detector, was also an indication of a leak.

Since there appeared to be a real possibility that all of the tritium might be released to the atmosphere in spite of the precautions, the total amount of tritium was kept to a minimum. As a result the tritium system volume had to be kept as small as possible. This led to a search for the smallest possible valves, gauges, and so forth, that could be used. The system described above appeared to be satisfactory.

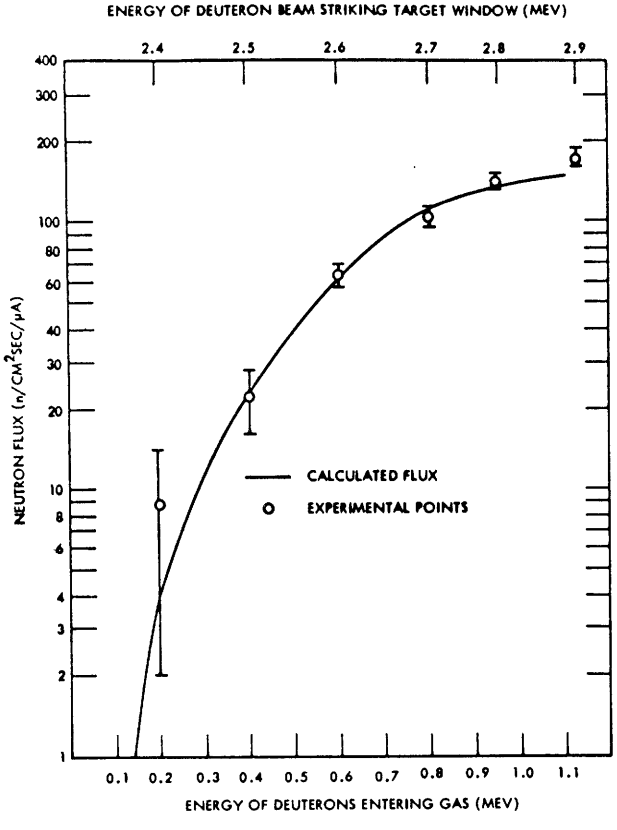

Fig. 12. Comparison of experimental and calculated values of neutron flux.

f. Preliminary Operations

Before tritium operations began, the system was operated with deuterium. Measurements were made of the integral flux of neutrons from the $H^2(d,n)He^3$ reaction with 1 atm of deuterium in the target, by means of a calibrated BF_3 neutron detector. In Fig. 12 the experimental results, corrected for the energy degradation in the aluminum window, and the background neutrons (which were measured in a similar run with 1 atm He in the target), are compared with the calculated results (see Sec. 4.4). A sharply focused deuteron beam of 3 μa was used for these runs.

After the tritium system shown in Fig. 11 was evacuated and checked, the valve connecting the inner and outer systems was closed, and the tritium reservoir was heated. Within approximately 20 minutes all of the tritium had been driven into the system, thereby raising the system to 0.6 atm. When the pressure had reached this (or a lower) limit, the target valve was closed, and the reservoir was allowed to cool, thereby reducing the pressure to less than 0.2 in. Hg within a few minutes. The reservoir valve was closed and the run was begun. After the run, the target and reservoir valves were opened to allow the gas in the target to be returned to the reservoir. Within a few minutes, the pressure was reduced to <0.2 in. Hg; within an hour, the pressure could be reduced to <10 μ Hg. (In spite of these splendid beginnings, the system did not operate satisfactorily.)

From the early runs we concluded that between the time that the tritium reservoir was removed from the filling manifold and it was sealed in a helium atmosphere for transportation, air had entered the reservoir through the reservoir valve, which had not been properly closed, thereby oxidizing some of the T_2 to T_2O. Overnight, between the time of installation of the reservoir and the first run, as much as 10 curies of tritium were pumped out of the valve and exhausted up the stack. We reached the conclusions mentioned above on the basis of the following facts: (i) When the reservoir valve was opened for the run, it was found to be loosely closed. (ii) A careful calculation of the system volume revealed that less than 30 curies of tritium was being released when the reservoir was heated – if all of the gas was assumed to be tritium. (iii) The neutron yield was low by a factor of 2. (iv) The shape of the curve of the neutron yield versus deuteron energy indicated the presence of a contaminant with a higher atomic number than 1. (v) The tritium contamination in the oil of the forepump was too high (8 mc/liter) after the first four runs to be explained as a holdup of the few microcuries of T_2 which were evacuated from the system at the end of each run; if there were T_2O in the gas, however, the high holdup was plausible.

At this point in the operations a leak developed at the joint at which the target line was soldered to the target valve – after the target had been filled and isolated from the system. The air leaked into the target to raise the pressure inside from 0.5 atm to ~1 atm. The two reservoirs were able to absorb all but a small amount of gas in the system (<5 mc had all of the gas been T_2); the remainder was exhausted through the forepump up the stack. It was necessary to dispose of both reservoirs. New ones were prepared under stricter specifications.

In the preparation of the second set of reservoirs, it became apparent that there was only a small difference between the tightness of the closure of the bellows valves that gave a satisfactory seal and the one that would crack the bellows. Two alternatives were possible. (i) A larger and more sturdy commercial valve could be used, thereby increasing the volume of the system. This procedure would require a change in the AEC by-product material license. (ii) A custom-made valve in the which the valve stem was supported by more than the bellows could be designed which would be sufficiently sturdy,

and would still have the requisite small volume. The delays entailed by either alternative, together with the fact that the Cockcroft-Walton accelerator was then available at M. I. T., led to the decision to terminate the gas target operations at AFCRL.

g. Tritium Contamination

During operations with tritium a program of wipe tests was conducted to control the spread of tritium contamination. The outside of the reservoir itself was highly contaminated from its presence in a tritium hood during the filling operations (and possibly by tritium leaking through the reservoir valve). Immediately after the installation of the reservoir in the asbestos box, the whole inside of the box showed a tritium contamination of approximately 500 dpm for a 10-cm^2 wipe. Within a few days, however, the air flowing through the box (vented to the outside) had reduced contamination below measureable levels.

The only other major source of contamination was tritium adsorbed on the inner walls of the target chamber, which was released when the target windows were changed after each run as required by the AEC by-product material license. During window changes a portable hose connected to the ventilation system was held close to the target to entrap any tritium that might otherwise be released to breathing zones.

An air monitor (manufactured by Radiation Technology, Inc., Atlanta, Georgia) was used throughout all operations and indicated that at no time did the tritium concentration in the air exceed permissible levels (2×10^{-3} $\mu c/cm^3$). After 4 runs, urine samples were collected from all personel in the building and analyzed for tritium content. In spite of the fact that disposable plastic gloves were worn by those handling potentially contaminated equipment, samples from the author and an assistant, who were involved in window changes, and from the technician who operated the accelerator, were 6.0, 4.0, and 0.6 μc/liter (uncertainty is ~0.2 μc/liter), all of which were less than the permissible level of 28 μc/liter. Samples from other personnel in the building, including those who supervised the window changes, showed no activity, indicating that contamination was spread by contact with contaminated equipment, rather than by inhalation of contaminated air.

4.3 SOLID TRITIUM TARGET

Operations with the solid-tritium target on the Cockcroft-Walton accelerator at M. I. T. were much less complicated than those with the gas target. The only tritium contamination came from the surface of the targets during target changes (once every 1-2 weeks). A portable vent hose was placed near the target during changing operations, and at the exhaust of the forepump when the accelerator was being roughed down afterwards. The accelerator vacuum was maintained by a titanium getter pump (manufactured by Varian Associates, Palo Alto, California), so that normally the accelerator was a closed system. The air monitor showed that the tritium concentration in the air of the accelerator room was negligible except in the immediate vicinity of a target surface

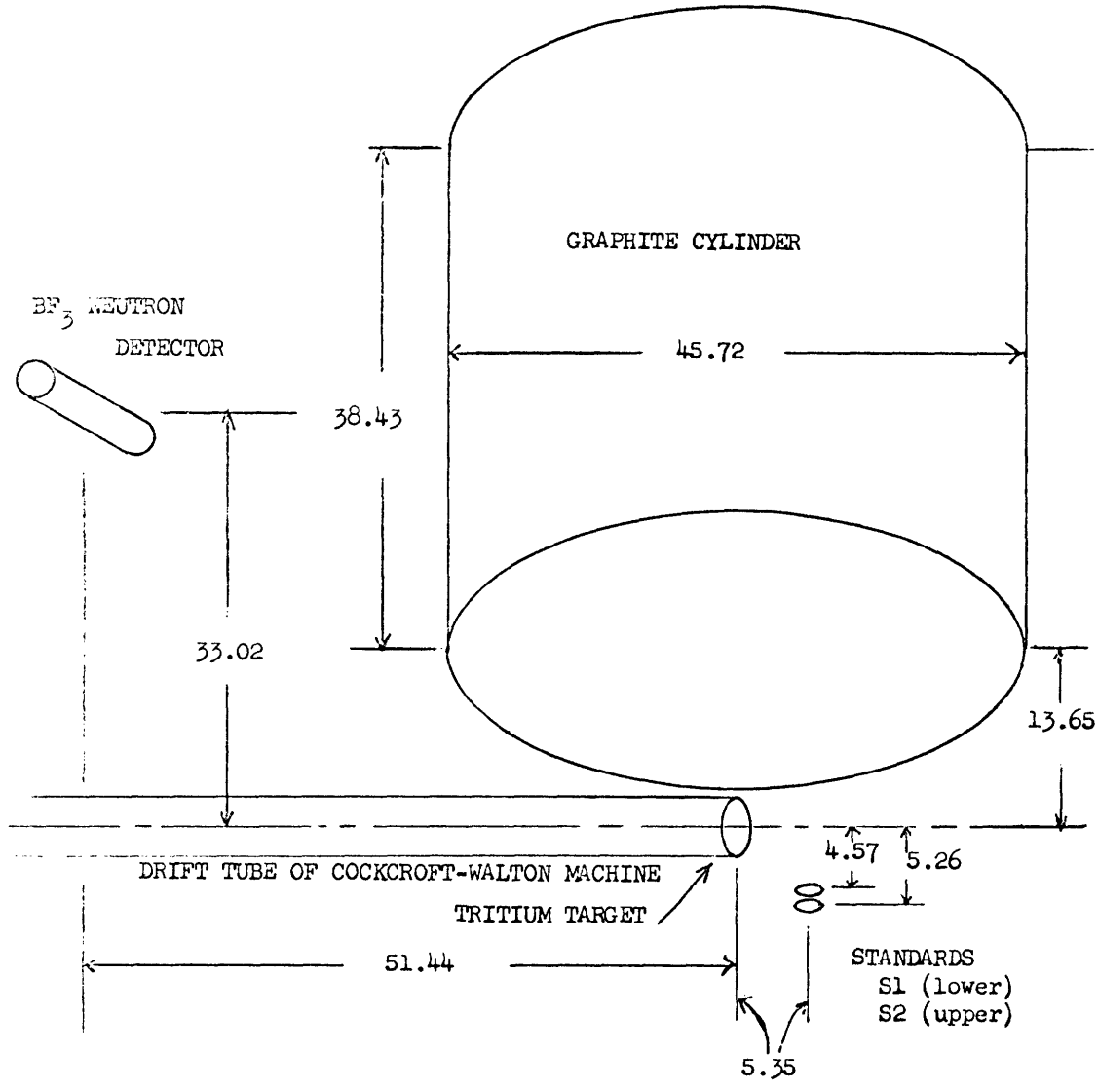

Fig. 13. Position of neutron detector, graphite cylinder, and foil standards with respect to the tritium target on the Cockcroft-Walton accelerator at M. I. T.

or the open accelerator tube.

The yield from the target was initially 10^8 neutrons per second per microampere, but decreased as the tritium was boiled off, and the active area of the target was blocked by deuterium build-up.

For blanket experiments the mock-up was placed over the target as shown in Fig. 13. The neutron flux was monitored by a BF_3 counter enclosed with a 2-inch OD plastic block. The BF_3 counter was close enough to the blanket to be affected by its presence. A calibration experiment with a second neutron counter that was placed across the room showed that the ratio of the neutron monitor sensitivity with the blanket in place to its sensitivity without the blanket was 1.205.

The effective neutron flux for each kind of threshold detector was measured by placing a foil in one of the two standard positions.

Details of the operation of the accelerator itself have been recorded elsewhere.[14]

4.4 NEUTRON ENERGY SPECTRUM FROM THE SOLID TRITIUM TARGET

A knowledge of the energy spectrum of the neutrons from the DT reaction is necessary for the calibration of the threshold detectors, and for the final evaluation of the experimental results. The neutrons produced by the Cockcroft-Walton machine behave as though they were produced by monoenergetic deuterons: their energy and intensity depend only on θ, the angle between the path of the deuteron beam and the path of the observed neutrons, and are almost isotropic. The derivation of the spectrum has been expanded to show the difference in yields of the solid and gas targets.

When deuterons of energy E' strike a thin titanium target of thickness $d\ell$, it is assumed that their energy loss within the target is negligibly small. The total number of neutrons produced is $n(E')\, d\ell$.

$$n(E')\, d\ell = IN_t\sigma_t(E')\, d\ell, \tag{5}$$

where I is the deuteron current, $\sigma_t(E')$ is the cross section for the $H^3(d,n)He^4$ reaction (DT reaction), N_t is the tritium number density, and $d\ell$ is the thickness of the target. For bombarding energies $E' < 0.4$ Mev, the DT reaction is isotropic in the center-of-mass (c.m.) coordinate system[15]; hence the fraction of neutrons that are emitted at an angle $\theta^* = \cos^{-1} x^*$ in center-of-mass coordinates within the solid angle $d\Omega^* = \sin\theta^*\, d\theta^* d\phi^*$ is just $d\Omega^*/4\pi$. The calculations are simplified if, instead of using θ^* as the independent variable, we use the direction cosine x^*; then $d\Omega^* = -dx^* d\phi^*$. The fraction in the solid angle $d\Omega = \sin\theta\, d\theta d\phi = -dx d\phi$ in the laboratory coordinate system at angle θ is found by using the appropriate transformation

$$d\Omega^* = -dx^* d\phi^* = -j(E', x)\, dx d\phi = j(E', x)\, d\Omega. \tag{6}$$

The fraction of neutrons that pass through the elemental area $dA = r^2 d\Omega$ at the point $(r, \cos^{-1} x, \phi)$ is then $j(E', x)\, dA/4\pi r^2$. Hence the number of neutrons that pass through this point, which are produced by deuterons of energy E' in the target of thickness $d\ell$, is $\phi_\ell(E', x, r)\, d\ell dA$.

$$\phi_\ell(E', x, r)\, d\ell dA = IN_t\sigma_t(E')\frac{j(E', x)}{4\pi r^2}\, d\ell dA. \tag{7}$$

All of these neutrons have an energy $E = f(E', x)$. A derivation of $f(E', x)$ and $j(E', x)$ has been given by Evans.[16] These functions, as well as the solution of the equation $E = f(E', x)$ for $E' \rightarrow E = g(E, x)$, are presented in Table 5.

The energy degradation of the deuterons in the thin target, which we have thus far neglected, is actually given by

$$dE'/d\ell = -N_t\tau_t(E') - N_s\tau_s(E'), \tag{8}$$

Table 5. Energy-angle relationships for the nuclear reaction $M_2(M_1, M_3)M_4$. Here, E' is the energy of the incident nuclide M_1 in laboratory coordinates; E is the laboratory energy of M_3 after the reaction; x is the cosine of the angle between the paths of M_3 and M_1 in laboratory coordinates; x^* is the same cosine in center-of-mass coordinates; m_i is the mass of the i^{th} nuclide M_i; and $Q = \{(m_1+m_2)-(m_3+m_4)\}c^2$, where c is the velocity of light. The derivation of these equations has been given elsewhere.[12]

Functions	Equations	Restrictions
$f(E', x) = E$	$\sqrt{E} = \frac{\sqrt{m_1 m_3}}{m_3 + m_4}\left[x\sqrt{E'} \pm \left[x^2E' + (m_4/m_3+1)\{(m_4/m_1)(Q+E')-E'\}\right]^{1/2}\right]$	$\sqrt{E}$ Real $\sqrt{E} \geq 0$ (See Note A)
	$x^* = -(1-x^2)\{a(E')\} \pm [1-(1-x^2)\{a(E')\}^2]^{1/2}$	x^* Real
	$a(E') = [(m_1 m_3/m_2 m_4)/\{1+(Q/E')(m_1/m_2+1)\}]^{1/2}$	$\lvert x^*\rvert \leq 1$
$j(E', x) = \partial x^*/\partial x$	$\partial x^*/\partial x = 2x\, a(E') \pm [1-(1-x^2)\{a(E')\}^2]^{1/2}\left[1 + \frac{x^2\{a(E')\}^2}{1-(1-x^2)\{a(E')\}^2}\right]$	(See Note A)
$g(E, x) = E'$	$\sqrt{E'} = \frac{\sqrt{m_1 m_3}}{m_4 - m_1}\left[-x\sqrt{E} \pm \left[x^2E + (m_4/m_1-1)\{E-(m_4/m_3)(Q-E)\}\right]^{1/2}\right]$	$\sqrt{E'}$ Real $\sqrt{E'} \geq 0$ (See Note B)

Note A: Where ± occurs, only the plus sign may be used if $Q > 0$ for restrictions to be satisfied; for $Q < 0$, both signs are sometimes possible; that is, the function is double-valued.

Note B: Reverse of Note A; only the plus sign may be used for $Q < 0$, but the function is sometimes double-valued when $Q > 0$.

where N_t, N_s and $\tau_t(E')$, $\tau_s(E')$ are the number densities and stopping cross sections (in Mev-barns) of the tritium and absorbant, respectively. We may write the neutron flux in terms of the deuteron energy loss dE' instead of the thickness $d\ell$ by inserting Eq. 8 into Eq. 7: that is, the flux of neutrons through the point $(r, \cos^{-1} x, \phi)$, produced by deuterons between energies E' and E' + dE' is

$$\phi'(E', x, r)\, dE' = I \frac{N_t \sigma_t(E')}{N_t \tau_t(E') + N_s \tau_s(E')} \frac{j(E', x)}{4\pi r^2}\, dE'. \tag{9}$$

Note that for a given deuteron energy E', the relative intensity and the neutron energy E are functions only of x. With the solid target, E' must be taken to be somewhat less than the bombarding energy (0.15 Mev for the Cockcroft-Walton machine) because the tritium-activated layer is not directly on the surface of the target. Comparison of the activities of the various threshold detectors placed at different angles θ led to the choice of E' = 0.1 Mev. For the angles θ subtended by the blanket (32°-148°), the neutron energy varies from 14.6 Mev to 13.5 Mev, and the relative intensity from 1.04 to 0.96 (normalized to 1.0 at θ = 90°).

The reason that a gas target has a better efficiency becomes apparent from an inspection of Eq. 9. In the gas target $N_s = 0$, so that the total flux is increased. In most solid targets $N_s/N_t \geq 1$, and $\tau(E')$ is roughly proportional to $\sqrt{Z_s}$, where Z_s is the atomic number of the absorbant. The increased slowing-down rate of the deuterons in the solid target decreases their chance of undergoing a DT reaction.

4.5 NEUTRON-ENERGY SPECTRUM FROM A TRITIUM GAS TARGET

For a very thin gas target, the equation for the flux per unit deuteron energy $\phi'(E', x, r)$ is just Eq. 9 with $N_s = 0$. A thick gas target is split into many slabs of thickness $d\ell$ within which the deuteron energy E' may be considered constant. The distance of each slab from the surface at which the deuterons enter the gas at energy E'_{max} is

$$\ell(E') = \int_{E'}^{E'_{max}} dE'/\tau(E'). \tag{10}$$

To obtain $\phi(E, x, r)$, the flux of neutrons per unit neutron energy, it is only necessary to change the energy width in Eq. 9 from dE' to dE:

$$dE' = \frac{dE}{(dE/dE')_{x=\text{const.}}}, \tag{11}$$

where

$$(dE/dE')_{x=\text{const}} = \partial f(E', x)/\partial E' \qquad \text{(point source)}, \tag{12}$$

if $r \gg \ell(E'_{min}) = \ell_o$, the thickness of the gas target. By substituting Eqs. 11 and 12 for dE' in Eq. 9, the desired expression for $\phi(E, x, r)$ is found to be

$$\phi(E, x, r) = I \frac{\sigma_t(E')}{\tau_t(E')} \frac{j(E', x)}{4\pi r^2} \{\partial f(E', x)/\partial E'\}^{-1}, \tag{13}$$

where $E' = g(E, x)$. Only the magnitudes of $j(E', x)$ and $\partial f(E', x)/\partial E'$ are used, since only the magnitudes of $(d\Omega^*/d\Omega)_{E'=\text{const}}$ and $(dE/dE')_{x=\text{const}}$ are of interest. A sample set of spectra at various angles, computed from Eq. 13, is plotted in Fig. 14 as $r^2\phi(E, x, r)$ versus E.

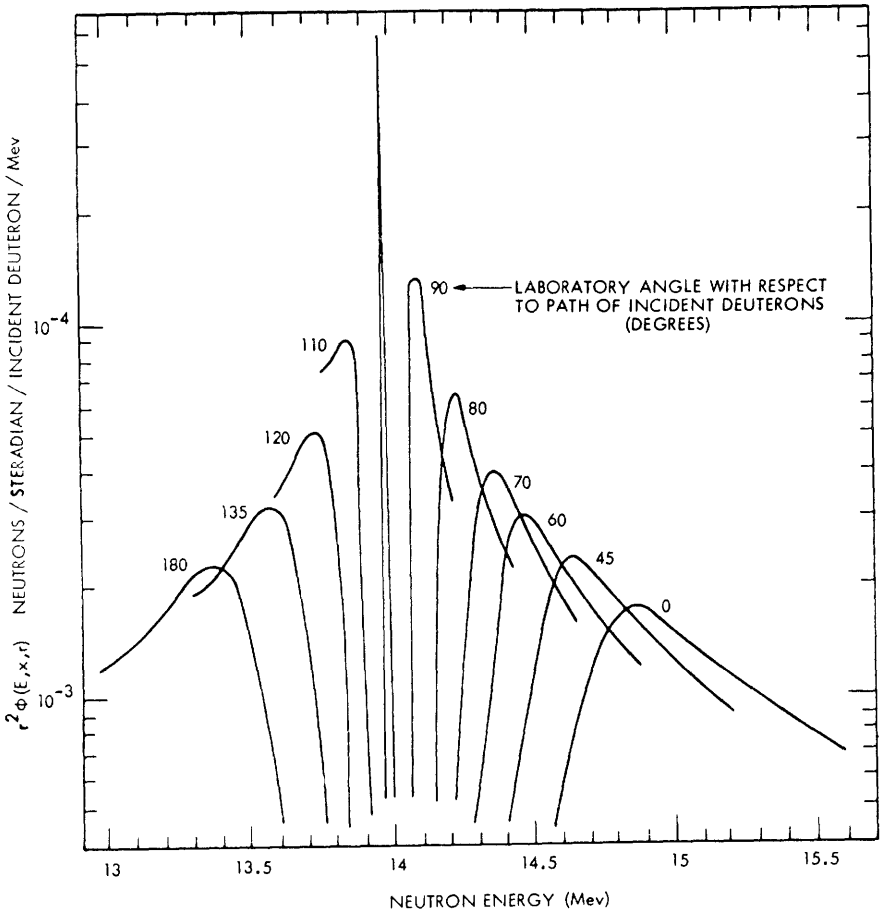

Fig. 14. Point-source calculation of the neutron-energy spectrum from the gas target.

a. Numerical Problems

The function $f(E', x) = E$ for a given value of x has the general shape shown in Fig. 15. From the figure it can be seen that if $E'_{max} > E'_m$ and $E'_{min} < E'_m$, where E'_{min} is the energy at which unreacted deuterons leave the gas, and

$$\partial f(E', x)/\partial E' = 0 \qquad (E' = E'_m), \tag{14}$$

there may be two deuteron energies E' that can produce neutrons of energy E. The fluxes from each E' are added.

Since $\partial f/\partial E'$ appears in the denominator of Eq. 13, $\phi(E_m, x, r)$ is singular if

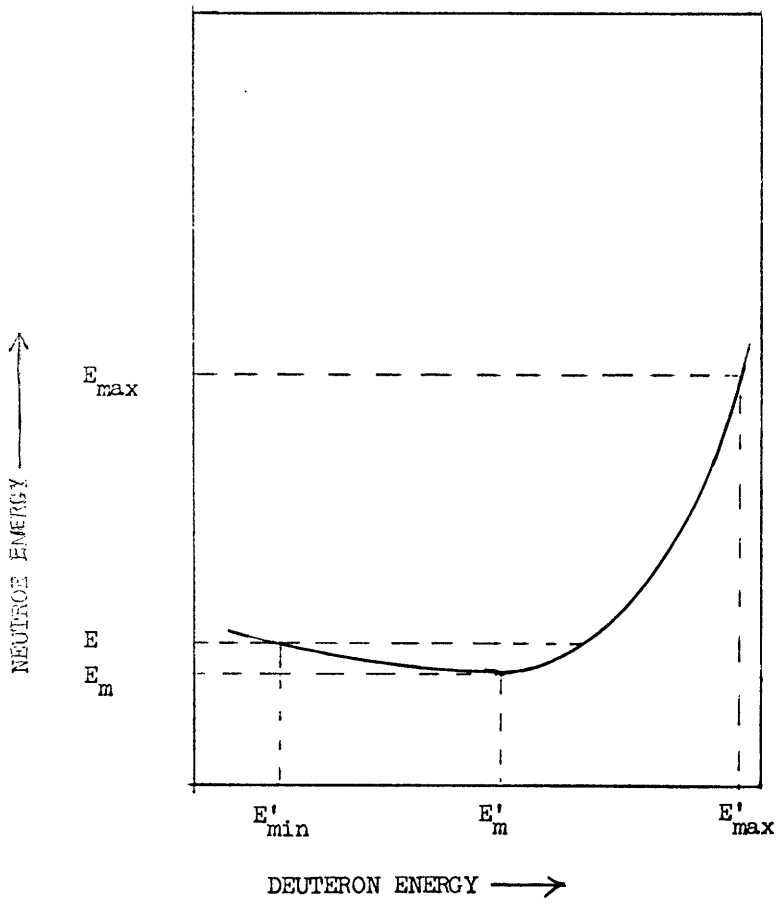

Fig. 15. Schematic curve of $E = f(E', x)$ for a constant value of x.

$E_m = f(E'_m, x)$. If $\phi(E, x, r)$ is being used in an integration (to find the average value of a cross section $\sigma(E)$, for instance, for which the detailed shape of the neutron energy is not desired), the singularity may be avoided by using Eq. 9, integrating over deuteron energy, and using $\sigma\{f(E', x)\}$ in the integral.

b. Finite-Source Calculation

If the distance r of the point of observation P from the target is of the same order as the thickness of the target ℓ_o (see Fig. 16), the distance $\ell(E')$ which the deuterons travel in slowing to energy E' (from Eq. 10) must be taken into account. As can be seen from Fig. 16, the neutrons that pass through P, which are produced by deuterons of energy E', now travel a distance R, given by

$$R^2 = r^2 + \{\ell(E')\}^2 - 2 \times r\ell(E'). \tag{15}$$

The cosine of the angle between R and the deuteron path is now not x but y,

$$y = \frac{r - \ell(E')}{R} \tag{16}$$

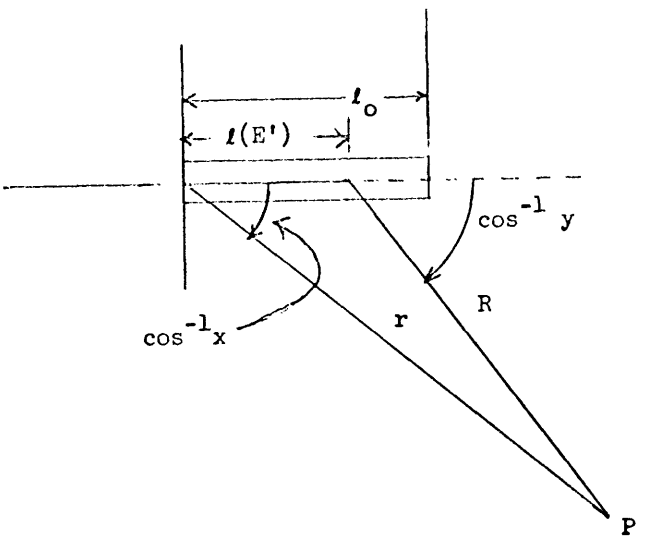

Fig. 16. Schematic diagram of a gas target for the finite-source calculation.

The energy of the neutrons is $E = f(E', y)$, and the ratio of the solid angles in center-of-mass and laboratory coordinates is $j(E', y)$. Furthermore, $(dE/dE')_{x=\text{const}}$ is no longer simply $\partial f/\partial E'$, but

$$(dE/dE')_{x=\text{const}} = \frac{\partial f(E', y)}{\partial E'} + \frac{\partial f(E', y)}{\partial y} \frac{dy}{d\ell} \frac{d\ell}{dE}, \qquad \text{(finite source)}. \tag{17}$$

We find $d\ell/dE'$ from Eq. 8 (with $N_s = 0$); $dy/d\ell$ can be found by differentiating Eq. 15:

$$dy/d\ell = (y^2-1)/R. \tag{18}$$

The expression for the neutron-energy spectrum $\phi(E, x, r)$ for a finite source is found from Eq. 13 by replacing x with y, r with R, and $\partial f/\partial E'$ by Eq. 16:

$$\phi(E, x, r) = I \frac{\sigma_t(E')}{\tau_t(E')} \frac{j(E', y)}{4\pi R^2} \left[\frac{\partial f(E', y)}{\partial E'} - \frac{\partial f(E', y)}{\partial y} \frac{(y^2-1)}{RN_t\tau_t(E')} \right]^{-1} \qquad \text{(finite source)}. \tag{19}$$

Here $dy/d\ell$ and $d\ell/dE'$ have been replaced by the right-hand side of Eqs. 18 and 8 (with $N_s = 0$). It is no longer possible to find the deuteron energy E' analytically from the neutron energy E and the coordinates of the point of observation $(r, \cos^{-1} x, \phi)$; a numerical approach must be used.

A sample calculation of the neutron-energy spectrum for $\cos^{-1} x = 70°$ is shown in Fig. 17 for various radii. Notice in Eq. 19 that as r becomes large $y \to x$, $R \to r$, and the second term in square brackets becomes much larger than the first; thus Eq. 19 approaches Eq. 13 for the point source. This is shown in Fig. 17, in which the results

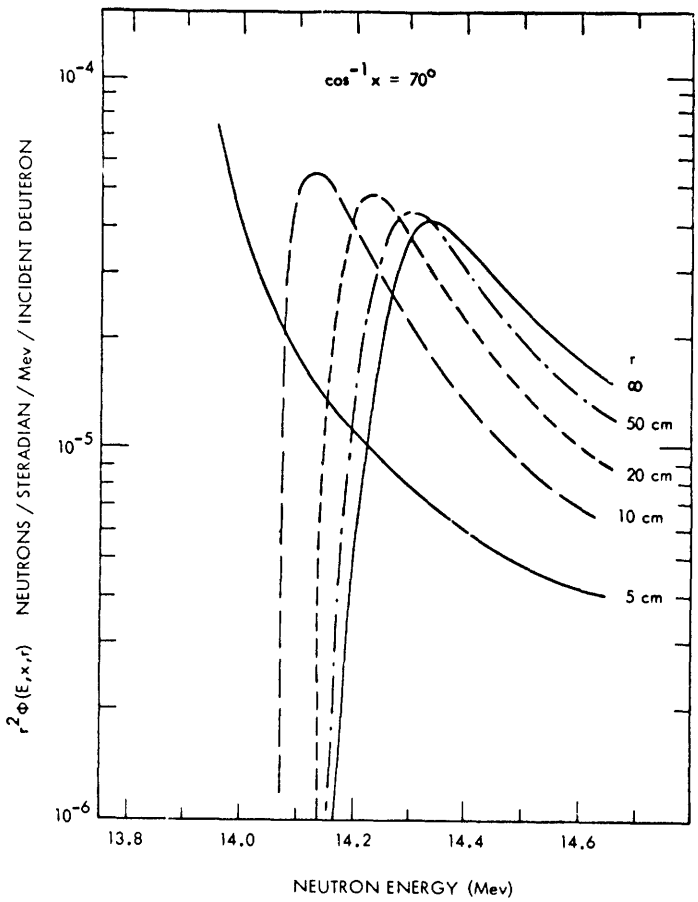

Fig. 17. Finite-source calculation of the neutron-energy spectrum from the tritium gas target.

of the finite-source calculation merge with those of the point-source calculation as r increases. The spectrum broadens as r decreases, since the neutrons that pass through the point of observation can come from a wider range of angles with the deuteron path. The continued increase of the spectrum as E approaches 13.93 Mev for r = 5 cm is caused by the fact that in this case the term in braces in Eq. 19 approaches zero. The problems of singularities in $\phi(E, x, r)$ for the finite-source calculations are similar to those discussed for the point-source calculations.

V. THRESHOLD DETECTORS

5.1 INTRODUCTION

The measurement of the neutron-energy spectrum above 1 Mev is of interest, because the computation of the behavior of the neutrons is most difficult in this energy region. Electronic systems for measuring the spectrum, in particular solid-state devices, were considered; they were rejected because the detectors were too large to be placed conveniently at various positions within the experimental assemblies. The other choice was a series of threshold detectors. After a search among publications, five suitable threshold reactions were found: $U^{238}(n, f)$, $P^{31}(n, p)Si^{31}$, $Fe^{56}(n, p)Mn^{56}$, $I^{127}(n, 2n)I^{126}$, and $F^{19}(n, 2n)F^{18}$.

The criteria for selecting the threshold detectors, the properties of the chosen threshold detectors, the irradiation procedures, and the calculations and preliminary experiments that were necessary to properly normalize the experimental results are described here. The method of deducing the differential neutron-energy spectrum $\phi(E)$ from the normalized detector responses is the subject of Section VI. The results of the threshold detector measurements are presented in Section VIII; the spectra computed from these results are discussed in Section IX.

Some of the discussion below has been published elsewhere[9, 11]; material from these sources will be used without further reference.

5.2 REQUIREMENTS FOR SUITABLE THRESHOLD DETECTORS

Several factors had to be considered in choosing the threshold detectors.

Cross Section. The cross section for the reaction must be an accurately known function of energy in the region <14.2 Mev. This requirement eliminates most of the prospective reactions because (a) the work with threshold detectors has usually been done for reactor systems, for which the highest energy of interest is ~2 Mev, and (b) a great deal of the data on threshold detectors results from measuring an effective cross section for a neutron spectrum that is almost a fission spectrum. The spectrum in the blanket is nothing like a fission spectrum; hence data on effective cross sections are of no value in the present work.

Half-life. Since it requires from 15 minutes to 2 hours after completion of an accelerator run to begin counting the foils, the half-life of the daughter products cannot be much less than one hour, or the activity produced will decay before it can be counted. On the other hand, if the half-life is more than several hours, not enough activity is produced unless the cross section for the reaction is large. The foils were counted on an automatic sample-changer that used a Geiger-Mueller counter, so different types of radiation (β-, γ-radiation; γ-rays of various energies) could not be discriminated. Therefore the half-life of the daughters of the main reactions must be larger or shorter by a factor of at least 3 than those of competing reactions, so that the decay from the various components can be separated by the Frantic analysis program (see Appendix A),

which was used to analyze the sample-changer data.

Foil Material. To ease the problem of counting the foils after an accelerator run, the parent isotope must be in a form that does not require special handling. Since the economic use of the tritium target required that at least 20 foils be irradiated per run, high-cost isotopically enriched foils were rejected. If a compound is used, the additional elements cannot contribute too much to the background.

Foil Size. Because of the low neutron fluxes in the experimental assemblies, the foils must be rather large to obtain enough activity for counting. On the other hand, the foils must be small enough to give some spatial resolution. Foils of 0.75-inch diameter and up to 0.125-inch thick were chosen as a reasonable compromise. The mean-free paths for neutrons in the energy range of interest are large (~2 cm); therefore corrections for the presence of the foils in the blanket are unnecessary.

5.3 THRESHOLD DETECTOR PROPERTIES

The properties of the five threshold detectors that were finally chosen are discussed below, and are summarized in Table 6. The cross sections appear in Fig. 18 (the actual values used in computations are listed in Appendix D). In general the cross sections are

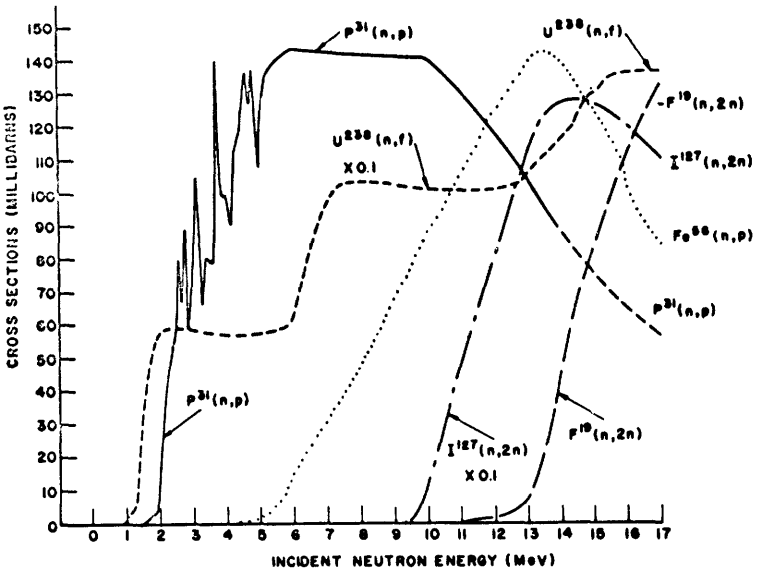

Fig. 18. Cross sections for threshold reactions. The curves are the best ones from available data (see Table 6). The curve for $P^{31}(n, p)$ has been averaged over the resonances in the 2-5 Mev region; beyond 14 Mev it was extrapolated on a logarithmic plot. The curve for $F^{19}(n, 2n)$ is a compromise between Russian[27] and French[26] data. Numerical values for the cross sections are given in Appendix D.

Table 6. Threshold detector properties.

Element	Uranium	Phosphorus	Iron	Iodine	Fluorine
Reaction	$U^{238}(n,f)$	$P^{31}(n,p)Si^{31}$	$Fe^{56}(n,p)Mn^{56}$	$I^{127}(n,2n)I^{126}$	$F^{19}(n,2n)F^{18}$
Threshold energy	1.0 Mev	2.0 Mev	4.5 Mev	9.5 Mev	11.1 Mev
Half-life of daughter(s)	31.6 min[a] 425 min	2.62 hr	2.58 hr	13 days	1.85 hr
Important competing reactions--half lives	---	---	$Mn^{55}(n,\gamma)Mn^{56}$[b] 2.58 hr	$I^{127}(n,\gamma)I^{128}$ 25 min	---
Foil material	Depleted metal foil, Mylar catchers	$Ca(PO_3)_2$ glass	Metal foil	C_6I_6 pellets	Teflon discs (CF_2)
Foil dimensions Diameter, thickness	0.75"d.,0.01"t.	0.75"d.,0.145"t.	0.75"d.,0.016"t.	0.625"d.,0.096"t.	0.75"d.,0.062"t.
References for cross sections	17	17, 18, 19	17, 20, 21, 22, 23, 24	17, 24, 25	25, 26, 27, 28, 29

Notes: a. Empirically determined pseudo half-lives.
b. From impurities. The foils used in these experiments had less than 10 ppm manganese.

those of BNL-325 modified by later measurements.[17] Certain alternatives to the chosen detectors are also mentioned.

a. $U^{238}(n, f)$

Cross Section. The 1-Mev threshold for the fast fission of U^{238} sets a lower limit to the neutron energies which could be measured. The cross-section values of BNL-325 are used for the entire energy range.

Half-life. If the various activities from the fission products are counted, as was true in our case, the decay of each of the fission products cannot be distinguished, and an empirical procedure must be used. We found that the fission product decay curves could be fitted reasonably well by the curve

$$A(t) \doteq A_1 \exp(-\lambda_1 t) + A_2 \exp(-\lambda_2 t), \tag{20}$$

where λ_1 and λ_2 are pseudo-decay constants corresponding to half lives of 31.6 and 425 minutes, respectively. The 31.6-minute half-life was used in the data analysis, since the activity of this component was not affected by the activity of small pieces of uranium oxide which occasionally rubbed off onto the Mylar catchers.

If 5 or more points could be measured on the decay curve, the constants A_1 and A_2 were determined by the Frantic analysis program. In some cases, however, only 2-4 points could be taken before the catcher activity decayed to background levels, and the following method was used: The curve of Eq. 20, plotted on logarithmic paper, is a straight line in the range $20 < t < 100$, where t is the time in minutes after the accelerator run. The slope of this line depends on the ratio A_1/A_2:

$$\frac{d(\log A(t))}{d(\log t)} = \frac{(A_1/A_2)x_1 \exp(-x_1) + x_2 \exp(-x_2)}{(A_1/A_2) \exp(-x_1) + \exp(-x_2)}, \tag{21}$$

where $x_1 = \lambda_1 t$ and $x_2 = \lambda_2 t$. The sample-changer observation points for each sample were plotted on logarithmic paper, and a visual fit was made to the points. The slope of the curve at t = 60 minutes after the accelerator run was compared with that computed from (21) to obtain the ratio A_1/A_2. This ratio, plus the total activity at t = 60 was used to compute the initial activity A_1. Comparison of this method with the results of the Frantic analysis (when there were at least 5 points) showed agreement within approximately 50 per cent.

Foil Material. The uranium foils were punched out of commercial grade depleted uranium foil (about 0.25% U^{235}). These foils have a background activity of about 10^5 cpm. Irradiation of the foils for several hours increased the activity only by a few per cent. As a result the activity of fission products that recoil into Mylar catchers was counted instead of the uranium itself. Although the efficiency of the catcher technique is less, the counting statistics are much better.

Alternative Reactions. The reaction $In^{115}(n, n')In^{115m}$ has a threshold of 0.5 Mev,

and produces activity from the isomeric transition (half-life = 4.5 hr). The required cross-section values are not available in the energy range 5-14 Mev. Good data are available[31,32] for the reaction $Np^{237}(n,f)$, which also has a threshold of 0.5 Mev, but the cost of a sufficient number of foils was prohibitive.

b. $P^{31}(n,p)Si^{31}$

Cross Section. The cross section for this reaction is basically that given in BNL-325, modified by later measurements made by Ricamo and his co-workers[18] in the 2-5 Mev region. Older data by Ricamo reported in BNL-325 are renormalized to these more recent values. For use as a threshold detector, the cross sections are averaged over the many narrow resonances in the 2-5 Mev region.

Half-life. The Si^{31} produced in this reaction decays with a 2.62-hr half-life.

Material. Although most authors suggest using ammonium phosphate for the foils, we found that calcium metaphosphate glass ($Ca(PO_3)_2$) is a better material.[30] The foils were manufactured in the following way.

Monobasic calcium phosphate powder ($Ca(H_2PO_4)_2 \cdot H_2O$) is heated in graphite crucibles to 2300°F, at which temperature it dehydrates, decomposes to $Ca(PO_3)_2$, and then melts. The resulting clear syrupy fluid is poured into graphite molds (which are heated by a hot plate), and pressed into shape before the molten fluid solidifies. The resultant clear glass pellets are annealed at 850°F for several hours to remove the thermal strains introduced in casting, and then slowly brought to room temperature. The pellets can be handled as ordinary glass, although they are not quite so brittle. They are of 90% theoretical density because of air bubbles and bits of graphite trapped during the casting process.

Five calibration runs were made to calibrate the 20 foils which were used in the blanket experiments. The foils were placed on a flux wheel which rotated about the neutron source. An average initial activity was computed for each run, and the activity of each foil was ratioed with the average. The averages of the ratios for the five calibration runs are shown in Table 7; the original data are shown in Appendix E. (Preliminary runs with other threshold detectors showed that the responses of the foils of each kind were the same within the limits of reproducibility – about 5%.)

Alternative Reactions. The $S^{32}(n,p)P^{32}$ reaction covers the same energy region as does the $P^{31}(n,p)Si^{31}$ reaction, and the cross section of the former reaction is better known. However, the 14.3-day half-life of P^{32}, coupled with an average cross section of only 100 mb made the activity too low to be used in these experiments. The cross section for the $Al^{27}(n,p)Mg^{27}$ is also similar to that of the $P^{31}(n,p)$ reaction, but the half-life of Mg^{27} is too short (9.5 minutes).

c. $Fe^{56}(n,p)Mn^{56}$

Cross Section. The cross-section measurements made by various workers are in good agreement. The data of Terrell and Holm, reported in BNL-325, have been

Table 7. Calibration of phosphorus foils.

Foil Identification[a]	Average Ratio[b]	Calibration factor F[c]
1	0.97	1.03
2	0.99	1.01
3	1.00	1.00
4	0.983	1.02
5	1.10	0.91
6	1.007	0.993
7	1.048	0.945
8	1.024	0.975
9	1.026	0.974
10 or U	0.998	1.002
11 or A	0.968	1.031
12 or B	1.016	0.985
13 or C	1.00	1.00
14 or D	0.999	1.001
15 or E	1.037	0.965
16 or F	0.94	1.06
17 or G	1.045	0.946
18 or H	0.975	1.027
19 or I	0.954	1.049
20 or J	1.006	0.995

Notes: a. Numbers were used in identifying the foils in the calibration runs. Since only one character was available for foil identification in the blanket runs, letters were used for foils 10-20.
b. Ratio is initial activity of given foil divided by average of all initial activities for a particular calibration run.
c. Inverse of previous column.

renormalized to agree with later measurements.

Half-life. The Mn^{56} produced in the $Fe^{56}(n, p)$ reaction decays with a 2.54-hr half-life.

Material. The decay of Mn^{56} from the $Mn^{55}(n, \gamma)Mn^{56}$ reaction provides an undesirable background to the desired $Fe^{56}(n, p)Mn^{56}$ reaction, even if there is only the 0.5% manganese present in commercially available high-purity iron. The iron foils used in these experiments were cut from a slug of iron (manganese content less than 10 ppm) obtained from the Department of Metallurgy, M.I.T. Preliminary measurements showed that these foils had identical responses. Cadmium ratios for these foils, measured in the graphite blanket, are 1.0, compared with 1.2 for commercial iron (and MnO_2 samples).

Alternative Reactions. The reaction $Al^{27}(n, \alpha)Na^{24}$ was also considered for this energy region. The cross section for this reaction is probably the best measured of any of the reactions that were studied, since it is used as a basis for measuring other cross sections in the region 6-20 Mev. The 31 mb effective cross section, coupled with a 15-hr half-life for the decay of the Na^{24} daughter product, led us to believe that the resultant activities would be too small. Since the count rates for the other foils were higher than expected, this reaction might still be useful in future experiments.

d. $I^{127}(n, 2n)I^{126}$

Cross Section. The cross section is mainly that given in BNL-325, modified at higher energies by more recent work by Borrmann and his co-workers.[24] The shape of the curve at lower energies is computed from a theoretical formula based on the compound-nucleus theory.[33]

Half-life. The cross section for the $I^{127}(n, 2n)I^{126}$ reaction is high enough so that the long half-life (13 days) of I^{126} can be tolerated. The $I^{127}(n, \gamma)I^{128}$ provides competing activity. The decay of I^{128} with a 25-min half-life can be separated from the I^{126} decay either by allowing the iodine foils to cool for one day before counting, or by fitting the iodine decay to the two half-lives, by using the Frantic analysis program.

Material. The foils are made by compressing 2 grams of hexaiodobenzine powder (manufactured by Distillation Products Industries, Rochester, New York) into a mold at a pressure of 100 ton/in^2. The resulting pellets are of uniform size, nonhydroscopic, and reasonably sturdy.

e. $F^{19}(n, 2n)F^{18}$

Cross Section. Most of the cross-section measurements are centered around 14 Mev, and are in good agreement. At other energies there are two widely varying sets of measurements, one by French researchers[26] and one by Russians.[27] Although the two curves have the same general shape, the Russian curve is higher, and rises and falls more steeply. The Russian curve is in better agreement with the data at 14 Mev, and is more consistent with the other data used in the spectral analyses (see Section IX). The

cross-section curve shown in Fig. 18 is based mainly on the Russian data. In the spectral analyses (Section IX) both sets of data are considered.

Half-life. The F^{18} produced in the $F^{19}(n, 2n)$ reaction decays with a 111-minute half-life.

Material. The foils were punched from 0.063-inch teflon sheet.

5.4 IRRADIATION PROCEDURES

Several foils of each kind of threshold detector are placed in the experimental assembly as the blanket configuration to be studied is constructed on an aluminum cart. The foils are irradiated in 0.020-inch cadmium foil holders, as shown in Fig. 19. Originally the holders were intended to reduce activities from competing thermal-neutron reactions. After we discovered that the thermal fluxes were negligible in the blanket assemblies, the holders still proved useful in handling the foils. Note in Fig. 19a and b that a phosphorus foil or an inverted holder is used to press the Mylar catchers to the uranium foils (which were slightly bowed when they were punched from 0.01-inch uranium sheet). A Mylar-uranium-Mylar sandwich might also be inserted between the teflon and cadmium lid (Fig. 19c). The cadmium covers, uranium foils, and Mylar catchers were cleaned with acetone before being inserted in the blanket. Phosphorus and uranium standards are placed in position S2; iron, iodine, and fluorine standards are placed in position S1 (see Fig. 13). After the blanket has been assembled, the aluminum cart is rolled into position, and the accelerator run is begun. (Because of the occupationally high neutron fluxes, all doors leading to the accelerator area were locked during runs.)

A reference code, including the foil type, foil number, and position number (see Sec. III) was used to identify each data point in later analysis. The composition of this code is shown in Fig. 20. Accelerator runs are referenced by blanket configuration and the date of the run.

Since the activities produced in the threshold detectors decay with half-lives of approximately 2 hours, the maximum useful length of an accelerator run is also approximately 2 hours. In general, at least three accelerator runs were required to gather the data for each configuration. The 13-day half-life of I^{126} makes it profitable to accumulate the dose given to the iodine foils over several runs for a particular configuration.

Except for I^{126}, the decay of the daughter products must be taken into account during the accelerator run. It is shown in Appendix A that the effective dose, considering decay, is

$$\phi_{eff}(L, \lambda) = \int_0^L \phi(t)\, e^{-\lambda(T-t)}\, dt, \tag{22}$$

where L is the length of the irradiation, and λ is the decay constant. During the runs the neutron flux was monitored with a BF_3 counter (see Fig. 13). The response of this

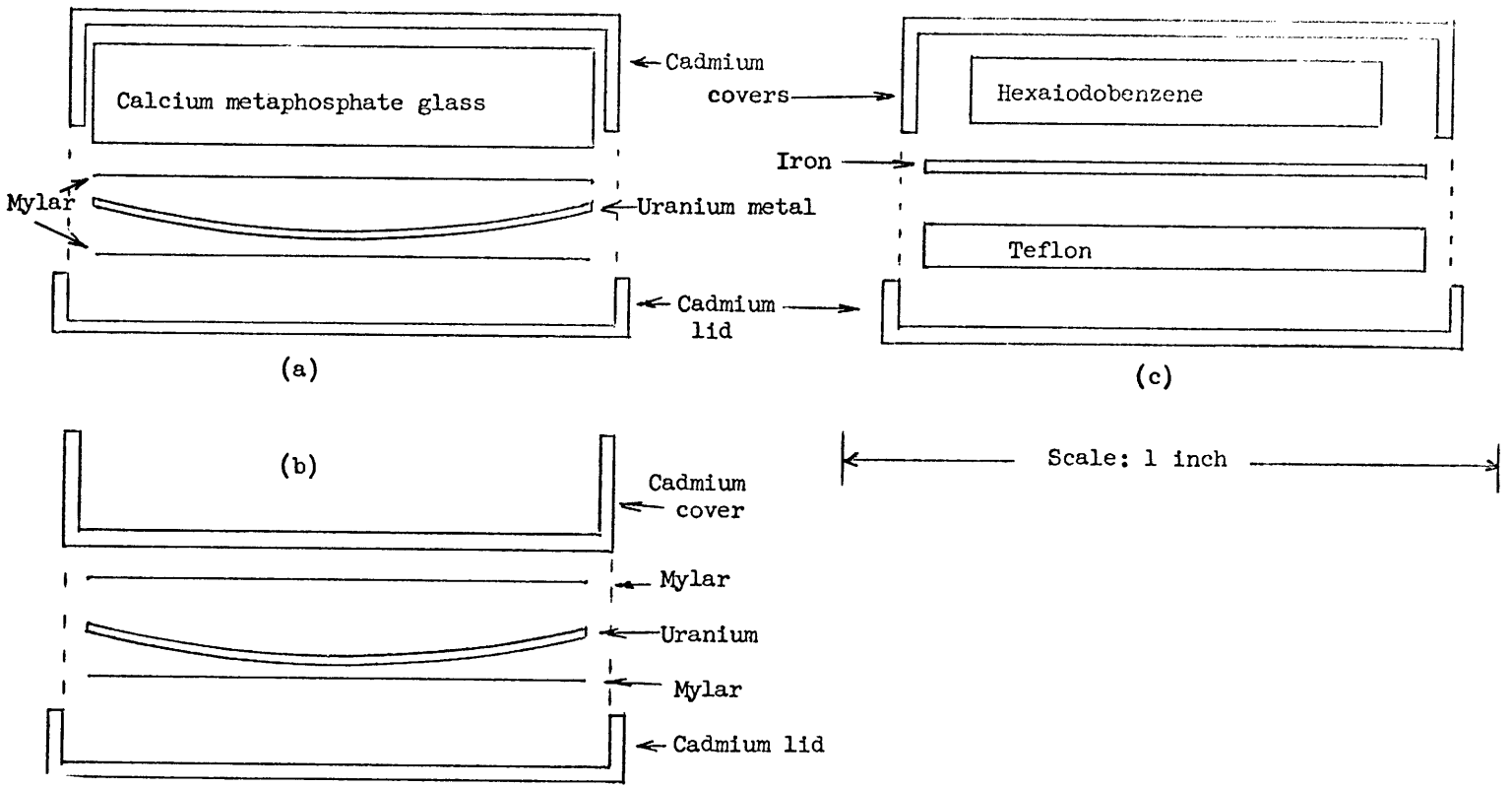

Fig. 19. Typical arrangements of threshold detectors in cadmium covers.

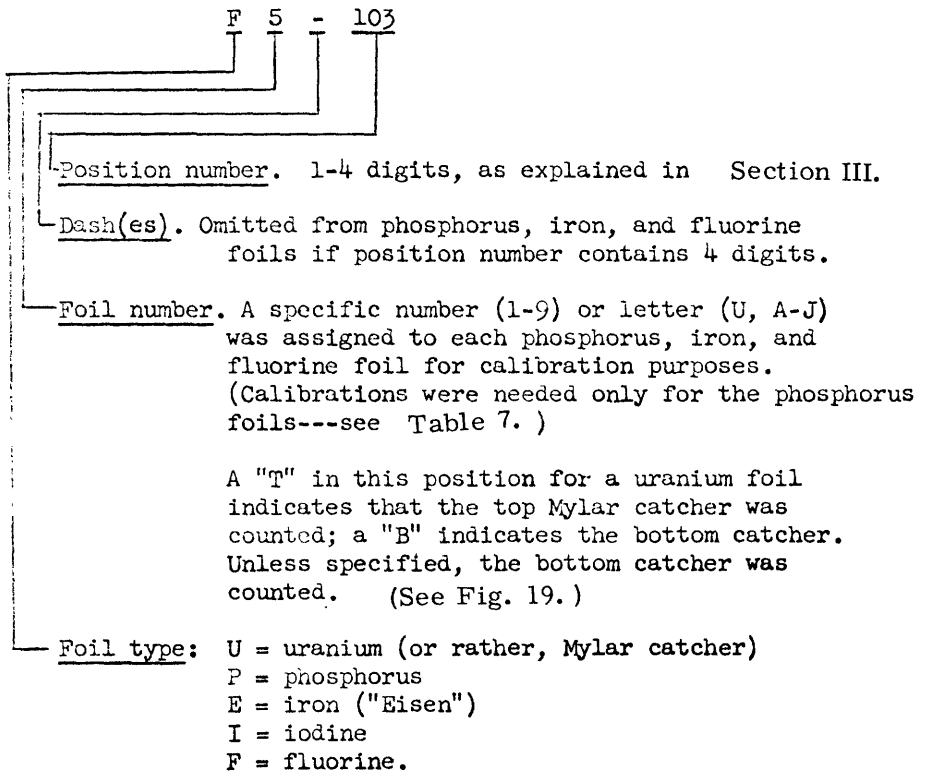

Fig. 20. Reference codes for threshold-detector data points.

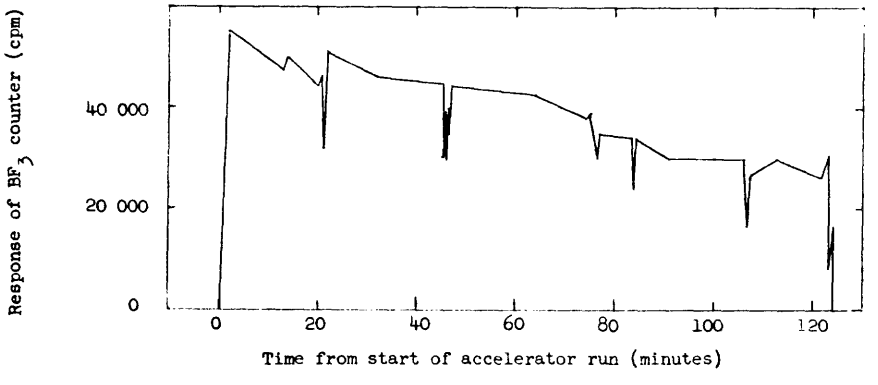

Fig. 21. Flux plot $\phi(t)$ for a typical accelerator run. (Data taken from run on March 24, 1964.) The effective doses for the various detectors are listed in Appendix E.

counter was fed through an amplifier-scaler and a count-rate meter to a chart recorder. The flux plot for a typical run is shown in Fig. 21.

5.5 COUNTING PROCEDURES

After the completion of an accelerator run the uranium catchers were counted as soon as possible. Two hours later, the catcher activity had decayed to background levels, and the phosphorus, iron, and fluorine foils were counted. The iodine foils were usually counted over the week end following the accelerator runs for a given blanket configuration. Figure 22 shows decay curves for four of the foils that were irradiated in the accelerator run shown in Fig. 21.

To monitor sensitivity changes in the flow-type GM counter, a Ba^{133} or Co^{60} standard was included in each batch of foils that was counted in the automatic sample changer.

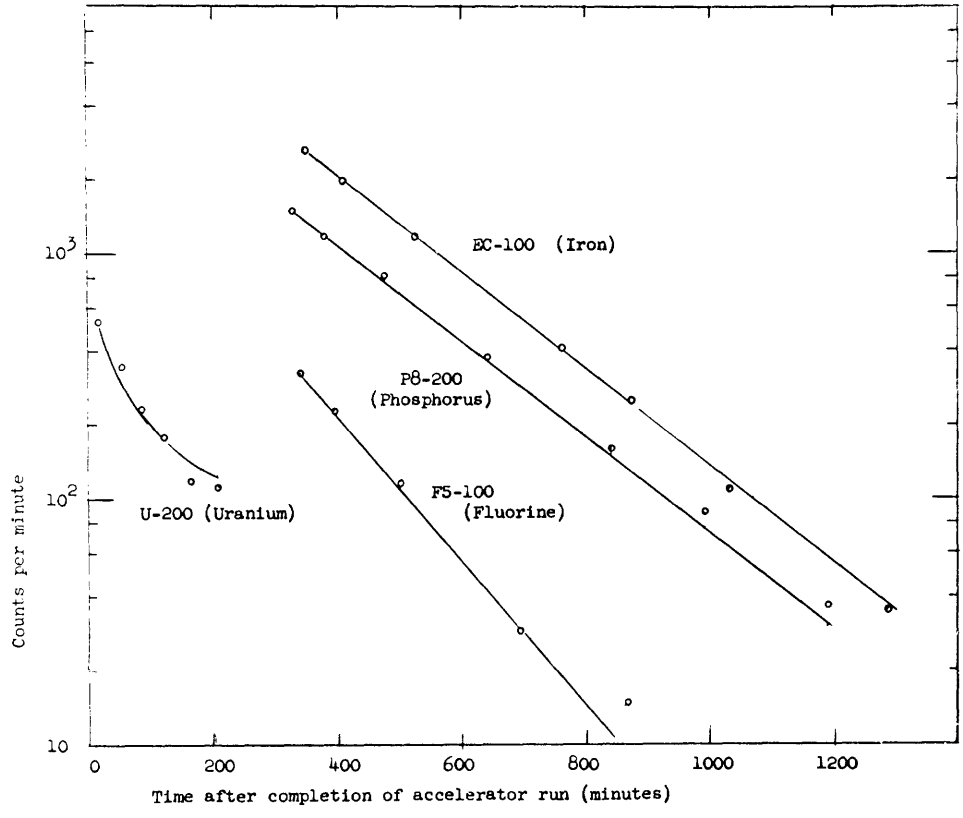

Fig. 22. Sample threshold detector activities. The foils were irradiated near the surface of the all-graphite blanket on March 24, 1964. Observed count rates are shown by the circles. Solid curves are weighted least-squares fits to the data, computed by Frantic analysis programs. The flux plot $\phi(t)$ for this run is shown in Fig. 21. The iodine foil I-10G, which was exposed to this and to similar runs (March 25 and 26, 1964) had an activity of approximately 150 cps on March 27, 1964.

Before April 26, 1964, P-10 gas was used as the counter gas; Q-gas was used after April 26. The operating plateau of the counter dropped from 2400 volts to 1000 volts with the change of gases, but the sensitivity of the counter was not noticeably changed. For each observation, the sample number (order number within the batch), length of the observation, and a code letter denoting the number of counts accumulated during the observation were recorded on a paper tape.

5.6 PRELIMINARY ANALYSIS

The data from the sample-changer tape and the chart recorder are transferred to cards, and fed with the SAMTAPE programs (see Appendix A) to an IBM 709 or 7094 computer. The SAMTAPE main program sorts the activation data by foil. The Frantic routines fit the activation data to the sum of one or more exponential decay curves, to give a number A.

$$A = \frac{(\text{cpm at end of accelerator run})}{\lambda}, \tag{23}$$

where λ (in min^{-1}) is the decay constant of the component of interest. The BEAM routines compute the effective dose for each λ from Eq. 22, and another number A' is computed.

$$A' = A/\phi_{\text{eff}}(L, \lambda). \tag{24}$$

A' is proportional to the saturation activity per unit neutron flux, and is independent of the half-life and irradiation and counting history of the foil.

The flow of information to this point is illustrated by Fig. 23. The values of the A' which were computed by the Frantic and BEAM programs are listed in Appendix E.

5.7 NORMALIZATION PROCEDURES

Additional normalization is necessary to convert the A' to numbers that can be used to determine the differential neutron-energy spectra by the method outlined in Section VI.

a. Normalized Activity

To be able to compare threshold-detector results from configuration to configuration, we define the normalized activity A_o.

$$A_o = FGA'. \tag{25}$$

Here, F is the foil calibration factor. The values of F for the phosphorus foils are given in Table 7. For other detectors in these experiments, F = 1. G is the neutron-counter normalization factor.

$$G = \frac{A'(\text{fluorine foil in standard position})}{0.11}, \tag{26}$$

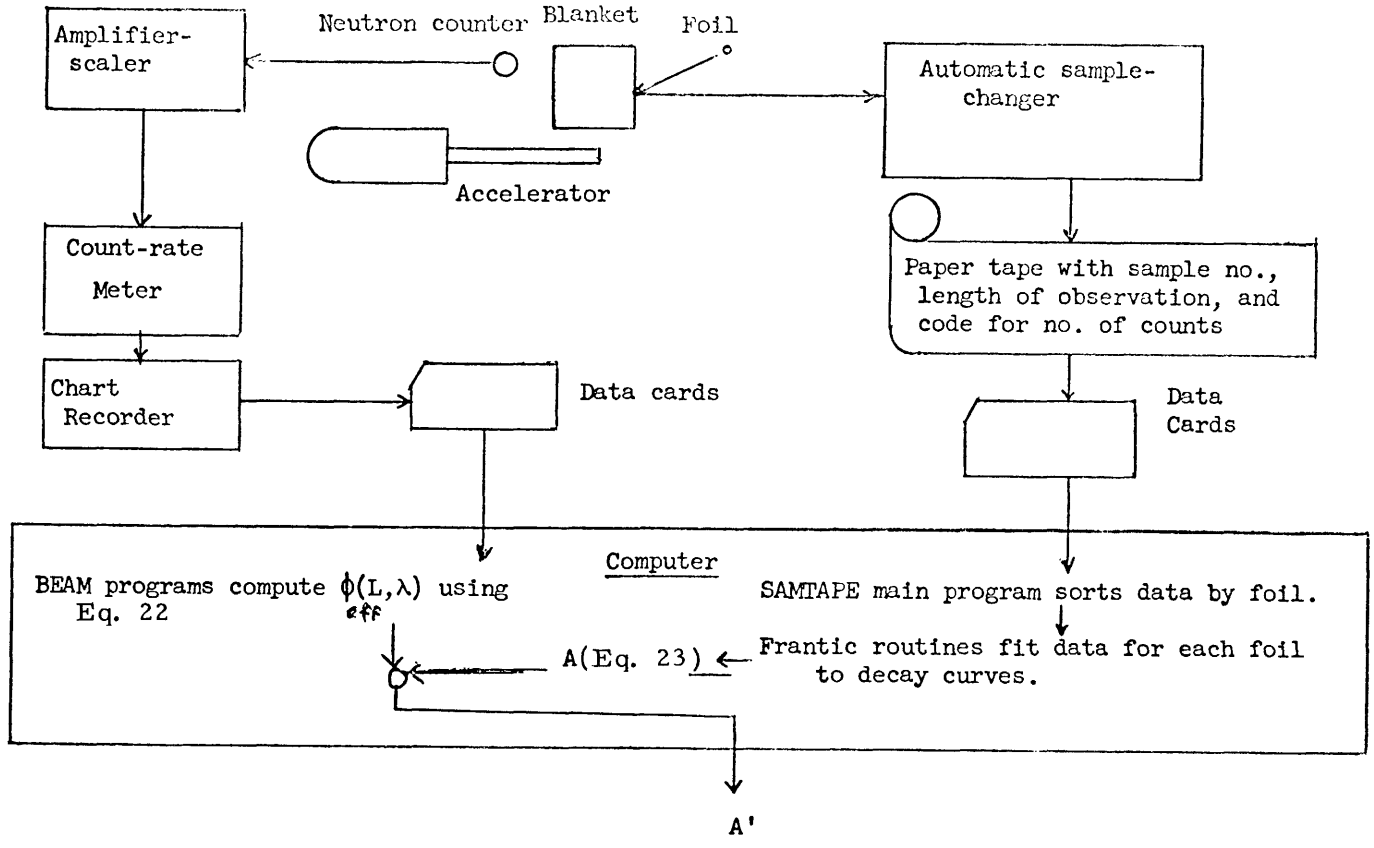

Fig. 23. Information flow in threshold-detector irradiations.

where 0.11 is the average value of A' for the fluorine standards for the all-graphite blanket runs. The BF_3 counter is sensitive mainly to neutrons with energies less than 2 Mev, and thus sees only neutrons that have undergone at least one inelastic scattering, either in the blanket assembly or in the walls of the target room. The 14-Mev neutrons from the tritium target are not counted directly. On the other hand, the fluorine foil in the standard position is sensitive only to the 14-Mev source neutrons; any scattering reduces the neutron energy below the threshold for the $F^{19}(n, 2n)$ reaction. The iodine standard foil might also be used for this purpose, but not as conveniently, since the iodine foils had to be irradiated for several runs to accumulate sufficient activity for counting. The iron, phosphorus, and uranium (catcher) foils are sensitive to the inelastically scattered neutrons; they can be used only as secondary standards within a given blanket configuration. The final positions for the standard foils (positions S1 and S2 in Fig. 13) were not fixed until March 3, 1964. Earlier threshold-detector data are normalized to runs made after this date, by using a blanket position near the first surface. These normalizations are indicated in Appendix E.

b. Normalized Reaction Rates

The responses of the five different threshold detectors must be brought to the same basis to perform the spectral analyses described in Section VI. The basis chosen is that used by Impink in his calculations: 1 source neutron per square centimeter per second at the first surface of the blanket. The rate of a threshold reaction at this position, per unit threshold-detector nuclide, is just the reaction cross section in millibarns for 14.07-Mev neutrons. The reaction rate T_x in millibarns for a threshold reaction at position x within the blanket is found from A_{ox}:

$$T_x = \sigma_1 R_x^2 A_{ox}/R_1^2 A_{o1} = \sigma_s R_x^2 A_{ox}/R_s^2 A_{os} = \alpha_s R_x^2 A_{ox}, \tag{27}$$

where

$$\alpha_s = \sigma_s/R_s^2 A_{os}. \tag{28}$$

Here, R is the distance from the source to the position indicated, and σ is the reaction cross section at the appropriate neutron energy. The subscript 1 refers to parameters at the first surface of the blanket, and s refers to the standard positions. A_{os} is measured with the blanket assembly not in place. The experimental values of the reaction rate calibration factors α_s are listed in Table 8.

This method of computing the normalized reaction rates T has the advantage of requiring a knowledge of only the relative shapes of the cross section curves, which are usually known to about 5%. The absolute values of the cross sections at various energies are seldom known to better than 10-30%. Another advantage is that no absolute calibrations are needed for the neutron and foil counters.

Table 8. Summary of calibration runs.

	Standard Position	Flux Wheel	First Surface of Blanket
Date of run	March 24,1964	April 26, 1964	
Distance to neutron source(R)	19.1[a],18.7[b] cm	8.02 cm	13.65 cm
$R^2(cm^2)$	366[a],350[b]	64.32	186.1
G(between neutron path and path of deuteron beam)	42°	75°	90°
Rel. neutron intens. j(θ)	1.036	1.012	1.000
Neutron energy E (Mev)	14.57	14.25	14.07
Reaction cross section (mb)			
U-238(n,f)	1234.	1275.	1167.
P-31(n,p)Si-31	79.9	84.4	86.3
Fe-56(n,p)Mn-56	131.4	135.5	138.2
I-127(n,2n)I-126	1272.	1275.	1273.
F-19(n,2n)F-18			
Russian data	77.	70.	64.8
French data	58.	54.	51.
Activity A' (See Note c.)			
U (31.6-min)	.020 ± .002	.079 ± .007	
U (425-min)	.0156 ± .0016	.063 ± .006	
P	.233 ± .001	.982 ± .006	
Fe	.432 ± .002	1.88 ± .01	
I	.383 ± .014		
F	.111 ± .001	.422 ± .002	

Detector	$R_w^2 A'_w \sigma_s / R_s^2 A'_s \sigma_w$	React. Rate Calib. Factor α_s
U (31.6 min)	.72 ± .10	177.
U (425 min)	.70 ± .10	
P	.714 ± .007	1.015
Fe	.721 ± .007	.831
I		8.75
F (Russian data)	.72 ± .02	1.89
F (French data)	.70 ± .01	1.44

Notes: a. Values for position S1 in Fig. 13: used for Fe, I, F foils.

b. Values for position S2 in Fig. 13: used for U, P foils.

c. Phosphorus data corrected by F-factor (Table 7); otherwise numbers are the A' computed by the Frantic program. Standard deviations are those computed by the Frantic program; they include only counting errors.

5.8 CALIBRATION EXPERIMENTS

Two calibration runs were made to test the normalization procedures delineated above. On March 26, 1964, foils were irradiated in the standard positions with no blanket assembly in place. On April 24, foils were rotated about the neutron source on a flux wheel. The pertinent data for these runs are shown in Table 8.

At the time of these runs we were unaware of the effect of the presence of the blanket on the response of the BF_3 counter. With no blanket in place, the counter sees only neutrons scattered from the walls of the target room, so that the neutron flux seems to be low. On March 24, the tritium target was almost depleted, so the "low" fluxes were not surprising. On April 26, however, we had just installed a fresh tritium target. Disturbed by the apparently low neutron output, we increased the deuteron current to bring the neutron fluxes to "normal" levels. The resulting very high neutron fluxes produced large competing activities that decayed with long half-lives (possibly Na^{24}). Except for the iodine foils, the competing activities could be separated by the Frantic program. The half-life of I^{126} is too long for such separation, so the iodine data for this run were lost.

To compare the results of these two runs we compute the ratio

$$\xi = A'_w R_w^2 \sigma_s / R_s^2 A'_s \sigma_w, \tag{29}$$

where the subscript w refers to the flux wheel, and s refers to the standard positions. If all of the parameters entering into ξ are correct, $\xi = 1.0$. The values of ξ in Table 8 hover about 0.72, thereby indicating a systematic error in the measurement of at least one of the parameters (an error of 0.5 inch in the measurement of R_w, for example). The important point is that the experimental values of ξ are the same for all foils, within the standard deviations.

From this similarity the following conclusions may be drawn:

1. All of the factors necessary to compute the normalized reaction rate have been taken into account.

2. The slopes of the cross-section curves near 14 Mev are correct, as taken from various publications.

3. No great distinction can be made between the shapes of the French and Russian cross-section curves for the F^{19}(n, 2n) reaction, although it does appear that the French values are somewhat low.

The errors reported in Table 8 include only the counting errors computed by the Frantic programs. Actually, an additional 5% should be included to account for uncertainties in determining the shapes of the cross-section curves.

VI. ANALYSIS OF THRESHOLD DETECTOR DATA

6.1 INTRODUCTION

The determination of the differential neutron-energy spectrum $\phi(E)$ from N different threshold reactions involves the solution of N simultaneous integral equations:

$$T_j = \int \phi(E)\, \sigma_j(E)\, dE \qquad (j=1, 2, \ldots, N). \tag{30}$$

Here, T_j is the reaction rate per nuclide of the j^{th} threshold detector, and $\sigma_j(E)$ is the activation cross section. The range of all integrals in this discussion is from the lowest threshold energy to the maximum neutron energy to be expected in the experiment. Since the general solution of (30) is intractable, some assumptions must be made about the $\sigma_j(E)$ and the neutron-energy spectrum $\phi(E)$. Of the available methods[34] the method of Lanning and Brown[35] has been chosen for two reasons: it is relatively simple, and allows additional knowledge of the spectrum – in this case, calculations made by Impink – to be taken into account by means of a weight function w(E).

We shall describe the method, as well as the tests that were performed to provide a basis for interpreting the spectra calculated from the threshold-detector measurements in the experimental blanket assemblies.

6.2 METHOD OF LANNING AND BROWN

In this method the differential neutron spectrum $\phi(E)$ is expanded as a product of w(E) and a weighted sum of polynomials $p_i(E)$.

$$\phi(E) \doteq w(E) \sum_{i=1}^{N} a_i p_i(E). \tag{31}$$

The polynomials $p_i(E)$ (of degree i - 1) are chosen so that

$$\int p_i(E)\, p_j(E)\, w(E)\, dE = \delta_{ij}. \tag{32}$$

The $\sigma_j(E)$ are approximated as a Fourier expansion of the $p_i(E)$.

$$\sigma_j(E) \doteq \overline{\sigma}_j(E) = \sum_{i=1}^{N} \tau_{ji} p_i(E), \tag{33}$$

where

$$\tau_{ji} = \int p_i(E)\, \sigma_j(E)\, w(E)\, dE. \tag{34}$$

The method gives a least-squares fit to the cross-section data.

$$\int w(E)\,[\sigma_j(E)-\bar{\sigma}_j(E)]^2\,dE = \text{minimum.} \tag{35}$$

Since the set of polynomials is not complete, the $\sigma_j(E)$ can only be approximated. If we use these equations, the activation of the j^{th} foil is given by

$$T_j = \sum_{i=1}^{N} \tau_{ji} a_i. \tag{36}$$

Note that (36) may be conveniently used to calculate additional activation rates that are not used to determine the spectrum.

The equations (36) can be written in matrix form:

$$\vec{T}_j = [\tau_{ji}]\vec{a}_i. \tag{37}$$

If we define the inverse of the matrix $[\tau_{ji}]$ as $[\tau'_{ij}]$, then the calculation of all of the parameters that are necessary to determine $\phi(E)$ by Eq. 31 may be completed by computing the a_i from the equation

$$a_i = \sum_{j=1}^{N} \tau'_{ij} T_j, \qquad (i=1,\ldots,N). \tag{38}$$

If many sets of activation rates are to be used to compute the spectrum at various points in the blanket assembly, it is convenient to precalculate the τ_{ji} for all threshold reactions, once the weight function and the energy range have been chosen. When the reactions that are to be used to compute the a_i have been selected, the proper τ_{ji} may be used to precalculate the τ'_{ij}.

6.3 ERROR PROPAGATION

Since all of the equations above are linear, the uncertainties in the various parameters caused by uncertainties in the input activations may be computed directly. If we define δx as the standard deviation in x, it follows that

$$(\delta a_i)^2 = \sum_{j=1}^{N} (\tau'_{ij}\delta T_j)^2, \qquad (i=1,\ldots,N) \tag{39}$$

$$(\delta\phi(E))^2 = \sum_{i=1}^{N} (\delta a_i p_i(E))^2 \tag{40}$$

and

$$(\delta T_j)^2 = \sum_{i=1}^{N} (\tau_{ji}\delta a_i)^2. \tag{41}$$

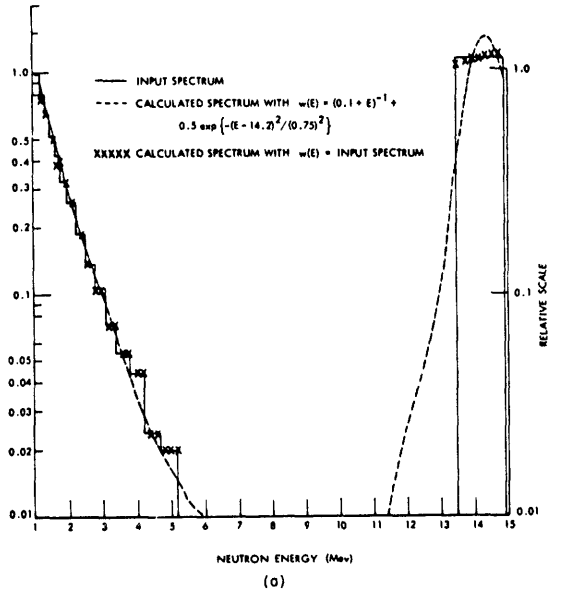

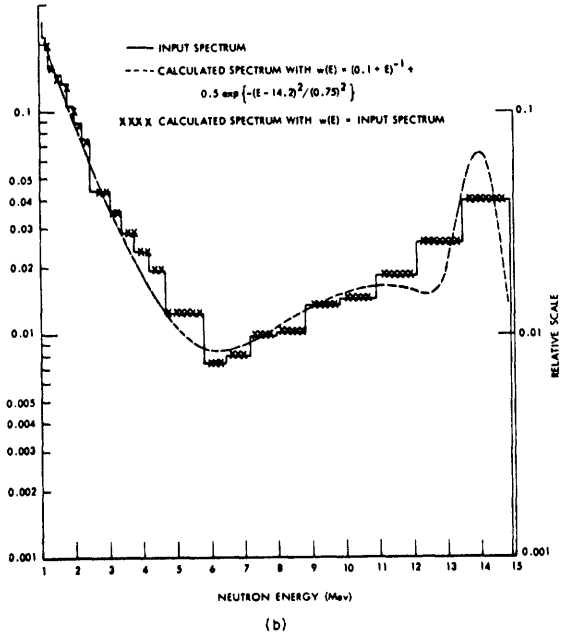

Fig. 24. Comparison of spectra calculated from Eq. 31 with input spectrum from Impink's codes. (a) Data from the first wall of the blanket. (b) Data from a point approximately 20 cm from the first wall.

Equation 41 is useful for determining uncertainties in the calculation of reaction rates that were not used to determine the spectrum.

6.4 PRELIMINARY TESTING

Computer programs were written to perform the computations described above. The use of these programs is discussed in Appendix D; the source-program listings are omitted from this report (see Preface).

The programs were tested[36] by using activities computed from spectra calculated by Impink.[37] Various aspects of the method of analysis were studied.

a. Weight Function

Since only five detectors are used, the spectrum that is computed from Eq. 31 is dependent on the function chosen for w(E). Two examples are shown in Fig. 24, in which the input spectrum is shown with two spectra computed from Eq. 31 with two sets of data. If the weight function w(E) is chosen to be the input spectrum, of course, the agreement is excellent. If a reasonable representation of the input spectrum is used, the fit of the calculated spectrum to the input spectrum is still good.

Figure 24 gives an example of such a weight function, which was computed from the equation

$$w(E) = c_1 + c_2(E+c_3)^{c_4} + c_5 \exp\left\{-(E-c_6)^2/c_7^2\right\}. \quad (42)$$

The values of the constants $c_1, \ldots, c_7$ were chosen somewhat arbitrarily: the fit of the calculated spectrum to the input spectrum is not too dependent upon the choice. Furthermore, the same w(E) gives a good fit to the data at the first wall (Fig. 24a), where the peak centered about 14.2 Mev predominates, as well as farther in the blanket (Fig. 24b) where this peak has been

attenuated, and the intervening energy regions have been filled by the moderated neutrons.

If an unreasonable weight function is used [w(E) = 1, for example], the computed spectrum still retains the general shape of the input spectrum, but oscillates about the origin in regions where the spectrum is small. The oscillations are a result of the limitations of the fourth-order polynomial, which must attempt to make up the difference between the input spectrum and the weight function. The retention of the general shape of the spectrum demonstrates that information from the activation data is not obscured by the weight function, and that the main features of the spectrum may be ascertained with even a poor guess for the weight function, although $\phi(E)$ may appear to be negative in some regions.

b. Orthonormalization Algorithm

The parameters in the orthogonal polynomials defined by Eq. 32 may be determined by several methods. Three algorithms were studied. While the results of the three algorithms should be the same, differences arise because of errors in the numerical integrations. The method which was finally chosen is as follows:

The $p_i(E)$ are written in the form

$$p_i(E) = B_i\left(1+b_{i2}E+b_{i3}E^2+\ldots+b_{ii}E^{i-1}\right). \tag{43}$$

Since E^{n-1} can be written as a linear combination of $p_i(E), \ldots, p_n(E)$, it can be seen from Eq. 32 that

$$\int E^{n-1}w(E)\left(1+b_{i2}E+\ldots+b_{ii}E^{i-1}\right)dE = 0, \qquad n < i. \tag{44}$$

If we define

$$S_j = \int E^{j-1}w(E)\,dE, \tag{45}$$

by successively setting $n = 1, 2, \ldots, i-1$ in (44), we obtain the following set of linear equations:

$$\begin{aligned}
&S_1 + b_{i2}S_2 + b_{i3}S_3 + \ldots + b_{ii}S_i = 0\\
&S_2 + b_{i2}S_3 + b_{i3}S_4 + \ldots + b_{ii}S_{i+1} = 0\\
&\cdots\cdots\cdots\cdots\cdots\cdots\cdots\cdots\cdots\\
&S_{i-1} + b_{i2}S_i + b_{i3}S_{i+1} + \ldots + b_{ii}S_{2i-2} = 0.
\end{aligned} \tag{46}$$

The equations (46) are solved for the b_{ij}. These coefficients, plus the normalization coefficients B_i are used in Eq. 38 to compute the $p_i(E)$. A test of the method showed that $\left|\int w(E)\,p_i(E)\,p_j(E)\,dE\right| < 10^{-3}$ for $i \neq j$, and that $\int w(E)\,p_j^2(E)\,dE = 1.000$.

The Gramm-Schmidt orthogonalization method[38] and an iterative method were also

tried, but the values of $\left| \int w(E)\, p_i(E)\, p_j(E)\, dE \right|$ $(i \neq j)$ were of the order of 0.7-0.99, so these methods were discarded.

In the iterative method, the $p_i(E)$ are written as follows:

$$p_i(E) = G_i[(E-H_i)\, p_{i-1}(E) - J_i p_{i-2}(E)], \tag{47}$$

where

$$H_i = \left[\int w(E)\{p_{i-1}(E)\}^2\, E\, dE \right] \Big/ \left[\int w(E)\{p_{i-1}(E)\}^2\, dE \right], \tag{48}$$

$$J_i = \left[\int w(E)\, p_{i-1}(E)\, p_{i-2}(E)\, E\, dE \right] \Big/ \left[\int w(E)\{p_{i-2}(E)\}^2\, dE \right], \tag{49}$$

and G_i is the normalization coefficient.

It was found that the values of $\phi(E)$ from Eq. 31 had little dependence on the orthogonality of the $p_i(E)$.

c. Effective Cross Sections

In the simplest type of threshold detector analysis[34] the cross section is approximated by a step function with an effective threshold energy, and an effective value of the cross section above this threshold. The strategem is equivalent to assigning an average value of the cross section for an assumed spectral shape (usually that of the fission spectrum). Here the range of integration is from the threshold energy to some maximum energy. The activation of the foils then is used with this effective cross section to determine the integral flux above the effective threshold energy. Comparison of the activation of several different detectors allows the construction of a histogram of the differential spectrum. Here the concept of an effective cross section is easy to recognize. The main objection to this method is that if the actual spectrum is much different from the assumed spectrum, serious errors can result.[35]

With the method of Lanning and Brown, the effective cross sections are those obtained from Eq. 33. These cross sections are plotted in Fig. 25 for two of the reactions: $U^{238}(n, f)$ and $I^{127}(n, 2n)$. It is found that the shape of the effective cross sections is dependent on the function chosen for $w(E)$ and on the orthogonality of the $p_i(E)$. For the $U^{238}(n, f)$ reaction Fig. 25 shows that a uniformly good fit to the experimental data is given by the effective cross section calculated with the Gaussian weight function (Eq. 42), which varies only an order of magnitude throughout the whole energy range. The effective cross section calculated with $w(E)$ equal to the first-wall input spectrum gives a better fit <4 Mev and >13 Mev by sacrificing a good fit in the region 4-13 Mev; but because $w(E)$ is small in this central region, the poor agreement between the experimental and effective cross sections is not important.

The effective cross sections for $I^{127}(n, 2n)$ shown in Fig. 25 are typical of reactions with higher threshold energies. There is some oscillation about zero below the

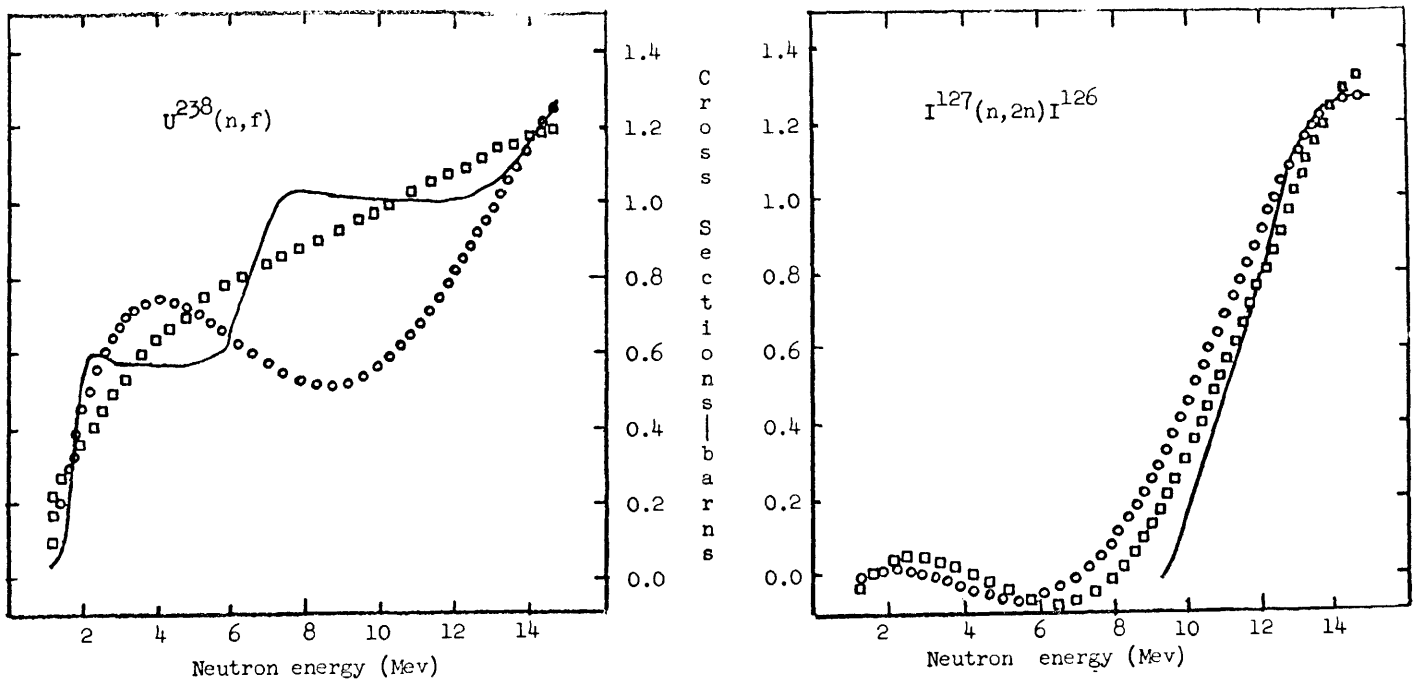

Fig. 25. Comparison of experimental cross sections for $U^{238}(n, f)$ and $I^{127}(n, 2n)I^{126}$ and those computed from Eq. 33. Solid curves represent experimental cross sections. Circles show the effective cross sections computed from Eq. 33 with w(E) = first-wall spectrum. Squares show the effective cross sections computed from Eq. 33 with $w(E) = (E+0.1)^{-1} + 0.5 \exp[-(E-14.2)^2/0.75^2]$.

threshold energy (9.5 Mev). The oscillations are less for the input-spectrum w(E) than for the Gaussian w(E) because in this region the input-spectrum w(E) takes on relatively larger values. Also, note the excellent fit >13 Mev for the input-spectrum w(E). Since the cross section for the $I^{127}(n, 2n)$ reaction is a smoother function of energy than that for the $U^{238}(n, f)$ reaction, the over-all fit is better for both weight functions.

The minimum of the left side of Eq. 35 occurs when the $p_i(E)$ are completely orthogonal. If the $p_i(E)$ are not orthogonal, the errors will be larger.

d. Uncertainties in Input Activities

In these calculations the false assumption is made that the T_j are known exactly. In a series of tests each of the T_j calculated from the input spectra shown in Fig. 24 were varied ±10% to determine the effect of these uncertainties on the calculated $\phi(E)$. The results of these tests are shown in Figs. 26-30. The weight function used in these runs is Eq. 42, with the c_j given in Fig. 24.

In all cases the sharp peak at 14.2 Mev is preserved. The presence of lower energy neutrons is still indicated, although their exact energies are uncertain. The T_j for the reactions with the highest and lowest threshold energies – $F^{19}(n, 2n)$ and $U^{238}(n, f)$, respectively – mainly distort the corresponding end of the spectrum. Uncertainties in the uranium activation destroy the shape of the spectrum below 2 Mev, since the $U^{238}(n, f)$ reaction is the only one that is sensitive to neutrons of these energies. The spectrum at 20 cm from the first wall (Fig. 24b) is a smoother function of energy; therefore, uncertainties in a single-threshold detector have much less effect on the shape of the calculated $\phi(E)$.

In evaluating the spectra calculated from the experimental threshold activations in the blanket assemblies the only curves considered are those of $\phi(E)$, $\phi(E) + \delta\phi(E)$, and $\phi(E) - \delta\phi(E)$. Roughly, the curves of $\phi(E) + \delta\phi(E)$ and $\phi(E) - \delta\phi(E)$ form an envelope of all the curves shown in Figs. 26-30.

e. Number of Foils.

When runs were made with an early version of the spectral analysis codes, we found that agreement between the calculated and input spectra did not improve, but became worse, as the number of foils for computing the spectrum was increased. Another investigator[39] obtained similar results. When the present version of the codes was completed, runs were made in which each of the δT_j was assumed to be 1 per cent. It was found that $\delta a_1/a_1 = 0.05$ if five foils were used to determine the spectrum, but that $\delta a_5/a_5$ ranged from 0.5 to 1.5, the value depending on the chosen w(E).

With two threshold reactions whose cross sections have similar shapes within the same energy range used, the errors are worse. The procedure implicitly involves differencing the cross sections, and the similar shapes result in small differences of large numbers, so that the effect of uncertainties in the cross sections are more acute.

Since analyses with up to 23 threshold detectors have been reported,[34] it should be

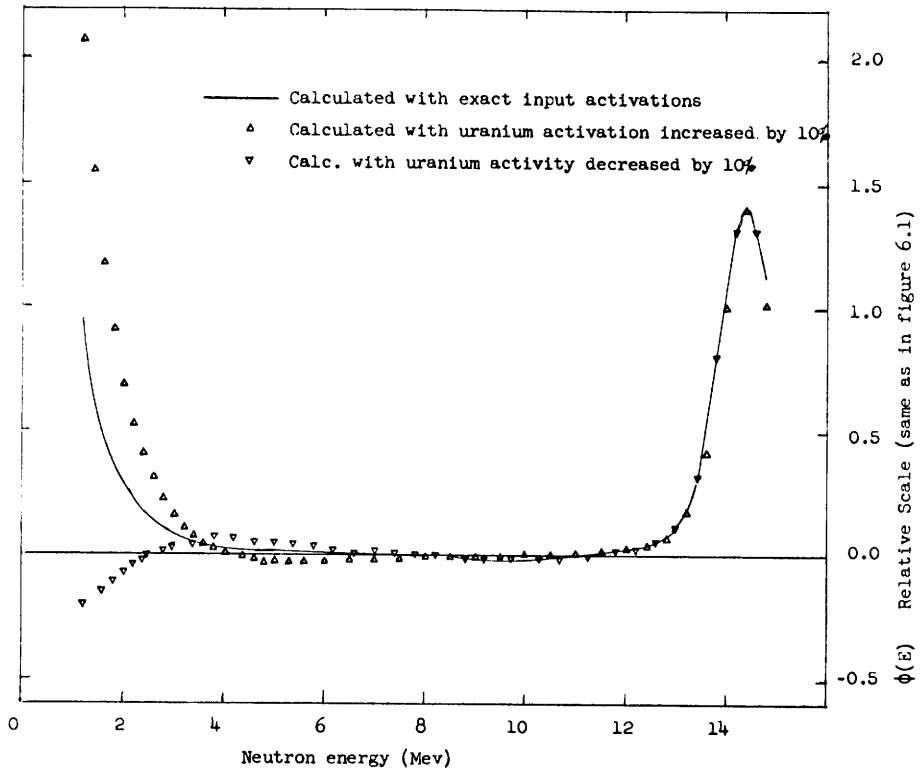

Fig. 26. Effect of 10% variation in uranium input activity. The exact input activities are the same as for Fig. 24a. The weight function is $w(E) = (0.1+E)^{-1} + 0.5 \exp[-(E-14.2)^2/0.75^2]$.

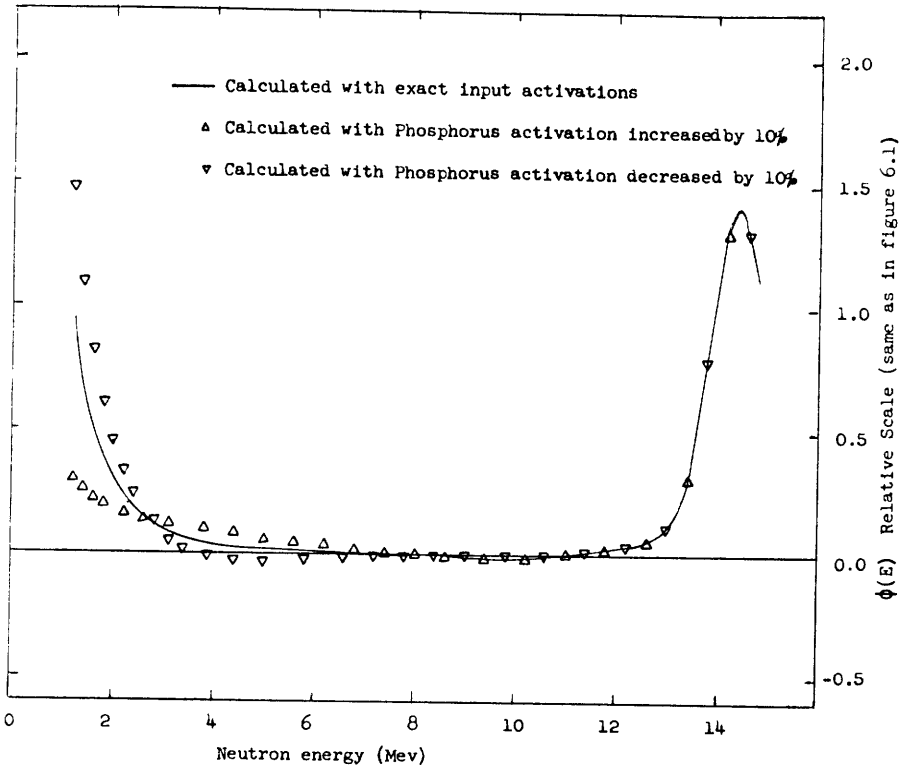

Fig. 27. Effect of 10% variation in phosphorus input activity. Input activities same as for Fig. 24a. Weight function same as for Fig. 26.

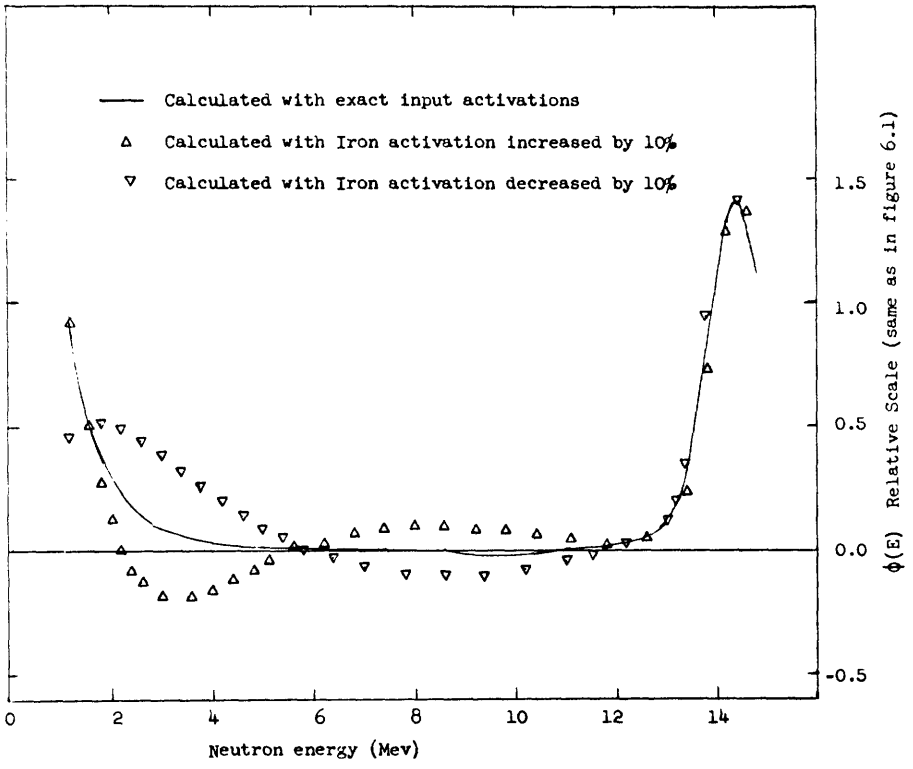

Fig. 28. Effect of 10% variation in iron input activity. Input activities and weight function same as for Fig. 26.

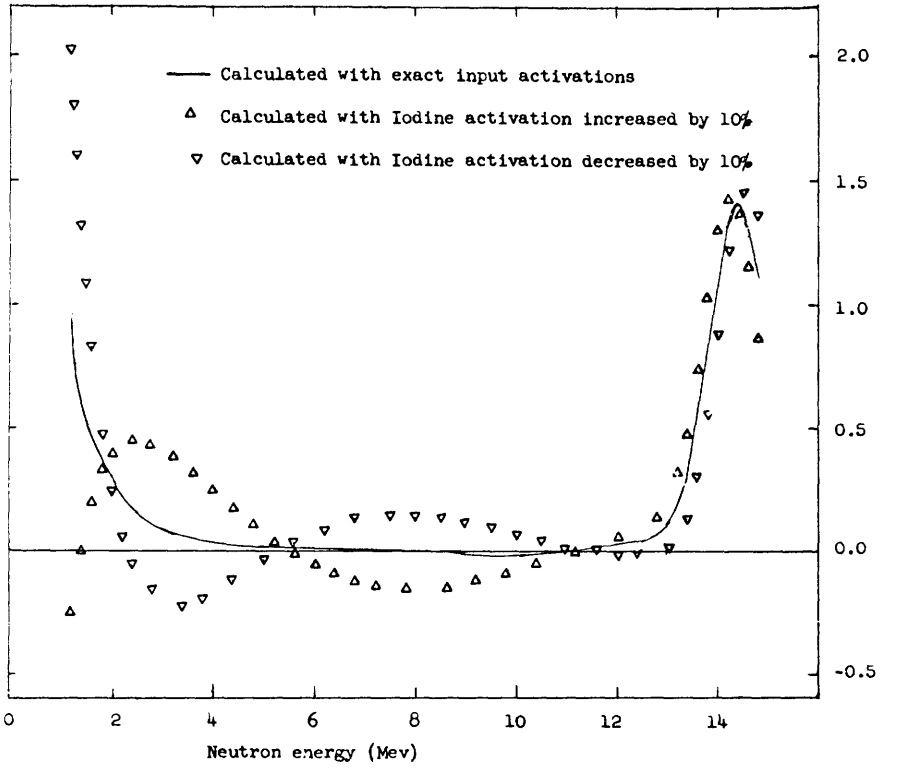

Fig. 29. Effect of 10% variation in iodine input activity. Input activities and weight function same as for Fig. 26.

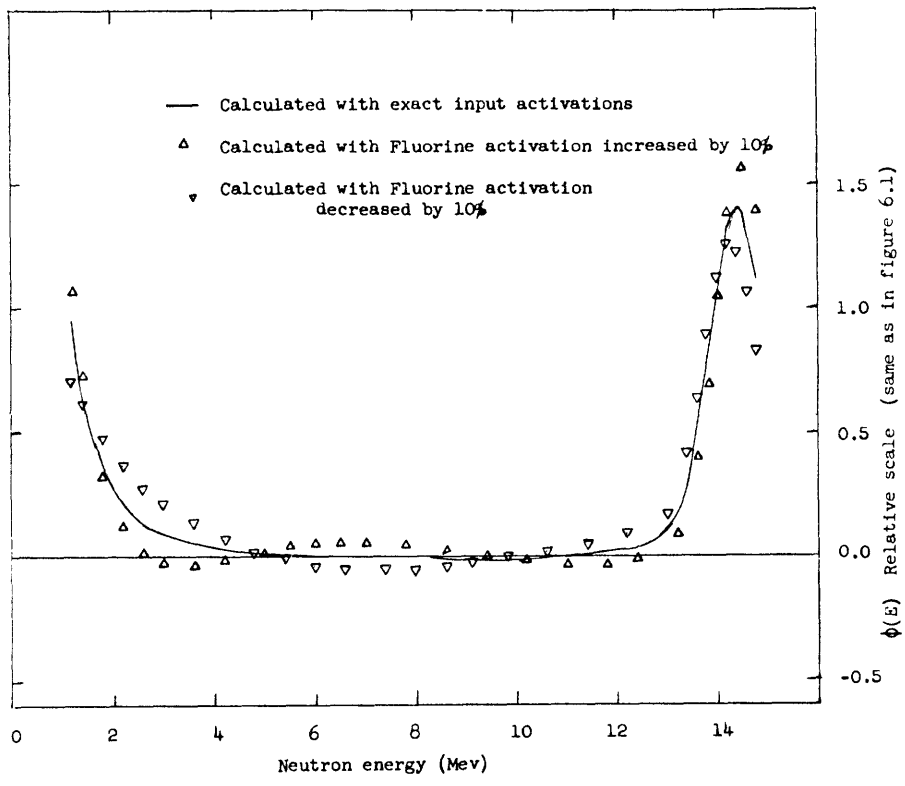

Fig. 30. Effect of 10% variation in fluorine input activity. Input activities and weight function same as for Fig. 26.

possible to overcome these difficulties by refinement of the numerical techniques. But, as the main restriction on the number of foils in our case is experimental rather than analytical, we feel that the machine codes as written are sufficient.

6.5 TESTS FOR GOODNESS OF FIT

The neutron spectrum in the experimental assemblies has not been determined analytically, so some empirical criteria had to be developed to determine how well the spectrum computed from Eq. 31 represents the actual spectrum in the assembly, and how successful we have been in finding the proper weight function.

Certainly an aesthetic criterion for goodness of fit is that the calculated spectrum be positive throughout the entire energy range. Because of limitations in this method, however, such a criterion cannot always be met.

Since the calculations are based on an integral method, information about $\phi(E)$ in the regions where it is small can be lost in uncertainties in either the calculations or the $\sigma_j(E)$ with $\phi(E)$ large. Therefore we feel that the fairest test of the method is its ability to reproduce rates of reactions which were not used to determine the spectrum. In performing the integration $\int \phi(E)\, \sigma_j(E)\, dE$ to determine these rates, errors in regions with $\phi(E)$ small are of less importance. In the preliminary runs[36] we found that the deviation between the rates obtained from the input spectrum, and those obtained from the

spectrum calculated with the Gaussian weight function, is approximately 1%. For calculations with the unit weight function the deviation is less than 30%. Recomputation of the reaction rates used to determine the spectrum merely involves re-inverting the matrix $[\tau'_{ij}]$; hence these rates are always reproduced exactly.

As the shape of w(E) approaches that of the actual spectrum, the contribution of the orthogonal polynomials diminishes. Thus the a_j decrease in magnitude with increasing j.

6.6 CONCLUSIONS

Four or five threshold detectors can be used with the method described above to obtain the general features of a neutron-energy spectrum, with only a rough guess as to its shape. Because of the rapid propagation of errors, the use of more than five detectors is not worth while unless the activities (and the reaction cross sections) are known with high precision. If additional information about the neutron spectrum is available, the method can furnish some of the fine structure of the spectrum. The comparison of calculated rates of reactions that were not used to determine the spectrum gives an estimate of how well the calculated spectrum represents the true spectrum.

VII. TRITIUM PRODUCTION MEASUREMENTS

7.1 INTRODUCTION

Since tritium production is a critical quantity in the design of a fusion reactor blanket, we hoped to measure the tritium produced by irradiating special samples of lithium-beryllium fluoride in the experimental blanket assemblies. An apparatus was designed and successfully tested with salt samples that were irradiated in the M. I. T. reactor. Since low tritium-production rates were expected in the blanket assemblies, only very small samples were used in the reactor irradiations. The impurities from the blanket in the larger samples were sufficient to quench the proportional counter that counted the tritium β^- decay, so that no data were obtained from the blanket. None of various schemes for removing the impurities seemed singularly promising, and an examination of all of them was considered to be beyond the scope of the present investigation. The design and operation of the apparatus, and the suggestions for removing the impurities are given below as a possible starting point for future work.

Because of the low tritium activities, and the general difficulties in counting the soft 16-kev β^- from the tritium decay, only two basic methods are available[40]: either the tritium must be intimately mixed with a liquid scintillator, or the tritium must be evolved as a gas, mixed with a counter gas, and counted in a windowless counter. The former method was rejected for three reasons: all known scintillators are organics and the lithium-beryllium fluoride dissolves only in a polar solvent; even if it were possible to dissolve salt samples in a scintillator, the fluorine would quench the counter; and any scheme for transferring the tritium to a suitable compound involves converting it into a relatively pure gas (T_2), and in such a state it might just as well be counted in a gas counter.

Since the same blocks of salt were used for several blanket configurations, special salt samples to be used for the tritium measurements were placed in the aluminum pans for each configuration. The tritium produced during accelerator irradiations by the $Li^6(n, \alpha)H^3$ and $Li^7(n, \alpha n)H^3$ reactions was trapped in the crystal lattice. That the tritium did not diffuse appreciably from the solid salt was demonstrated by the fact that salt samples which were counted almost a year after irradiation in the M. I. T. reactor showed almost the same activity per gram as samples that were counted shortly after irradiation.

7.2 APPARATUS FOR TRITIUM MEASUREMENTS

The basic components of the tritium-measuring apparatus, shown in Fig. 31, are a proportional counter, a furnace, and a glass Toepler pump.

The furnace, in which the samples of salt are melted to drive off the tritium is a copper tube, 1 inch OD and 30 inches long, heated at one end by a muffle furnace (manufactured by Hevi-Duty Electric Company, Watertown, Wisconsin). One end of the tube is brazed to a brass flange to which a removable end plate is sealed through an O-ring.

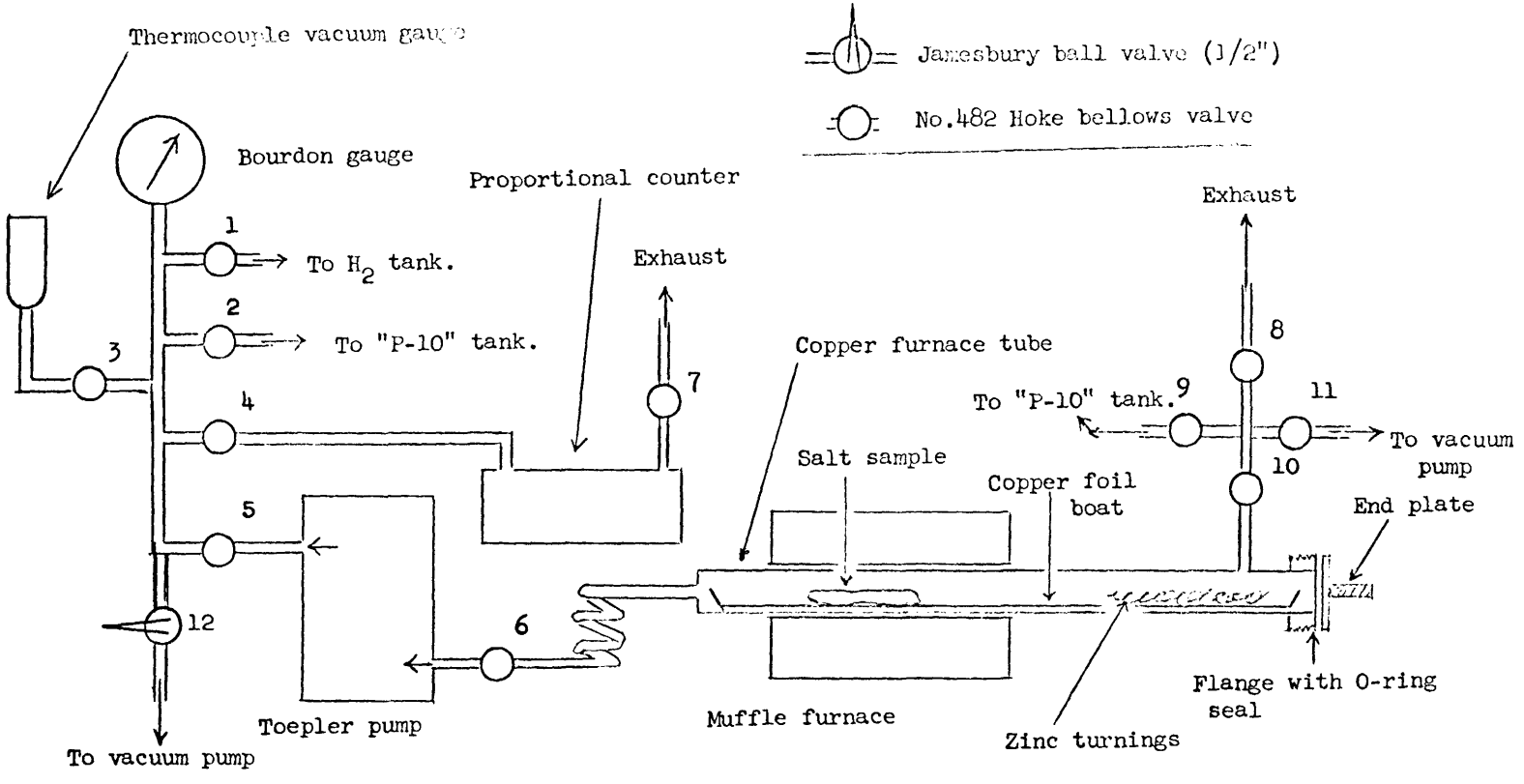

Fig. 31. Original system for measuring tritium production in samples of lithium-beryllium fluoride.

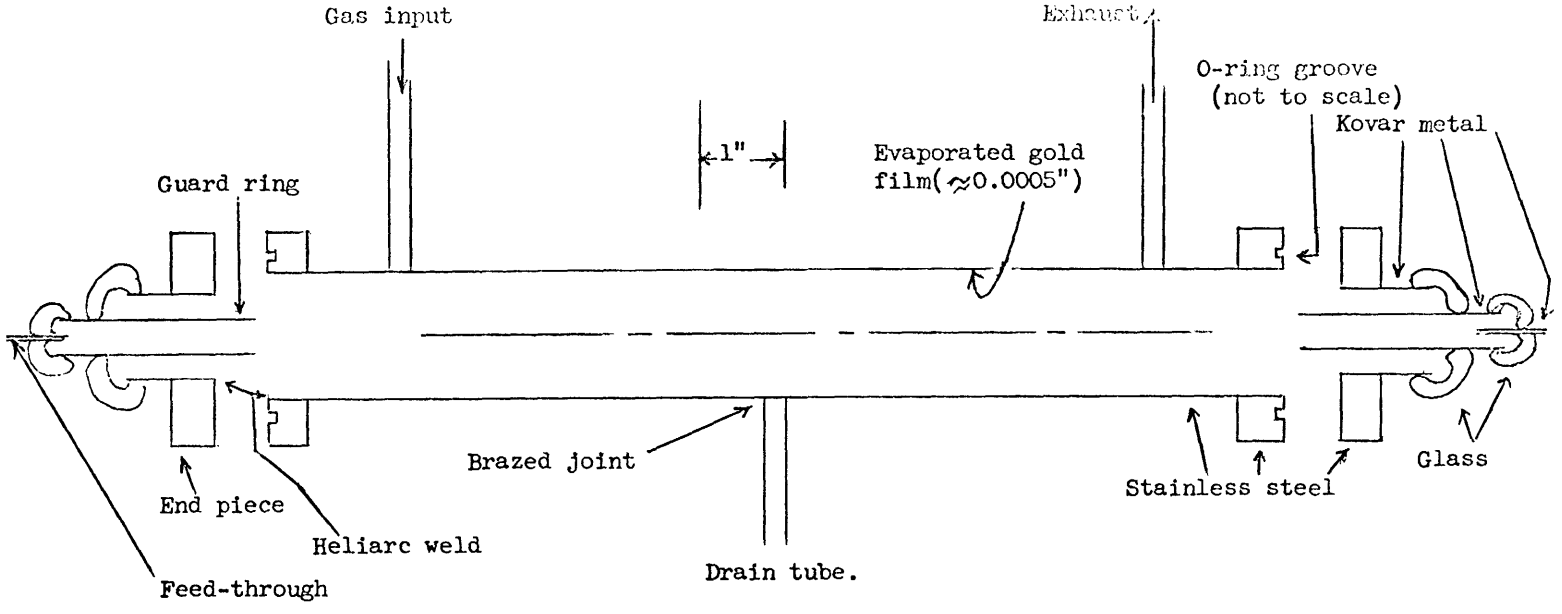

Fig. 32. Proportional counter. The center wire (0.002-inch nickel) is soft-soldered through the center of the feed-through in each end piece. The end pieces are held to the main body of the counter by stainless-steel bolts.

This end is placed approximately 18 inches from the muffle furnace to avoid overheating the O-ring. The other end is heliarc-welded to a plug into which a 2-ft length of 0.25-inch copper tubing was welded. The other end of the 0.25-inch tubing is connected by Swage-Lok fittings to a Hoke bellows valve (valve 6 in Fig. 31). The function of the 0.25-inch tubing is to provide thermal insulation to protect the teflon seat in the Hoke valve. Another valve (10) is brazed to the lateral surface of the flanged end of the copper-tube furnace. Copper is used in the construction because it is neither corroded nor wetted by the molten salt.

The proportional counter is shown in Fig. 32. The internal lateral surface is covered with an evaporated gold film to decrease tritium adsorption on the counter walls. The counter can be flushed in place with acetone to remove contamination from large activities. The signal from the counter is taken through a preamplifier to a scaler with a built-in amplifier. With the attached electronic equipment the counter has a plateau of 2875 volts; the scaled pulses have an amplitude of 5 volts (representing the maximum energy loss of an energetic electron passing through the counter). The average pulse height from tritium decay is approximately 2 volts. When cased in 2 inches of lead, the counter has a background of 200 cpm. The first tritium measurements were made with a 3-inch diameter counter that had a plateau of 2500 volts and a background of 300 cpm. This counter was discarded when a leak developed.

The glass Toepler pump is a standard model (manufactured by the Scientific Glass Apparatus Company, Inc., Bloomfield, New Jersey); details are given in Appendix C. Connections to the metal tubing are by glass-Kovar seals. All make-and-break connections are with 0.25-inch stainless-steel Swage-Lok fittings (manufactured by the Crawford Fitting Company, Cleveland, Ohio).

7.3 PROCEDURE FOR TRITIUM MEASUREMENTS

The following procedure was used to measure the tritium in the salt samples which were irradiated in the M.I.T. reactor.

1. A weighed amount of desiccated salt is placed in a copper-foil boat. Zinc turnings are added (to getter fluorine and oxygen), and the boat is inserted in the furnace tube. Note that the zinc is placed so that it is outside the section of the tube heated by the muffle furnace. The zinc must be hot, but must not melt, since the molten zinc attacks the copper (note that copper + zinc = brass).

2. After the furnace tube has been sealed and evacuated through valves 10 and 11 (see Fig. 31), the muffle furnace is heated to 500-600°C and held there 15-60 minutes. The actual values of time and temperature are not critical, provided the salt is completely melted.

3. During the heating cycle the proportional counter is filled with 1 atm of "P-10" gas (90% argon and 10% methane), and the background is measured. A Co^{60} source is placed next to the counter, and the rate is noted (~3500 cpm). The high voltage is then turned off, and the counter, Toepler pump, and connecting tubing are evacuated.

4. The muffle furnace is turned off, and the furnace is allowed to cool below 100°C.

5. Valves 4, 5, and 6, and by-pass valve on the Toepler pump (not shown in Fig. 31), are opened to connect the furnace tube with the previously evacuated system.

6. P-10 gas is admitted through valves 9 and 10 to bring the pressure of the whole system to 0.2 atm, as measured on the Bourdon gauge. Note that if the furnace is too hot, the methane in the P-10 gas is decomposed.

7. The by-pass valve on the Toepler pump is closed, and the pump is started to transfer the gas remaining in the furnace to the proportional counter.

8. When the first charge of gas has been transferred, the pressure of the high-pressure side of the Toepler pump should be at 0.5 atm. A second charge of gas is admitted through valves 9 and 10 and pumped to the counter.

9. After the second charge has been transferred, valve 5 is closed, and enough gas is admitted through valve 2 to bring the counter pressure to 1 atm.

10. Valve 4 is closed, and the gas in the counter is counted, first with the Co^{60} source in place, and then without. The count rate because of the Co^{60} source gives a measure of the sensitivity of the counter.

11. During the counting hydrogen is admitted to the rest of the system through valve 1, and swept through the furnace through valves 5, 6, and the Toepler-pump by-pass valve, and exhausted outside the building through valve 8.

12. After the counting is completed, hydrogen is swept through the counter through valve 7. Sweeping with hydrogen for 15-30 minutes was sufficient to remove all tritium contamination.

7.4 ATTEMPTS WITH BLANKET SAMPLES

The system was checked out with samples irradiated in the M. I. T. reactor, and it appeared that with care a reproducibility of at least 10% could be obtained. When the first blanket samples were run, however, the counting procedure in step 10 yielded a total count rate which was less than background, thereby indicating that the counter was being quenched by impurities. Since the most likely source of impurities was water which had been adsorbed by the salt, a dry ice and acetone cold trap was installed between valve 6 and the Toepler pump, and larger quantities of zinc were put into the furnace. So that the zinc could be allowed to melt, the furnace tube was redesigned, as shown in Fig. 33. Now the furnace tube, just a 30-inch length of 1-inch OD copper tubing with a welded end plug, was used for only one run. The first run after these modifications were made yielded a count rate which was 10 times the expected value, but these results could not be repeated: the quenching reappeared. A careful check showed that there were no leaks in the system. A second cold trap was added between valve 4 and the manifold to no avail.

A comparison of the conditions of the reactor and blanket irradiations is given in Table 9. Since such a small quantity of salt was used in the reactor samples, the effects of impurities was not noticeable. Furthermore, the salt samples used in the blanket

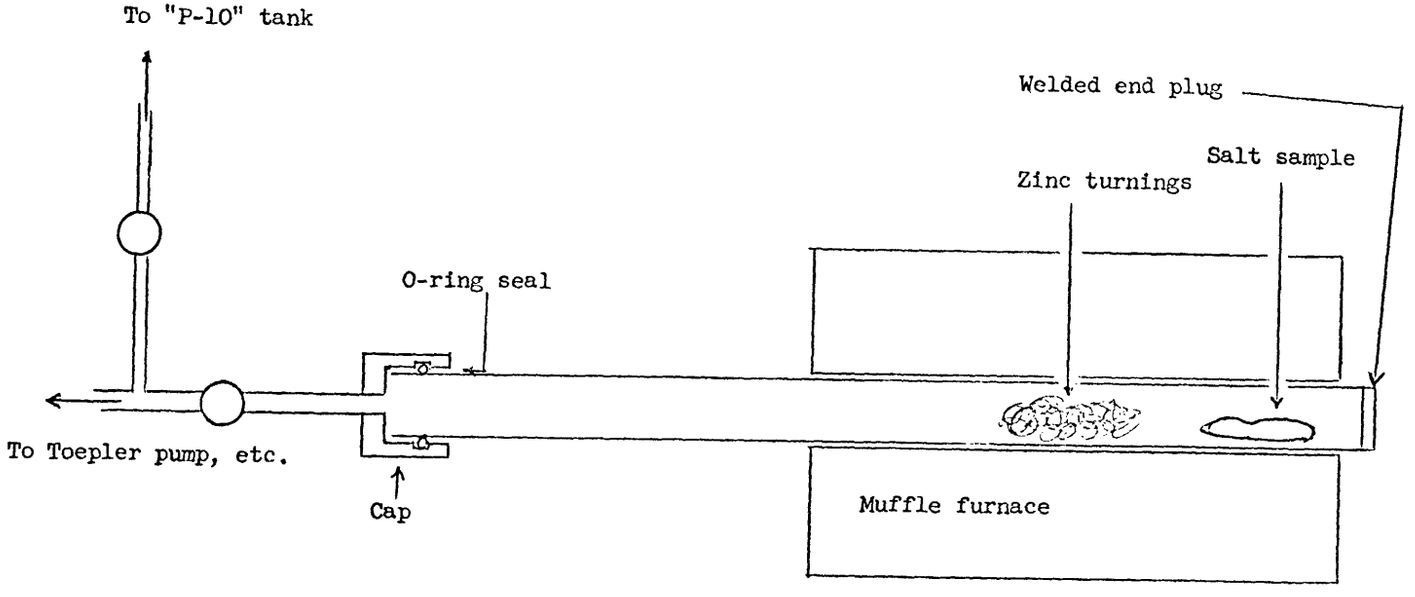

Fig. 33. Disposable furnace tube.

Table 9. Comparison of expected tritium activities from M. I. T. reactor and irradiations in experimental blanket assemblies.

Quantity	MIT Reactor	Blanket
Total neutron flux (n/cm^2sec)	8×10^9 (in "rabbit" at 2 kw power)	3.5×10^6 (at a point 15 cm from target with 4π-intensity of 10^{10} n/sec)
Irradiation time	1 minute	5 hours
Cross section for $Li^6(n,\alpha)H^3$ reaction	950 barns (thermal)	3 barns[a] (computed from Impink spectrum)
Sample weight	0.1 g	120 g
Expected count rate above background	300 cpm[b]	300 cpm

a. Since in the infinite blanket most of the neutrons are removed by the $Li^6(n,\alpha)H^3$ reaction, this number is almost independent of the blanket configuration. Where $\sigma(E)$ is high, the $\phi(E)$ is low, and visa versa.

b. Average experimental value.

irradiations appeared to be less pure than those used for the reactor irradiations. The exact nature of the impurities, and the reason for the one successful run are uncertain. The only explanation which is offered is that either the sample used for this run happened to be exceptionally pure or the activity that was counted included tritium held up in the Toepler pump and furnace from previous unsuccessful runs.

7.5 SUGGESTED REMEDIES

Further consideration of the problem, and consultation with others yielded an effervescence of possible solutions.

1. Magnesium, uranium, calcium, and other metals are better getters than zinc; however, some are more dangerous to handle.

2. So that the more efficient liquid-nitrogen cold traps could be used, pure argon could be used as the sweeping gas – with the required methane added directly to the counter. Liquid nitrogen cannot be used with P-10 gas, since liquid nitrogen condenses methane. This scheme would require a redevelopment of the counting techniques.

3. Especially purified salt samples could be prepared for irradiation. Since the

impurities are obviously volatile, purification could probably be accomplished by melting under a vacuum the samples to be irradiated, and sealing these samples in a polyethylene container during the irradiation. A dry-box would have to be designed for the packaging and unpackaging, to be sure that these operations are carried out in an inert atmosphere.

4. Since most of the background appeared to result from radiation originating outside the counter, surrounding the tritium counter with an outer counter, and using anticoincidence circuitry should reduce the background to approximately 1 cpm, effectively increasing the sensitivity of the counter to the point where perhaps smaller samples could be used.

5. Passing hydrogen through a palladium or nickel metal is a standard technique for purifying hydrogen, but the quantities of tritium involved are so small that it is doubtful whether such a technique could be used in this case. It might work if hydrogen were used as the sweeping gas; up to 50% hydrogen can be used in a proportional counter.[40]

6. With proper amplification of the output signal, the counter could be operated as an ionization chamber, and the effect of impurities would be much less.[40]

While it would not be too difficult to try any one of these schemes, none of them seemed particularly promising; and to reopen the whole examination of tritium-counting methods was considered to be beyond the scope of the present investigation. This discussion is offered as a starting point for future effort, since, in principle, the tritium produced in the blanket experiments is countable. Furthermore, irradiation times that are higher by a factor of 10 are inconvenient, but not impossible.

VIII. RESULTS OF THE THRESHOLD DETECTOR MEASUREMENTS

The results of the measurements made with the threshold detectors in the various experimental blanket assemblies are presented here, and general trends are outlined. Over-all conclusions will be drawn about these measurements following the discussion of the spectral analyses in Section IX.

Figures 35-40 show semi-logarithmic plots of R^2A_o versus R for traverses made along the axis z of the various assemblies. Here, R is the distance from the neutron source, A_o is the normalized activity defined by Eq. 25, and z is the distance along the axis of the blanket from the first surface (see Fig. 34). The composition of the blankets is indicated by the bars at the bottom of the figures.

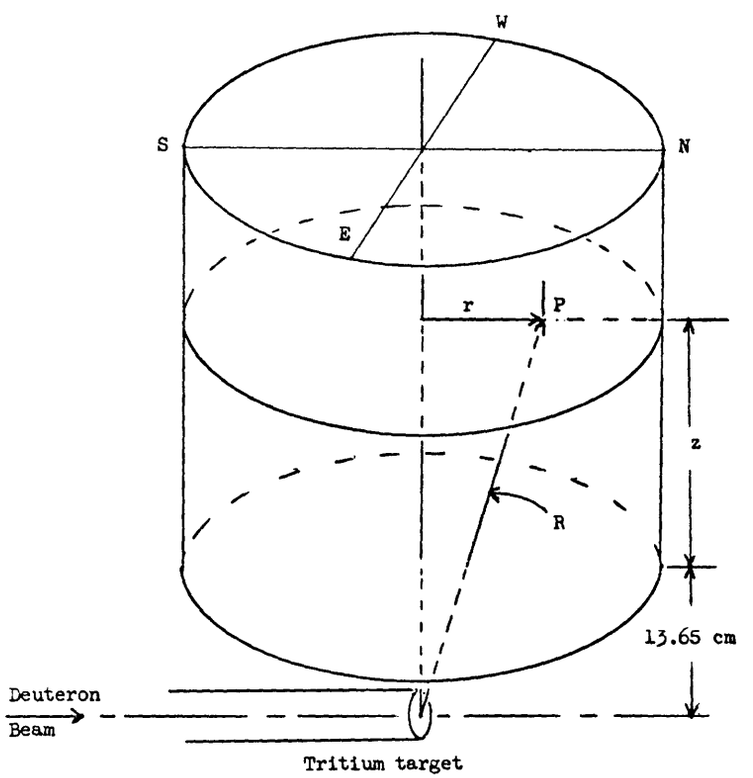

Fig. 34. Irradiation positions in experimental blanket assemblies. z = axial distance to point P. r = radial distance to point P.

For radial traverses in these assemblies the quantity $\ln\left(R^2A_o\right)$ is constant for points with $z \doteq 3$ cm. For larger z, $\ln\left(R^2A_o\right)$ tends to decrease linearly with R at approximately the same rate as the axial plot for the corresponding detector and blanket. The small asymmetries of the earlier radial traverses (before April 1964) are inconsistent, and are due, most likely, to variations in the positioning of the blanket assembly over the neutron source. The rest of this discussion will be

concerned with the axial traverses.

The size of the points generally indicates the standard deviations computed by the Frantic programs. The errors in the uranium data are approximately 30% for $z > 15$ cm.

The dates listed for the various points are those on which the foils were counted, and correspond to the dates in the data listings (omitted in this report). Except for the iodine

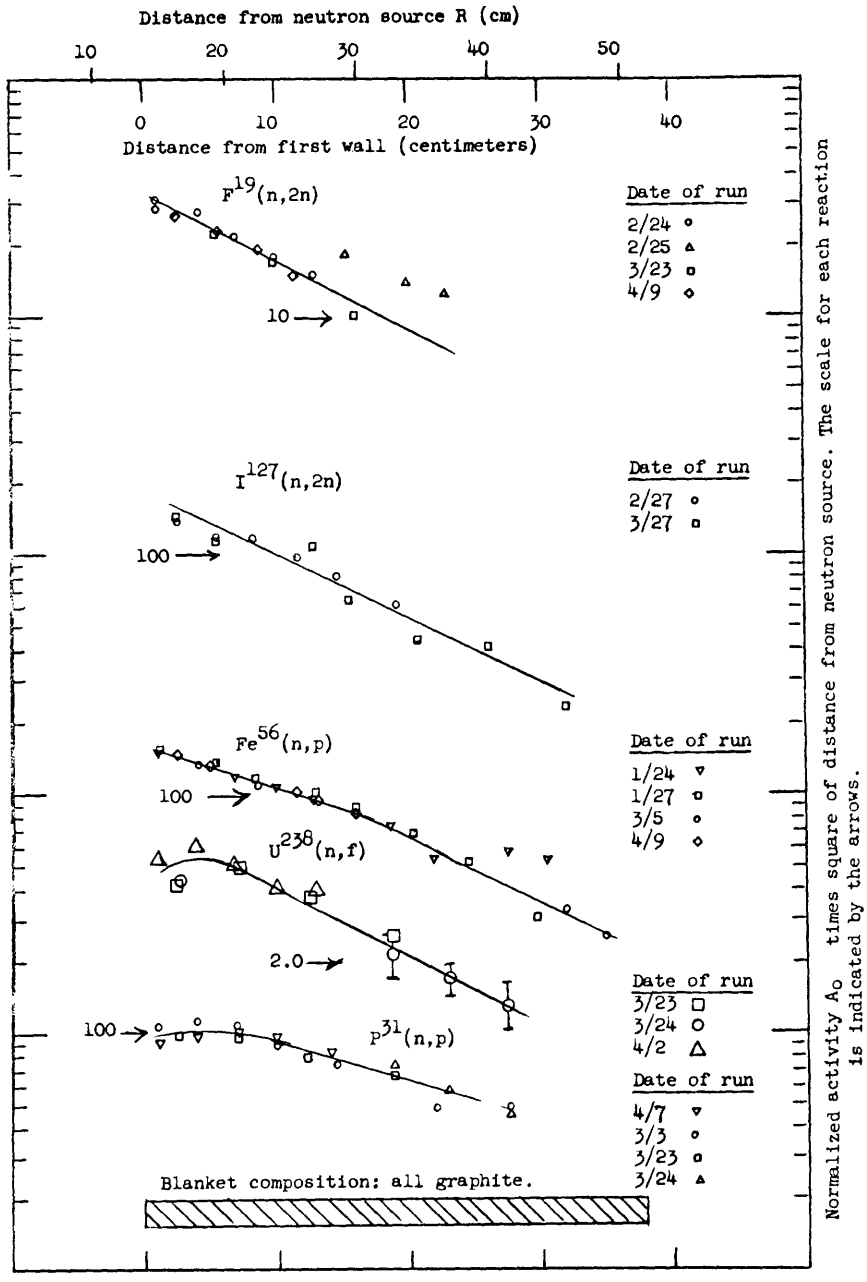

Fig. 35. Axial traverse with threshold detectors in the all-graphite blanket with no wall. Solid curves are visual fits to the data. (Blankets irradiated on April 2, 7, and 9 had aluminum plates between several of the graphite slabs.

foils these are also the dates of the accelerator runs. The iodine foils were usually irradiated in several accelerator runs; the dates of these runs are indicated by a code number for each foil in the iodine-counting runs.

Because of high uncertainties in the graphical procedures used to analyze some of the uranium data, these data have not been included in listings, although the axial points are included in the graphs.

8.1 ALL-GRAPHITE BLANKET, NO FIRST WALL (NOS. 1 AND 3 IN TABLE 3)

If the neutrons in the assemblies experience only attenuation,

$$A_o = \text{const.} \frac{e^{-R/\ell}}{R^2}, \tag{50}$$

where ℓ is the attenuation length. In the all-graphite blanket (Fig. 35) the relation (50) is true for the responses of the fluorine and iodine detectors, since any collision except a straight-ahead elastic scattering[41] reduces the energy of the neutron below the thresholds for the $F^{19}(n, 2n)$ and $I^{127}(n, 2n)$ reactions. The occurrence of forward scattering is indicated by the fact that from the fluorine and iodine curves ℓ = 16 cm, compared with 9.21 cm, the total mean-free path of the 14-Mev neutrons in graphite.[42] The data for the $Fe^{56}(n, p)$ reaction show slight curvature, indicating the contribution of inelastically scattered neutrons to the reaction rate. This curvature becomes successively more pronounced in the responses of the phosphorus and uranium detectors, whose thresholds are still lower.

Aluminum plates were inserted between the graphite slabs on several runs (March 11, April 2, 7, 9). Within the accuracies of the measurements, the presence of the aluminum had no effect on the detector responses. Some of these data are included in Fig. 35.

Repetition of measurements at several points within the blanket showed that the responses of the detectors were generally reproducible within the standard deviations computed by the Frantic programs. In a few cases all numbers for a given run were off by a constant factor, but were internally consistent. The difference could be attributed to the failure to properly position the neutron counter before the run. In these cases the data for the run were normalized to a convenient point for another run.

8.2 ALL-GRAPHITE BLANKET, 3-CM MOLYBDENUM WALL (NO. 2 IN TABLE 3)

The addition of 3 cm of molybdenum (actually 1.125 inches) to the first wall of the graphite blanket depresses the threshold detector responses approximately 20%, except for those of the $U^{238}(n, f)$ reaction (Fig. 36). Within the scatter of the points the responses of the uranium detectors remain the same, or increase slightly, thereby indicating the production of low-energy neutrons at the expense of the 14-Mev neutrons. The over-all shapes of the curves are generally unchanged.

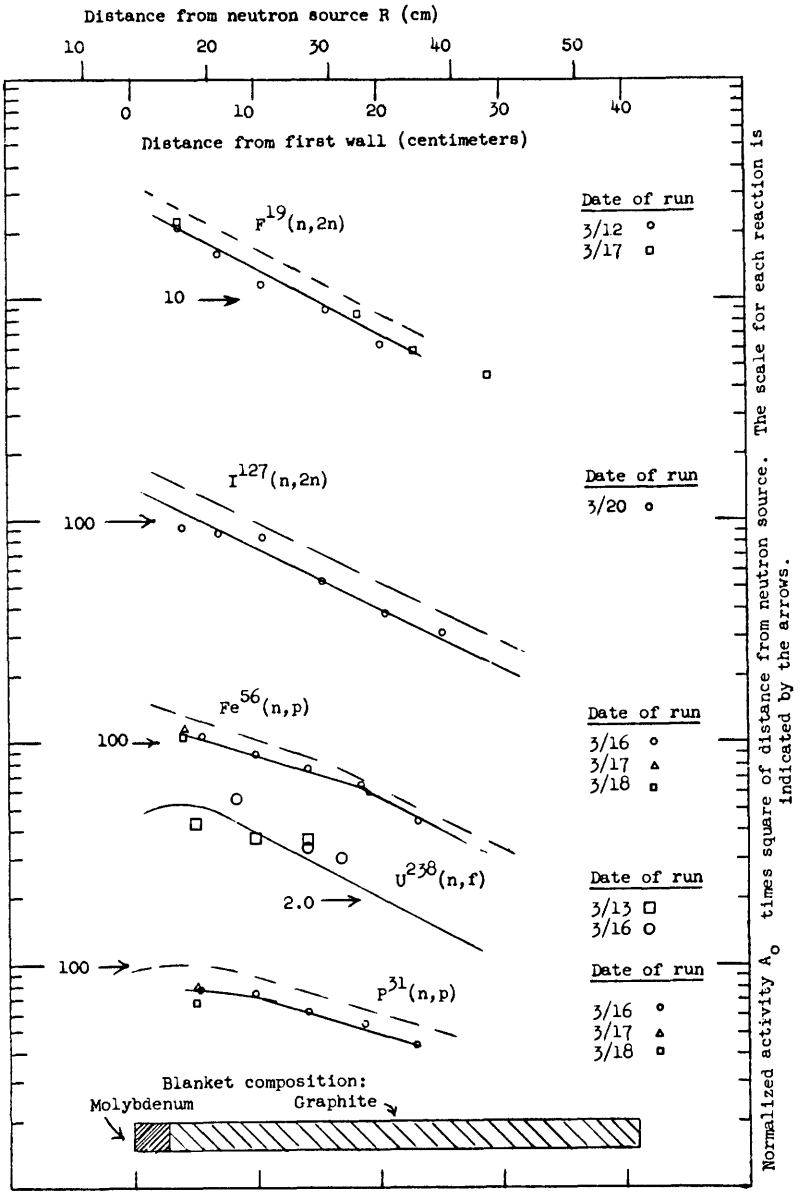

Fig. 36. Axial traverse with threshold detectors in the all-graphite blanket with 3-cm molybdenum wall. Solid curves are visual fits to the data. Dashed curves are visual fits to the data for the all-graphite blanket with no wall (Fig. 35). The solid and dashed curves for the $U^{238}(n,f)$ reaction coincide.

8.3 BLANKETS WITH LITHIUM-BERYLLIUM FLUORIDE SALT (NOS. 4-7 IN TABLE 3)

The absence of any general trend as the thickness of the molybdenum wall is increased (Figs. 37-39), or as the salt-to-graphite ratio is changed (Fig. 40), is not surprising for three reasons:

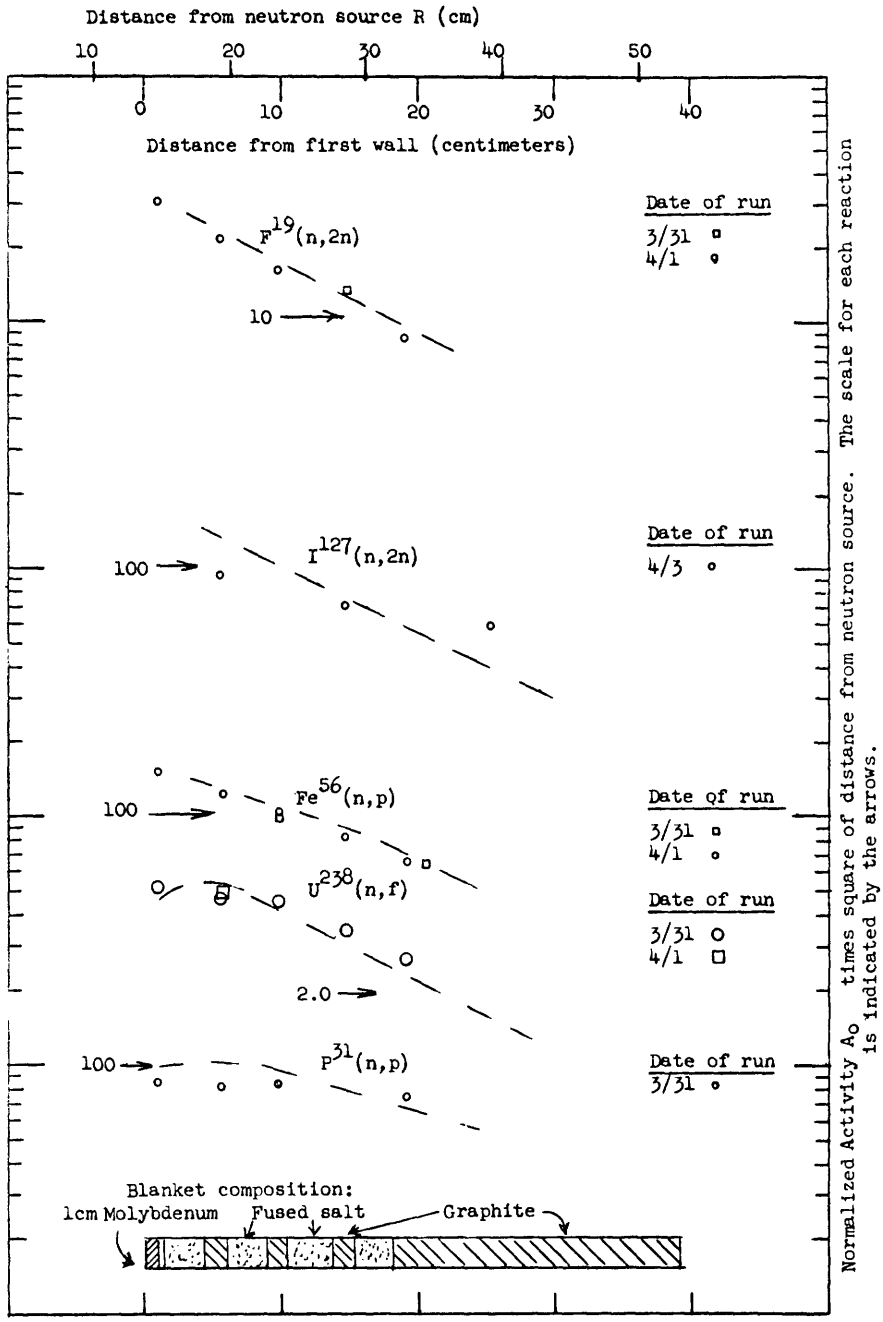

Fig. 37. Axial traverse with threshold detectors in the 33% graphite, 67% salt blanket with 1-cm molybdenum wall. Dashed curves are visual fits to the all-graphite blanket data.

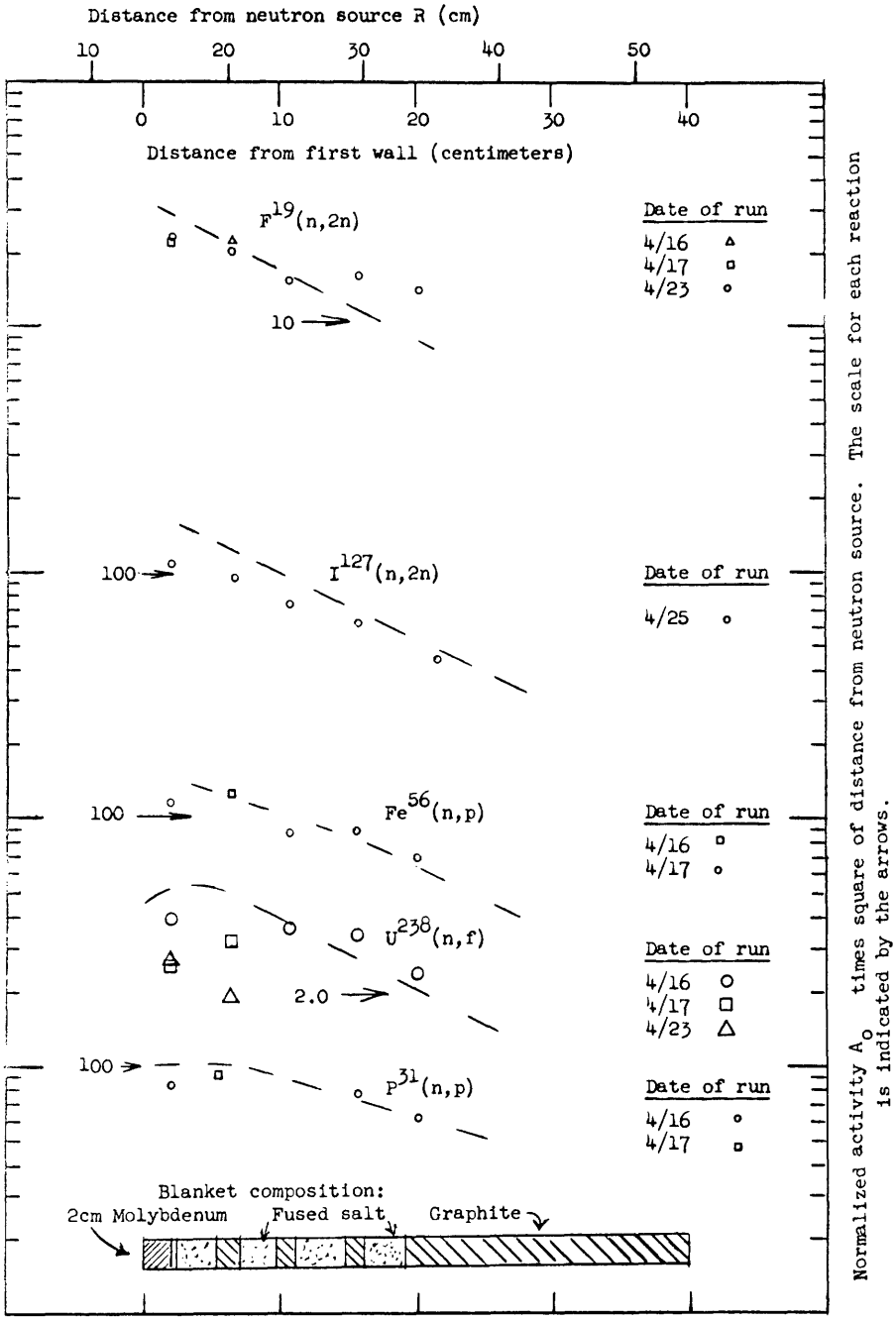

Fig. 38. Axial traverse with threshold detectors in the 33% graphite, 67% salt blanket with 2-cm molybdenum wall. Dashed curves are visual fits to the all-graphite blanket data.

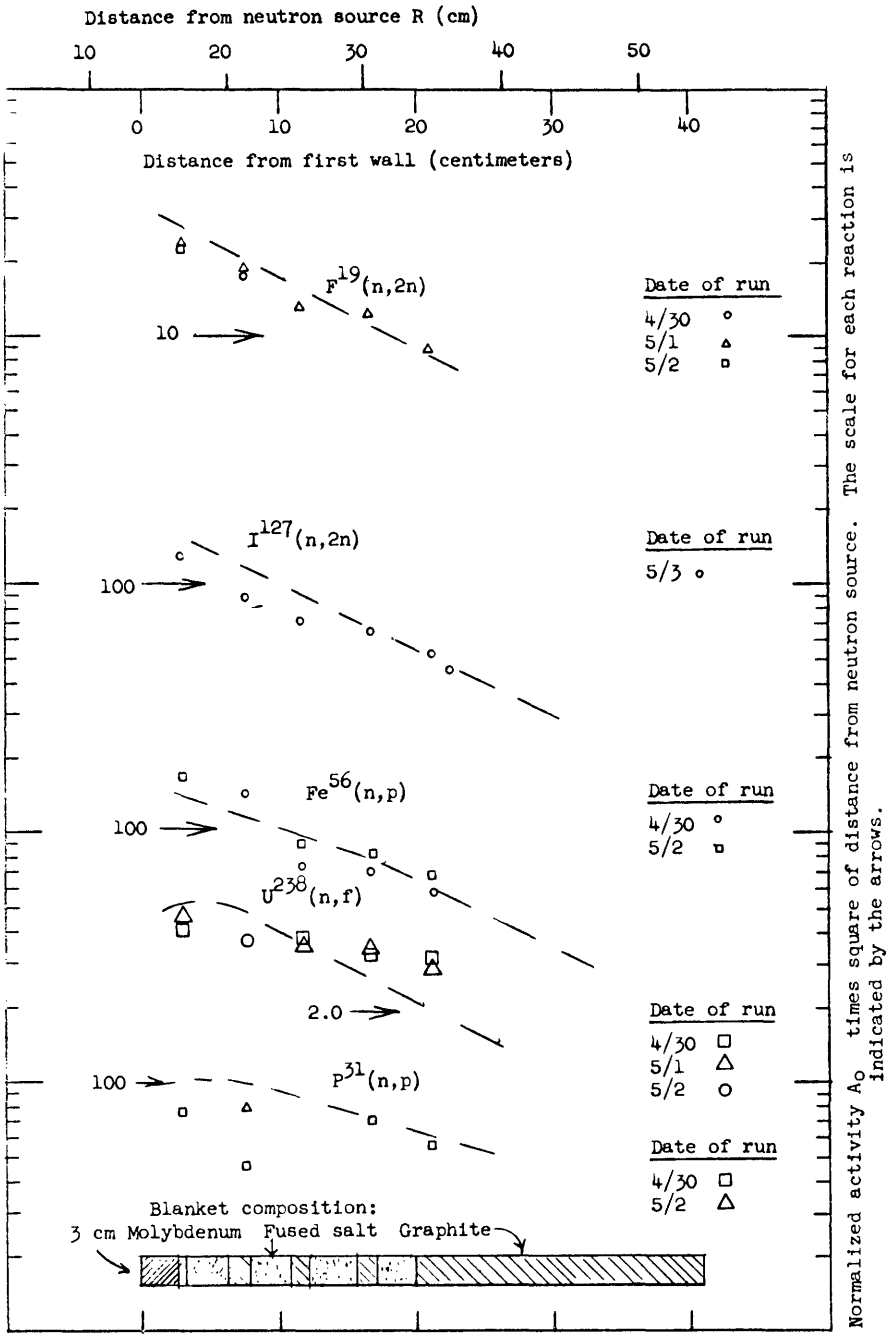

Fig. 39. Axial traverse with threshold detectors in the 33% graphite, 67% salt blanket with 3-cm molybdenum wall. Dashed curves are visual fits to the all-graphite blanket data.

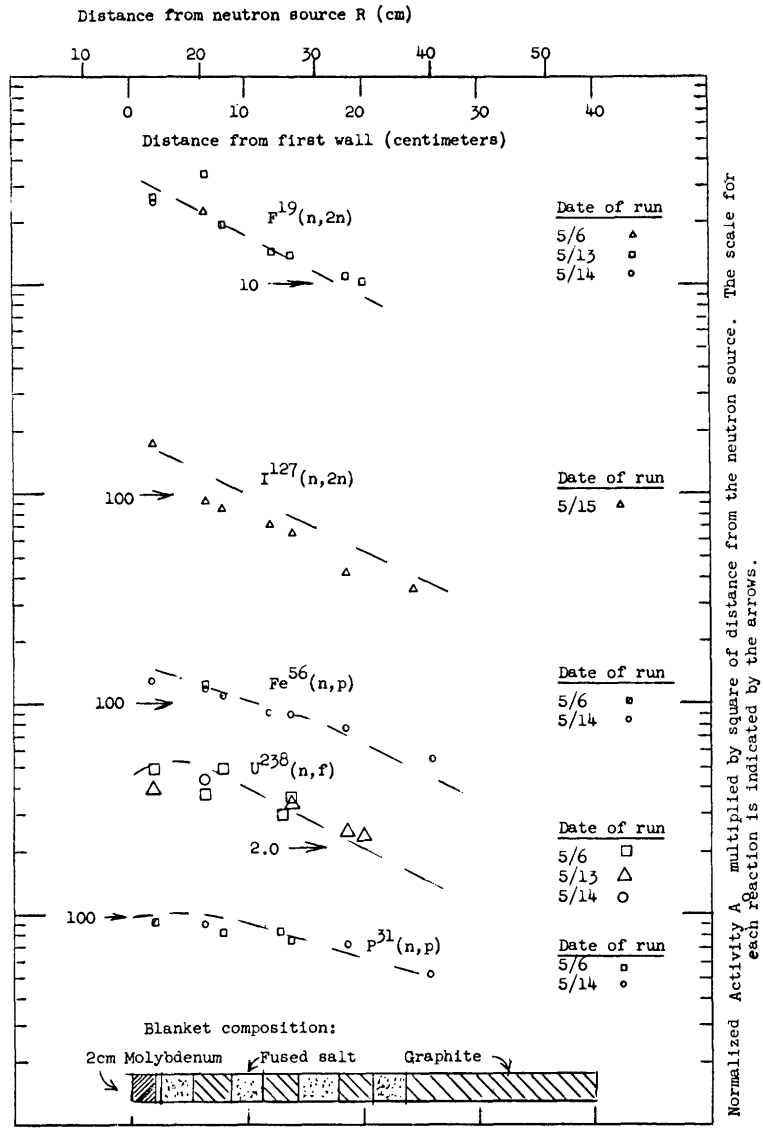

Fig. 40. Axial traverse with threshold detectors in 50% graphite, 50% salt blanket with 2-cm molybdenum wall. Dashed curves are visual fits to the all-graphite blanket data.

1. The scattering properties of the salt and the graphite are almost the same. In calculations[43] the main difference is that the salt removes neutrons through the $Li^6(n,t)$ reaction. The lithium in the salt used for these experiments contains only 1-3% Li^6 compared with 7.42% Li^6 in natural lithium (used for the calculations).

2. A rough calculation for a point source of thermal neutrons show that 99% would leak out of a graphite cylinder of the same size as the experimental assembly.[42] Since the leakage for 14-Mev neutrons is worse, very few neutrons are absorbed in any reaction in the assembly.

3. The salt wedges are not as smooth as those shown in Fig. 4. One third of the wedges were cracked in shipping; the lateral surfaces of the others were rough, and did not fit together very well. (Originally we planned to insert special samples along the radii between the wedges for tritium measurements, so a good fit was not considered necessary when the salt was being cast.) The pea-sized salt samples in the central void could not be tightly packed. Because of the toxicity of beryllium-fluoride dust, smaller samples could not be handled safely. A solid salt cylinder in the central void would have been more desirable.

Because of these conditions it was never certain just how much salt was in the pans at points where threshold-detector measurements were made in a given run. For example, it is felt that the responses of the fluorine detector in Fig. 37 for $z > 15$ cm are too high.

The salt is hygroscopic; for the tritium measurements the salt had to be kept dry. (Also, we were uncertain about the effects of the presence of moisture on the neutronic properties of the salt.) It was thus necessary to have half of the salt drying in plastic bags filled with calcium chloride, while the other half was being used in the assemblies – leaving insufficient salt to build a full-sized cylinder. We took advantage of the similarity in the properties of the salt and the graphite, and in the high neutron-leakage rates. The source intensities were too low to allow threshold detector measurements to be made for $z > 20$ cm, so the upper half of the salt assemblies are all graphite (as shown in the bars at the bottom of the figures) to maintain a constant geometry.

Further discussion will be given in Section IX after the presentation of the spectral analyses.

IX. RESULTS OF SPECTRAL ANALYSES

9.1 PRELIMINARY REMARK

Visual fits were made to the threshold detector responses shown in Figs. 35-40, and the normalized reaction rates T (in millibarns) were calculated from these curves, with the use of Eq. 27. The standard deviations δT were estimated from the scatter of the points.

a. Weight Functions

The differential neutron spectra $\phi(E)$ were calculated by the method outlined in Section VI, by using the SPECTRUM programs described in Appendix B with several types of weight functions w(E). Two weight functions are discussed here: the "Impink" weight function

$$w_I(E) = 0.5(E-1)^{-1} + 0.5\, e^{-(E-13.3)^2/(0.65)^2} \qquad (E>1 \text{ Mev}), \tag{51}$$

and the "Gaussian" weight function

$$w_G(E) = 0.05 + 0.5\, e^{-(E-5.5)^2/4} + 0.5\, e^{-(E-13.3)^2/(0.65)^2}, \tag{52}$$

where E is the neutron energy in Mev. Because of the large δT, a concerted effort to guess a theoretically correct, or aesthetically pleasing, weight function was not considered to be worth while. These weight functions are merely rough guesses about the shape of the spectra; they are sufficient for comparisons among various data sets. A theoretical treatment of the experiment, with a Monte Carlo calculation used, will give a better w(E).[44]

b. Energy Range

The $\phi(E)$ have been calculated between 2.1 Mev and 14.1 Mev. The upper limit represents the maximum energy of the source neutrons (to the nearest 0.1 Mev). The lower limit was chosen to be 2.1 Mev instead of the $U^{238}(n, f)$ threshold because early calculations indicated that there were few neutrons below 2 Mev, and the small values of the $U^{238}(n, f)$ cross section in this region are implicitly divided into the response of the uranium detectors, thereby accentuating the large errors already present in the $U^{238}(n, f)$ reaction rate.

c. Fluorine Cross Sections

Because of the large δT, four foils gave just as good or better results than did five. The activity of the fifth foil was calculated with the use of Eq. 36 and compared with the experimental value as a check on the applicability of the method of analysis. When the fluorine reaction rate was omitted from the analysis, the calculated and experimental

values of the fluorine reaction rate were in better agreement when the Russian[27] values of the cross sections were used than they were with the French[26] values. Therefore the Russian values were used in all subsequent runs.

9.2 SPECTRA IN THE GRAPHITE BLANKETS

The calculated spectrum $\phi(E)$ at the point $z = 5$ cm in the graphite blanket with no first wall is shown in Fig. 41a. The weight function is that of Eq. 51. The scale for $\phi(E)$ is the same as in Fig. 24: n/cm^2 sec per Mev for an incident neutron current at the first wall of 1 n/cm^2 sec. The prominent features of the curve are a sharp peak at approximately 13.3 Mev, and a smaller, broader peak centered near 3 Mev (the energy of neutrons scattered inelastically from 14 Mev in the forward direction by the 9.61-Mev level in carbon). The height of the peak at 13.3 Mev is within the range calculated by Impink (see Fig. 24). Roughly speaking, the neutrons enter the assembly at 14 Mev, experience one inelastic scattering to 3 Mev, and leave with little further moderation.

Figure 41b shows that farther into the assembly (z=20 cm) the high-energy peak is attenuated, but the spectrum at lower energies is approximately the same. The apparent shift in the low-energy peak is not significant, because of the large $\delta\phi(E)$.

The molybdenum first wall attenuates the high-energy peak (see Fig. 42a, $z = 5$ cm), and the average energy of the low-energy peak is reduced. The values of $\phi(E)$ at 3 Mev are the same for Figs. 41a and 42a, thereby indicating that the molybdenum contributes the lower energy neutrons by the (n, 2n) reaction. Farther into the assembly (see Fig. 42b, for $z = 20$ cm) the high-energy peak is again attenuated and the rest of the spectrum is essentially unchanged.

The negative $\phi(E)$ for $E < 2.5$ Mev in Fig. 41 are caused in part by the fact that $w_I(E)$ is large at energies for which $\phi(E)$ is small. The Gaussian weight function $w_G(E)$ (Eq. 52) was chosen to approximate the $\phi(E)$ in Fig. 41a. Figure 43a indicates that this choice is at least partially successful, in that at least $\phi + \delta\phi \geq 0$ almost everywhere. Adding the molybdenum wall (see Fig. 43b) still reduces the average energy of the low-energy peak. Since the center of the low-energy peak in $w_G(E)$ is too high (5.5 Mev), negative $\phi(E)$ result at energies >3 Mev. The corresponding curves for $z = 20$ cm look like those at $z = 5$ cm: the high-energy peaks are attenuated, while the low-energy portions of the spectra remain the same, but with sharper negative dips at approximately 7 Mev.

The negative $\phi(E)$ are due partially to inconsistencies in the activation data. From the errors indicated in Figs. 35 and 36, and the results of such errors in the preliminary analyses (see Figs. 26-30), negative $\phi(E)$ from this cause are not surprising.

The spectral analyses in the graphite blankets are summarized in Table 10, giving the experimental values of T, the computed values of T when that foil was omitted from the determination of $\phi(E)$, and the calculated values of the $Li^7(n, tn)$ reaction rate (for comparison purposes). The plots of $\phi(E)$ are evaluated as "excellent," "good," "fair," and "poor." The criteria for these evaluations are stated in notes to the table. Note

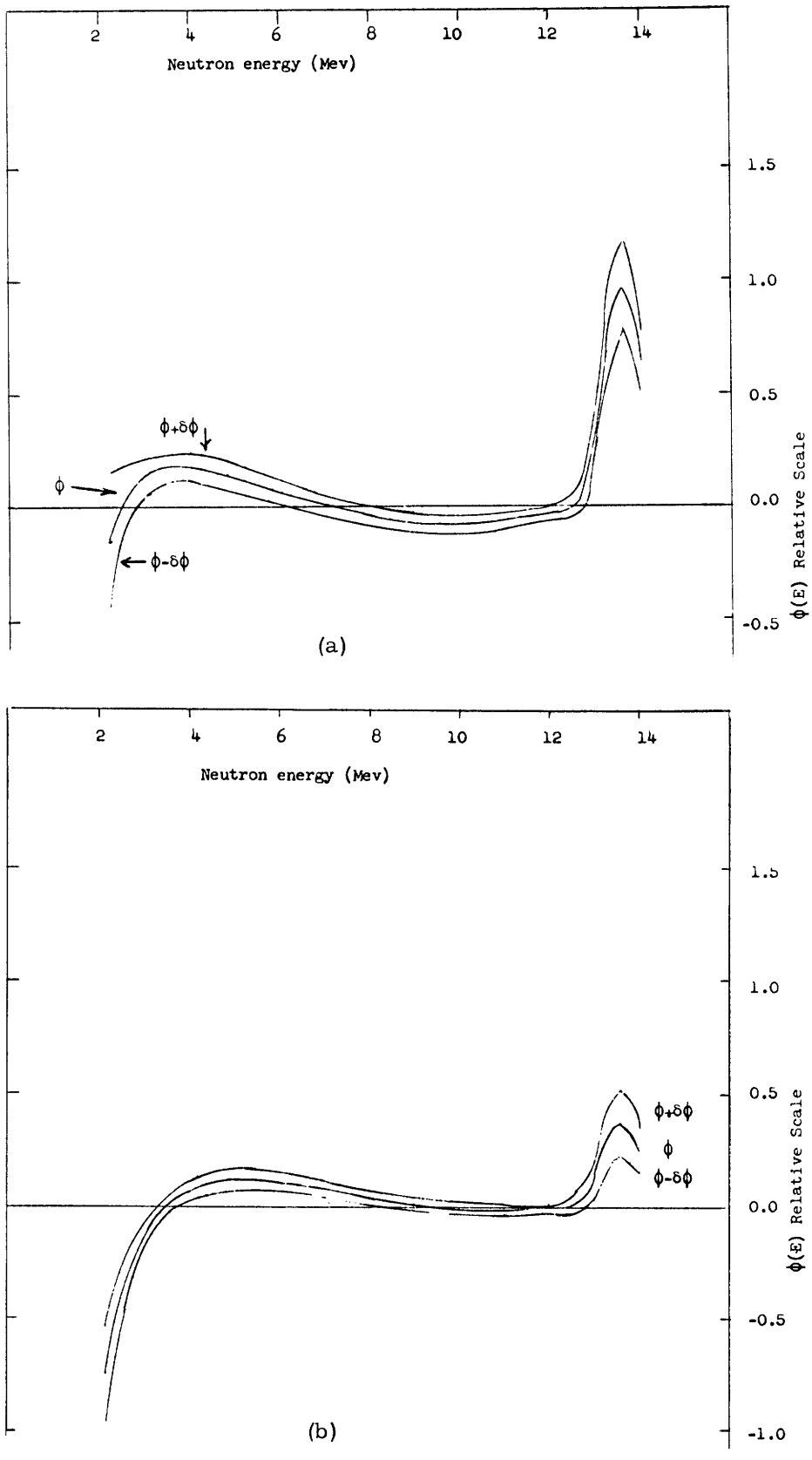

Fig. 41.

(a) Calculated spectrum in graphite blanket with no first wall at 5 cm from first surface. (Eq. 51 used for w(E).)

(b) Calculated spectrum in graphite blanket with no first wall at 20 cm from first surface. (Eq. 51 used for w(E).)

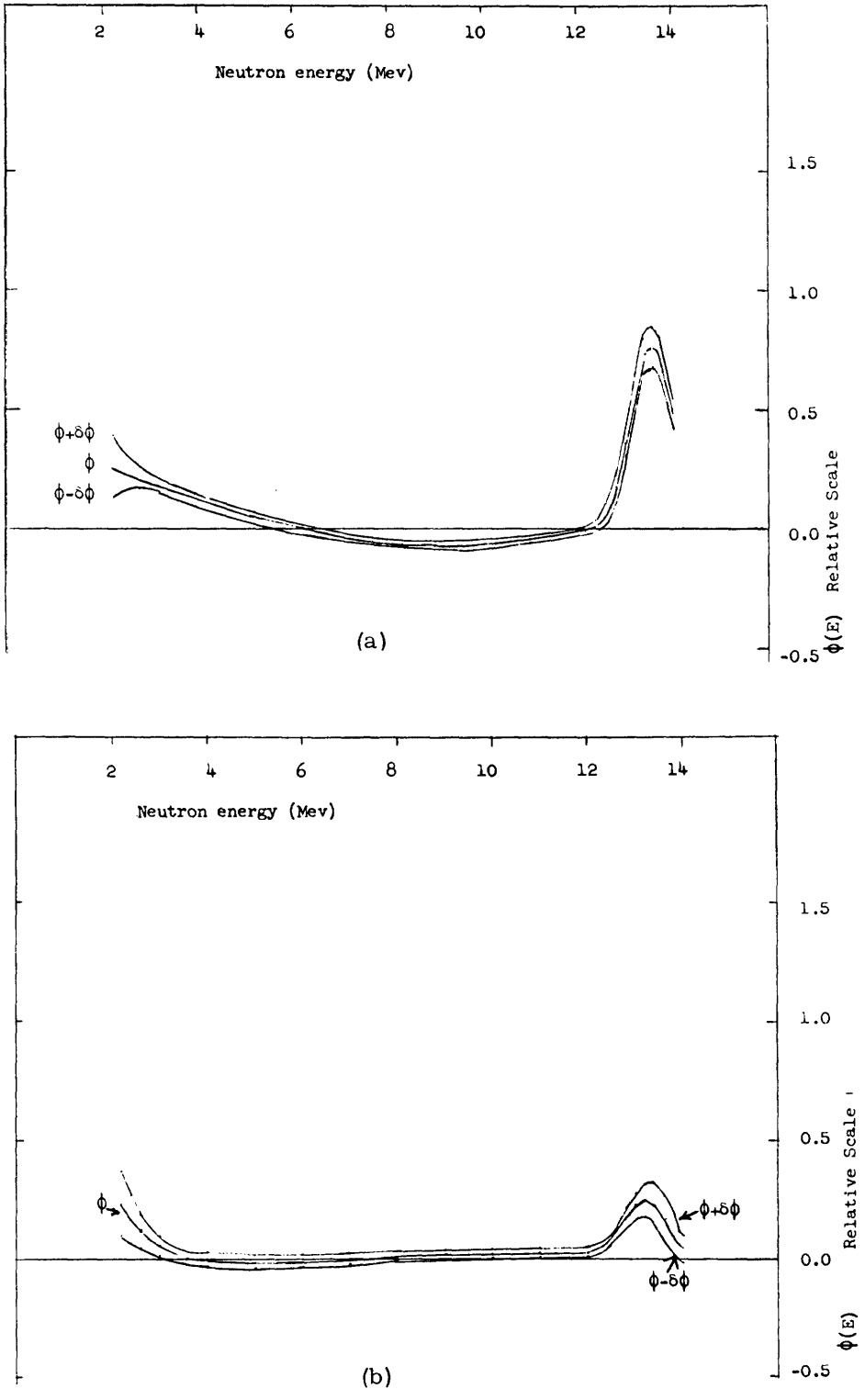

Fig. 42.

(a) Calculated spectrum in graphite blanket with 1.125-inch molybdenum wall at 5 cm from first surface. (Eq. 51 used for w(E).)

(b) Calculated spectrum in graphite blanket with 1.125-inch molybdenum wall at 20 cm from first surface. (Eq. 51 used for w(E).)

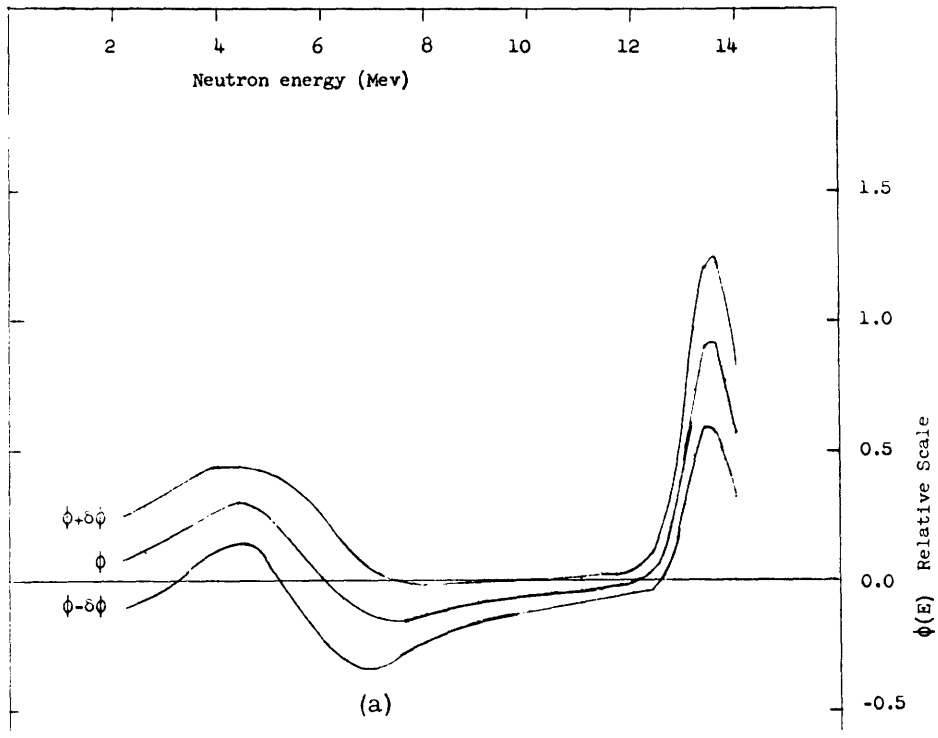

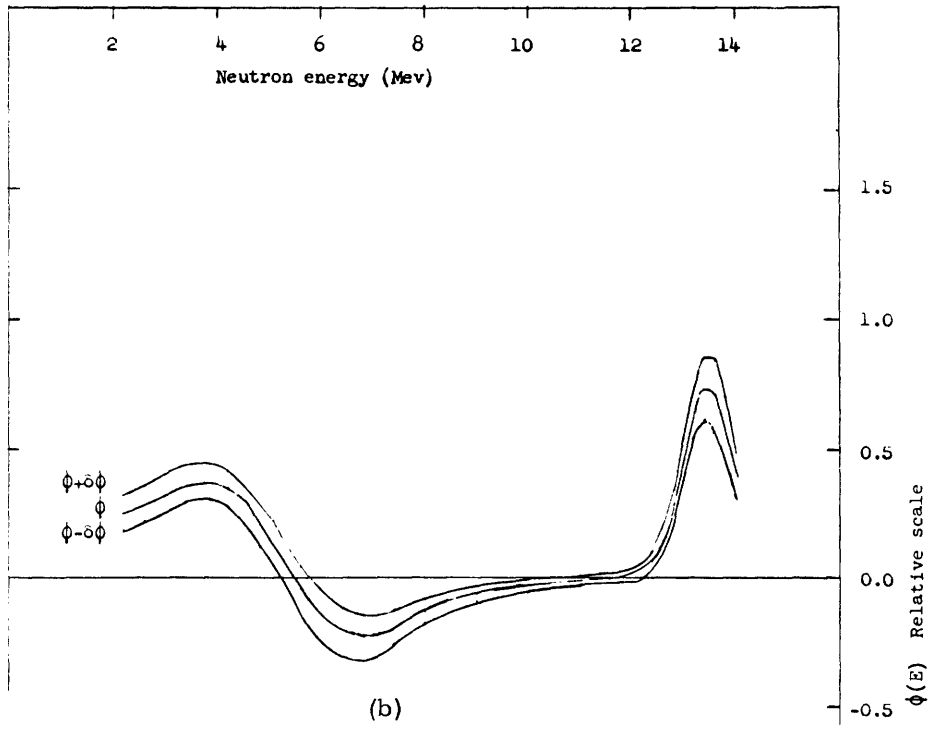

Fig. 43.

(a) Calculated spectrum in graphite blanket with no first wall at 5 cm from first surface. (Eq. 52 used for w(E).)

(b) Calculated spectrum in graphite blanket with 1.125-in. molybdenum wall at 5 cm from first surface. (Eq. 52 used for w(E).)

Table 10. Summary of spectral analyses for graphite blankets.

Blanket Configuration	z (cm)	Foil	Foil Input T	Foil Input δT	Impink W(E) (Eq. 9.1) Foil Calc. T	Foil Calc. δT	Li-7(n,tn) T	Li-7(n,tn) δT	Fit	Gaussian W(E) (Eq. 9.2) Foil Calc. T	Foil Calc. δT	Li-7(n,tn) T	Li-7(n,tn) δT	Fit
All-graphite blanket, no wall.	5	U	1000	100	1400	800	70	400	G	1100	470	120	30	G
		P	100	70	55	57	40	240	G	90	60	100	270	G
		Fe	109	4	130	60	380	190	G	150	300	500	1300	G
		I	1150	90	1070	230	260	90	F	1100	360	200	180	G
		F	46	2	52	10	240	90	F	48	15	200	160	G
	10	U	800	200	1100	750	130	380	G	900	450	160	330	G
		P	93	5	54	62	110	250	G	75	65	140	280	G
		Fe	89	4	110	80	370	270	G	140	390	700	1700	G
		I	850	90	790	410	280	170	G	800	680	280	340	G
		F	33	1	37	17	260	160	G	36	27	260	270	G
	20	U	410	70	640	190	130	100	E	570	120	150	80	G
		P	44	2	33	20	120	70	G	34	20	115	80	G
		Fe	56	2	70	30	320	100	P	140	140	1000	600	P
		I	470	20	430	170	250	70	P	400	270	340	140	P
		F	18	1	21	7	240	60	P	23	11	310	110	P
All-graphite blanket, 9/8" (3cm) Molybdenum wall.	5	U	860	40	580	370	300	60	P	620	200	340	140	P
		P	78	1	114	23	330	100	P	120	23	390	110	P
		Fe	89	3	71	26	84	81	F	-30	130	-930	560	F
		I	831	26	890	90	170	40	F	950	150	70	75	F
		F	38	2	34	4	180	35	G	31	6	120	65	F
	10	U	800	90	500	580	240	300	F	500	360	290	260	G
		P	76	3	115	42	270	170	G	130	43	350	200	G
		Fe	57	3	40	50	0	70	G	-100	260	-1300	1200	P
		I	542	44	610	210	90	90	G	690	350	-60	180	G
		F	26	4	22	9	110	80	G	18	13	-3	150	F
	20	U	510	50	520	160	150	80	G	500	100	150	70	G
		P	52	2	51	14	150	65	E	55	15	150	60	G
		Fe	50	2	50	20	150	65	G	42	93	70	410	G
		I	360	20	360	110	150	43	E	370	170	130	90	G
		F	12	4	12	5	150	41	G	12	7	130	70	G

T = Normalized reaction rate defined by Eq. 27 (in millibarns); δT = standard deviation in T.
z = Distance along axis of blanket from first surface (see figure 34).

Foil Input values of T and δT are calculated from the data in figures 35-4 and the α_s in Table 8. The Russian data are used for the F-19(n,2n) reaction.

Foil Calculated values of T and δT are computed by the SPECTRUM program, using the $\phi(E)$ determined from the other four foils, and the indicated W(E). The values of T and δT for the Li-7(n,tn) reaction in the adjacent column are calculated from the same $\phi(E)$.

The Fit is a subjective evaluation of the $\phi(E)$ described above:

E = Excellent Fit: $\phi(E)+\delta\phi(E) \geq 0$ everywhere within the range of calculation (2.1-14.1 Mev).
Also $\phi(E) > -0.05\ \mathrm{Max}(|\phi(E)|)$.

G = Good Fit: $\phi(E)+\delta\phi(E) > -0.05\ \mathrm{Max}(|\phi(E)|)$.

F = Fair Fit: $\phi(E)+\delta\phi(E) > -0.2\ \mathrm{Max}(|\phi(E)|)$.

P = Poor Fit: $\phi(E)+\delta\phi(E) < -0.2\ \mathrm{Max}(|\phi(E)|)$ for some E within the range.

$\mathrm{Max}(|\phi(E)|)$ is the maximum value of $|\phi(E)|$ for $2.1 \leq E \leq 14.1$.

that the $\phi(E)$ are "excellent" in Figs. 42b and 44; "good" in Fig. 43a; "fair" in Figs. 41a, 42a, and 43b; and "poor" in Fig. 41b.

The main features of the data in Table 10 are the following:

1. The choice of w(E) has little effect on either the fit, or the reproducibility of the normalized reaction rates T.

2. The input values of the $U^{238}(n, f)$ reaction rate for the graphite blanket with no first wall are consistently lower than the calculated values. The input values would be low if the uranium foils in the calibration experiments (see Table 8) were partially activated by neutrons scattered from the walls of the target room, since the blanket data are divided by the value of this activity.

3. The good agreement of the calculated and input values of T for the fluorine and iodine foils, even when other calculated activities differ widely, indicates that the fluorine and iodine cross sections may be too similar for this method of analysis.

4. The occurrence of $\phi(E) < 0$ ("good" and "fair" fits) does not prevent agreement between the calculated and experimental threshold reaction rates, or consistent values of the $Li^7(n, tn)$ reaction rate (and vice versa); although "poor" fits usually give poor agreement.

5. The data at 20 cm in the blanket with the molybdenum wall are in excellent agreement with the calculated values. The calculated $Li^7(n, tn)$ reaction rates are almost

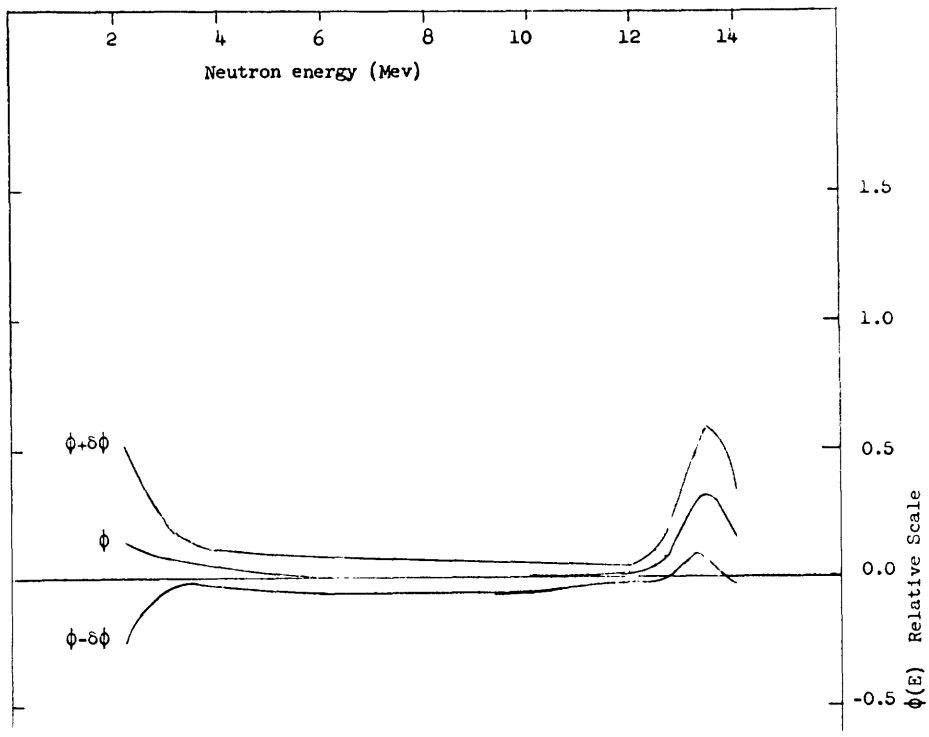

Fig. 44. Calculated spectrum in blanket with 33% graphite and 67% salt at 20 cm from first surface. (Eq. 51 used for w(E).)

Table 11. Summary of spectral analyses for blankets with lithium-beryllium fluoride salt.

Blanket Configuration	z (cm)	Foil	Impink W(E) Foil Input T	Impink W(E) Foil Input δT	(Eq. 9.1) Foil Calc. T	(Eq. 9.1) Foil Calc. δT	Li-7(n,tn) T	Li-7(n,tn) δT	Fit	Gaussian W(E) Foil Calc. T	Gaussian W(E) Foil Calc. δT	(Eq. 9.2) Li-7(n,tn) T	(Eq. 9.2) Li-7(n,tn) δT	Fit
67%2Li1F-BeF$_2$	5	U	990	170	2	800	-430	130	P	460	470	750	340	P
Blanket with		P	85	10	210	70	770	260	P	180	70	840	300	P
3/8" (1 cm)		Fe	109	8	40	80	-90	260	F	-160	370	-2200	1600	P
Molybdenum		I	830	90	1000	400	200	160	G	1100	650	100	320	G
Wall		F	43	1	28	17	260	150	G	28	26	210	280	G
	20	U	450	60	1300	600	-130	320	F	850	380	-110	270	F
		P	73	10	-30	45	-200	200	P	-90	45	-200	200	P
		Fe	54	3	110	50	515	150	P	270	240	2100	1000	P
		I	560	70	390	160	270	70	P	360	260	370	130	P
		F	17	2	28	8	250	65	P	28	11	290	120	F
67% 2Li1F-BeF$_2$	5	U	670	90	600	600	420	300	P	720	370	450	260	F
Blanket with		P	91	5	101	43	420	180	P	82	44	430	200	P
3/4" (2 cm)		Fe	104	4	99	53	360	170	P	130	260	750	1200	G
Molybdenum		I	875	44	890	220	380	90	P	850	360	510	180	P
Wall		F	39	4	38	9	385	84	P	40	14	500	150	P
	20	U	465	93	-180	400	510	200	P	180	250	540	170	P
		P	61	5	140	30	560	120	P	110	30	600	140	P
		Fe	56	3	13	43	-3	140	P	-90	220	-1000	1000	P
		I	416	22	550	210	190	90	P	560	350	280	180	G
		F	26	3	16	9	220	80	P	17	14	260	150	F
67% 2Li1F-BeF$_2$	5	U	740	190	420	720	580	370	P	750	410	560	300	P
Blanket with		P	79	5	120	60	600	260	P	80	70	560	290	P
9/8" (3 cm)		Fe	133	17	110	73	320	240	G	130	340	600	1500	G
Molybdenum		I	963	45	1030	480	420	190	P	960	790	570	380	F
Wall		F	40	2	35	20	430	180	P	40	31	560	340	P
	20	U	560	130	700	500	80	250	G	600	300	90	200	G
		P	60	5	40	40	70	170	G	53	45	80	190	G
		Fe	54	8	64	5	200	180	E	70	240	300	1100	G
		I	472	44	440	320	160	120	E	460	520	130	250	G
		F	17	1	19	13	150	120	E	18	20	120	220	G
50% 2Li1F-BeF$_2$	5	U	890	190	910	770	220	400	G	800	470	270	340	G
Blanket with		P	91	5	90	64	220	250	G	110	70	290	290	G
3/4" (2 cm)		Fe	100	5	100	80	230	270	G	50	400	-200	1700	G
Molybdenum		I	1020	90	1020	410	220	170	G	1070	680	170	340	G
Wall		F	45	2	46	17	220	160	G	43	27	180	290	G
	20	U	446	93	-10	300	490	140	P	310	180	510	110	P
		P	68	5	130	30	520	90	P	94	27	540	110	P
		Fe	58	3	30	40	130	130	F	-20	200	-270	830	G
		I	360	20	460	210	260	90	P	430	350	340	170	P
		F	20	2	13	9	290	80	P	16	14	380	150	P

constant, regardless of the weight function or combination of threshold reaction rates used to determine $\phi(E)$.

9.3 SPECTRA IN THE BLANKETS WITH LITHIUM-BERYLLIUM FLUORIDE

One of the spectra calculated from data in the blankets with lithium-beryllium fluoride (67% salt, 3-cm molybdenum wall) is shown in Fig. 44. The correspondence between this spectrum and that shown in Fig. 42b substantiates the insensitivity of the spectra to the presence of the salt – at least at high energies. The large δT for the uranium data allow almost any shape for the low-energy spectrum.

The analyses of the salt-blanket data are summarized in Table 11. There is a large number of "poor" fits, and wide disagreement between calculated and experimental threshold reaction rates. The scatter of the points discussed in Section VIII allows but one conclusion: poor data are poor data are poor data . . . .

9.4 CONCLUSIONS

The applicability of the method of spectral analysis described in Section VI has been demonstrated – at least for the graphite-blanket data. The semiquantitative agreement between the experimentally determined spectra and the spectra computed by Impink indicates that there are no serious errors in the approximations that he used to compute his spectra. His conclusions about the feasibility of various blanket configurations can therefore be accepted within the resolution of these experiments.

The shape of the spectrum <3 Mev is almost totally determined by the uranium-foil data, which contain the largest errors. The difficulty in counting the activities on the uranium catchers could be circumvented by measuring the $U^{238}(n, f)$ reaction rate with a small fission chamber, which could be inserted at various points within the experimental assemblies. With a fission chamber, the $Np^{237}(n, f)$ reaction could also be used. If the electronic problems of the fission chamber are insurmountable, the $In^{115}(n, n')In^{115m}$ reaction might be used, with a theoretical extrapolation of the cross section for energies >5 Mev.

X. FINAL EXPERIMENT

A run was made on July 26, 1964, to verify the effect of the presence and composition of the blanket assemblies on the neutron monitor. The response of the monitor was compared with the response of a BF_3 long counter that was placed in the target room as far as possible from the source. We had determined previously that in this position the long counter was insensitive to the presence or absence of the blanket assembly. The results, presented in Table 12, are somewhat scrofulous for three reasons:

1. The tritium target was practically depleted, so there was a large percentage of 2.5-Mev source neutrons from the $H^2(d,n)He^3$ reactions.
2. The neutron monitor is mainly sensitive to neutrons scattered from the walls.
3. The operation of the monitor BF_3 counter became erratic toward the end of the experiment, because of electronic difficulties.

Table 12. Relative neutron production rates.

Blanket Composition	First Wall	Ratio[a]	Position of Neutron Monitor
None	None	.127 ± .001	Standard Position (See Fig. 13)
100% Graphite	None	.130	
67% salt, 33% graphite	1 cm Mo	.142	
" "	2 cm Mo	.146	
" "	3 cm Mo	.148	
50% salt,50% graphite	2 cm Mo	.147	
100% Graphite	None	.30 ± .005	Top of blanket
"	1 cm Mo	.31	
"	2 cm Mo	.32	
"	3 cm Mo	.32	
"	2.5 cm Pb	.31	

a. Ratio = (cpm of neutron monitor)/(cpm of long counter far from accelerator) for a simultaneous two-minute count.

Nonetheless, the numbers in Table 12 provide a relative measure of the total neutron population at energies of interest in tritium production because the energy response of the BF_3 tube is roughly similar to the $Li^6(n,t)$ cross section. A comparison of numbers in Table 12 with the total tritium production computed by Impink (Runs 3-110, 3-111, 3-113, and 3-114 in Table 2) shows that 2 cm is, indeed, the maximum useful thickness for a molybdenum wall. Also, 2.54 cm of lead has about the same neutron-production value as 2 cm of molybdenum.

XI. CONCLUSIONS AND RECOMMENDATIONS

11.1 CONCLUSIONS

The feasibility of studying proposed fusion reactor blanket configurations has been demonstrated by using finite blanket assemblies and a point source of accelerator-produced neutrons. The techniques that were developed in the course of this work are listed in Table 13.

Table 13. Techniques developed in the Fusion Reactor Blanket Experiment.

Neutron Source using $H^3(d,n)He^4$ reaction.
- Use of Cockcroft-Walton machine with solid tritium target.
- Gas target for 1-3 Mev Van de Graaff accelerator.

Construction of Blanket Assemblies

Measurement of neutron-energy spectrum above 1 Mev
- System of threshold detectors using uranium, phosphorus, iron, iodine, and fluorine reactions.
  - Fabrication of phosphorus and iodine foils from calcium phosphate glass and hexaiodobenzene, respectively.
- Irradiation techniques
- Computer programs for handling large quanities of activation and irradiation data.
- Computer programs for determining neutron spectrum from reduced threshold-detector data
- Interpretation of spectra

Measurement of tritium produced in experimental assemblies
- Measurement of small amounts of tritium produced in small samples of lithium-beryllium fluoride salt

The semiquantitative agreement of our spectral measurements and Impink's theoretical results[3] implies the validity of his calculations, and hence his conclusions concerning the feasibility of various blanket configurations – within the limitations of the present experiments. The main differences between the theoretical and experimental results are attributable to the finite size of the experimental assemblies. A more direct comparison of the experimental results with Impink's calculations will require a Monte Carlo calculation.

11.2 RECOMMENDATIONS FOR FUTURE WORK

As we indicated initially, this work is a first look at experimental techniques for evaluating proposed fusion reactor blanket systems from the point of view of neutron economy. While the techniques listed in Table 13 provide data for a tentative evaluation, much experimental and theoretical work remains to be done.

a. Tritium-Production Measurements

The preliminary work indicates that the tritium production in the experimental assemblies can be measured directly, although the present efforts were not successful. Since the ability to produce enough tritium to sustain the plasma may be a deciding factor in the over-all feasibility of fusion power, further investigation is needed in this area. The suggestions at the end of Section VII offer a starting point for such investigation.

b. Construction of Experimental Assemblies

The difficulties with the fissures in the layers of lithium-beryllium salt in the experimental assemblies could be avoided by casting each layer as one piece in a graphite mold.[45] After proper cleaning to remove any salt on the outside surfaces, these molds could be used to contain the salt for the irradiation experiments. Facilities for casting the salt exist at Oak Ridge National Laboratory. If such salt layers are to be fabricated, the experimenter should consider personally supervising the operations.

If procurement of the salt in a more suitable form is not possible, fruitful experiments can be conducted with graphite assemblies with various first-wall materials. Of special interest are ceramic materials that are just becoming available, such as the molybdenum and niobium beryllides.

Spectral measurements in a "semi-infinite" graphite blanket will be needed to provide a transition between the finite assemblies and the geometry used in previous theoretical studies by Impink.

c. Spectral Measurements

Uranium and neptunium fission chambers should be investigated for measuring the neutron spectra below 2 Mev, in conjunction with the present set of threshold detectors. The $In^{115}(n, n')In^{115m}$ reaction might also be useful in this energy region.

The computational corrections for the sensitivity of the neutron monitor to scattered neutrons can be avoided by using a monitor that is sensitive only to 14-Mev neutrons. Schemes that should be investigated are knock-on proton counters and measurement of the N^{16} activity in the cooling water for the tritium target. This activity arises from the $O^{16}(n, p)N^{16}$ reaction.

d. Theoretical Work

The need for Monte Carlo calculations to evaluate the present experiments has already been mentioned. The results of these experiments should be combined with

concurrent measurements of γ-production in the experimental assemblies[46] and previous theoretical efforts,[3,4,47] and further studies should be made to investigate the blanket problem from other points of view, such as shielding, radiation damage, and economics.

APPENDIX A

SAMTAPE Data-Reduction Programs

A.1 INTRODUCTION TO THE SAMTAPE PROGRAMS

SAMTAPE is a collection of 31 FAP and Fortran subprograms written for the IBM 709/7090/7094 computers, operating under the Fortran-II Monitor System. In particular, it is compatible with the operating systems in use at the Computation Center, M.I.T., and the Cooperative Computation Laboratory, M.I.T., in the summer of 1964. SAMTAPE is divided into three parts: 1) the main program, which sorts data from an automatic sample changer, and corrects for certain changes in the operation of the sample changer; 2) the Frantic routines,[48] which fit the sorted data from the sample changer to exponential decay curves; and 3) the Beam programs, which compute the effective dose given to the samples, including the effects of decay of the active nuclei during the irradiation. The subroutine ZPRINT combines the results of the Frantic and Beam programs to give ratios for each sample which are independent of its irradiation and counting history.

SAMTAPE was written with these criteria in mind:

1. Continuity. In many cases computation errors that would normally result in termination of the programs are trapped internally, and cause the program to proceed to the next operation. This criterion applies mainly to the curve-fitting routines.

2. Direct Data Input. The activation data from the sample-changer tape and the neutron-flux data from the chart-recorder tape can be punched directly onto data cards. No preliminary computations are necessary.

Because of the limitations of the library input/output routines, most of the data cards are read under one of two standard input formats. In a few cases ("HEDING," "FRANIC," and "DOSE" cards), the appearance of a control card temporarily suspends the standard format to read one or more cards under a special format.

3. Versatility. Program flow is controlled by a mnemonic in the first 6 columns of each data card. Changes in parameters used in the computations, variations in the operation of the sample changer, unusual conditions in the flux plot, or the initiation of output or analysis may be accomplished by inserting the appropriate control card in the data deck.

Because of this versatility, the following description of the SAMTAPE program is mainly in terms of data cards. The cards for the operation of the automatic sample changer are given first, followed by the data cards for the Frantic analysis. Both sets of cards are read by the SAMTAPE main program. Since the curve-fitting routines are somewhat complex, a description of the Frantic routines is inserted here. There follows a description of the Beam programs and the Beam data deck, which uses a different standard format from that used by the SAMTAPE main program. Finally, there is a brief description of the comparison program ZPRINT. A sample input deck and the

Location		Length
0-100	Monitor System locations	100
03212	Locations used for SAMTAPE programs	8212
15296	Locations used for library routines	6986
17062	Not used.	1766
17521	Erasable storage for data	457
23921	"Saved Tape" Common Storage. Sorted sample-changer data and other parameters stored here.	6400
24315	"Saved Frantic" Common Storage	394
24378	"Saved Beam" Common Storage	63
32561	"Bottom Common" Storage. Unsorted sample-changer data stored here; also used by Beam and Frantic routines for temporary storage	8183
32767	Erasable storage locations*	206

* Used as temporary storage by library routines.

Fig. A-1. Computer storage for SAMTAPE programs.

resulting output from the ZPRINT comparisons are included to illustrate the use of the SAMTAPE programs.

In general, the operation of the various subroutines is outlined under the appropriate card description. The service subroutines, which are used by many of the other subroutines for various purposes, are described at the end of this appendix. A listing of the FAP and Fortran source decks is given in Appendix F.

The SAMTAPE programs require that the computer have a 32,768-word memory. The number of locations which are used depends slightly on the library programs at each installation. The storage distribution for a typical run at the Computation Center, M.I.T., is shown in Fig. A-1.

At any large computer installation, all input/output is from/to magnetic tapes which are processed off-line. Thus the phrase "read a card" as used in this discussion really means "read a record from the input tape, onto which the cards were read off-line." Similarly, the words "print" and "punch" really mean "written onto the output tape for off-line printing (or punching)."

A.2 SAMTAPE MAIN PROGRAM

The main purpose of the SAMTAPE main program is to prepare data from the automatic sample changer for the Frantic analysis routines. Additional cards for the Frantic routines, cards to initiate analysis or output, and the "BEAM" card to transfer control to the Beam programs are also read by the main program. The operation of the sample changer for which the main program was designed is described here.

Sample-Changer Operation

The samples to be counted are placed in coded planchets which are stacked in a magazine. After the sample changer is started, the first sample is moved into position and counted until a preset number of counts has been accumulated. The number of counts can depend upon the count rate of the sample and the planchet coding. After the count (or observation) of the sample is completed, the sample number, the length of the observation, and a code letter denoting the number of counts accumulated are printed on a paper tape, and the next sample is counted. After the last sample in the stack has been counted, the magazine is recycled to repeat the counting cycle.

The Elapsed-Time Counter

In order to plot a decay curve for a sample, it is necessary to know the time at which each observation began. SAMTAPE does this by means of an elapsed-time counter, which is set to zero at the beginning of each counting run. Into this register are added the observation lengths, the times required to change samples within a stack, the recycle time, and any changes in the normal operation of the sample changer which are signaled by "PAUSE," "RESTAR," or "CHECK" cards. The elapsed timer always contains the time at which the next observation should begin.

A.3 STANDARD INPUT FORMAT FOR THE SAMTAPE MAIN PROGRAM

Most of the data cards for the SAMTAPE Main Program are read under a standard format. Only the "HEDING," "DOSE," and "FRANIC" cards temporarily suspend the standard format to read one or more cards under a special format. The standard format consists of four fields:

Field 1: Columns 1-6 contain a control mnemonic which must be left-adjusted and followed by blanks. An improper or misadjusted mnemonic will terminate the programs. A card with an asterisk (*) in column 1 and blanks in columns 2-6 is ignored, and may be used for comments. Cards which are blank in columns 1-20 are also ignored.

Field 2: Columns 7-10 contain a fixed-point integer which must be right-adjusted, since blanks within this field are treated as zeros.

Field 3: Columns 11-20 contain a floating-point number (such as 10.35). If the decimal point is punched, it and the number may be anywhere within the field. If the decimal point is not punched, and if the places to the right of the last significant digit are filled with zeros, the decimal point is assumed to lie between columns 18 and 19.

Columns 21-24 are ignored.

Field 4: Columns 25-30 contain alphanumerical information for labels, dates, count symbols, or secondary control words. The data in this field must be left-adjusted.

The Fortran Format Statement for this card is (A6, I4, F10.2, 4XA6).

A.4 DATA CARDS FOR THE SAMTAPE MAIN PROGRAM

The data cards for the SAMTAPE main program are described on the following pages. In the description, these conventions will be used:

1. Control mnemonics are in capitals and enclosed in quotation marks (examples: "HEDING," "BEAM").

2. Names of subroutines are in capitals, but not enclosed in quotation marks (examples: TAPE, BEAM). Note that sometimes the same word is both a mnemonic and a subroutine name.

3. When a mnemonic is given in data fields 1 or 4 there will always be 6 spaces between the quotation marks, regardless of the number of characters in the mnemonic to emphasize that mnemonics must be left-adjusted and followed by blanks.

4. The SAMTAPE main program is referred to as (MAIN), the name used internally by the computer.

5. When the word "ignored" is used in a data field, it means that the field is not interpreted by the library input routines, and may contain any identification information.

6. The words "not used" in a data field mean that although no data are extracted from the field, it is interpreted by the library input routines. Such fields should be left blank.

7. To aid the programmer who wishes to follow the program flow, the names of the major subroutines that are used to process a card are given under the field descriptions for that card. The so-called service routines, which are frequently used for conversions and other computations are described in this appendix.

Cards for Normal Sample-Changer Operation.

1. The SAMTAPE Observation Card.

Field 1: Must be blank.

Field 2: Sample number (Set minus if this observation is to be omitted from the Frantic analysis).

Field 3: Length of the sample observation in minutes (Set minus if this observation is to be corrected by a subsequent "CHECK" card -- see page 209.)

Field 4: Either

A. The number of counts which are accumulated during the observation. This number must be left-adjusted to column 25. The first non-numeric character or blank terminates the field. If the first non-numeric character is a "K" or "M" the number will be multiplied by 10^3 or 10^6.

B. A symbol representing the number of counts, which symbol has been identified by a preceding "COUNT" card. The symbol may be all blanks (if only one preset count is used, for example), but may not include a number which falls in column 25.

Subroutines Called: TAPE,COUNTR.

Use: The data from the sample-changer tape are entered on observation cards, one observation per card. (MAIN) calls TAPE, which a) calls COUNTR to convert Field 4 to the number of counts; b) lists the observation data in bottom common storage, including the sample-number, the observation length, the number of counts (set minus if the sample number was minus), and the computed starting time for the observation; and c) advances the elapsed-time counter for the next count. NOTE: If the sample number on the observation card

is $\leq$ the sample number on the previous observation card, the starting time for the present observation will include a recycle time.

2. The SAMTAPE "START" Card.

Field 1: "START "

Field 2: Not used (see note A.)on page 234)

Field 3: Clock time at the start of the first observation in the counting run (see note B. on page 234)

Field 4: The date (see note C. on page 234)

Subroutines called: Service routines.

Use: This card must precede the first observation card in each run. (MAIN) sets the elapsed-time counter to zero, erases any references to previous observations, and defines the time and date listed in Fields 3 and 4 as the starting time for the run. NOTE: The BEAM program also uses a "START" card, but has different formats for the following fields.

3. The "BETWN" Card.

Field 1: "BETWN "

Field 2: Not used.

Field 3: The time in minutes which is required to change samples within a stack.

Field 4: Not used.

Subroutines Called: None.

Use: One "BETWN" card must appear before the first observation card of the first run. Thereafter "BETWN" cards need be inserted in the data deck only if the time required to change samples changes. The "BETWN" time is measured from the end of one observation to the beginning of the next (within the same stack).

4. The "RECYC" Card.

Field 1: "RECYC "

Field 2: Not used.

Field 3: The time in minutes which is required to recycle the stack.

Field 4: Not used.

Subroutines Called: None.

Use: One "RECYC" card must appear before the first observation card of the first run. Thereafter a "RECYC" card need be inserted in the data deck only if the recycle time is changed (by the addition or removal of samples from the stack, for example). The recycle time is measured from the end of the observation of the last sample in the stack to the beginning of the first observation after the stack has been recycled.

5. The "COUNT" Card.

Field 1: "COUNT "

Field 2: Not used.

Field 3: The number of counts to be identified with the count symbol in Field 4.

Field 4: The count symbol, exactly as it will appear on subsequent observation cards. The symbol may include any combination of letters, numbers, or blanks; but it may not include a number which falls in column 25.

Subroutines Called: NEWSET

Use: One "COUNT" card for each different symbol must appear in the data deck before the first observation card on which that symbol is used. Thereafter a "COUNT" card need be inserted in the data deck only if the number of counts identified with a particular symbol is changed. An entry is made in a symbol-number table for each new symbol. Redefining a symbol only changes the number identified with that symbol; it does not cause a new entry in the symbol-number table. The maximum number of symbols which may be used at one time is ten. The symbol-number table may be erased with a "CLEAR" card.

6. The "CLEAR" Card.

Field 1: "CLEAR "

Fields 2-4: Ignored.

Subroutine Called: RESET

Use: The appearance of a "CLEAR" card in the deck erases the symbol-number table. It may be used to prevent a symbol-number table overflow.

7. The "MAXSAM" Card.

Field 1: "MAXSAM"

Field 2: The maximum number of samples which will be encountered in the following runs(≤ 50).

Fields 3-4: Not used.

Subroutine Called: SETX

Use: Storage is available for 2000 observation points. Normally SAMTAPE assumes that 50 samples will be used, with 40 observations per sample. If it is desired to use less samples with more than 40 observations per sample, a "MAXSAM" card may be used.

8. The "PAUSE" Card.

Field 1: "PAUSE "

Field 2: Not used.

Field 3: Length of pause in minutes. The time is measured from the end of the observation before the pause to the beginning of the observation which follows.

Field 4: Not used.

Subroutines Called: None.

Use: A "PAUSE" card may be used if it is necessary to interrupt the operation of the sample changer to add or delete samples, to change the coding of a planchet, etc. A stopwatch would be started at the end of the observation before the interruption, and stopped when the first observation after the interruption began. Note that if the sample being counted before the interruption is, say, number 5, it is not necessary for the sample after the interruption to be number 6, etc. Also, no recycle time will be added, even though the first sample to be counted after the interruption is number 1.

9. The "RESTAR" Card.

Field 1: "RESTAR"

Field 2: Not used (See note A. on p. 234)

Field 3: Clock time at the start of the following observation (See note B. on p. 234)

Field 4: The Date (See note C. on p. 234)

Subroutines Called: Service Routines.

Use: The "RESTAR" card is used for the same purpose as the "PAUSE" card, except that the time at the beginning of the first observation after the interruption is given instead of the length of the pause (which is computed internally).

Observation Length Correction.

1C. The "CHECK" Card.

Field 1: "CHECK "

Field 2: Not used (See note A. on p. 234).

Field 3: The clock time at the start of the following observation (See note B. on p. 234).

Field 4: The date (See note C. on p. 234)

Subroutines Called: Service Routines, CHECK.

Use: If the length of an observation has been misprinted by the sample-changer, the elapsed-time counter, and the starting times for the observations which follow will be in error. If the misprinted time is flagged with a minus sign (see p.204), the appearance of a "CHECK" card leter in the deck will cause the offending observation length, and the intervening starting times to be corrected.

If more than one observation length is misprinted before the situation is discovered, the observations occurring between the first and last misprints in the series are lost. However if Fields 2 and 3 of the last misprinted observation are flagged with minus signs, a "CHECK" card may be used to retrieve the observations which followed the last misprint. A similar procedure could be used in case of a power-failure, etc.

NOTE: The "CHECK" correction feature may be used only before the observation data have been moved from bottom common to "saved tape" common by the CHANGE routine.

Cards to Delete Bad Observations.

11. The "ERROR" Card.

Field 1: "ERROR "

Field 2: The sample number.

Field 3: The length of the observation.

Field 4: Not used.

Subroutines Called: None.

Use: The elapsed time counter is advanced as for a normal observation, but the point is otherwise ignored. An"ERROR" card may be used, for example, in case of a count-symbol misprint by the sample-changer.

12. The "IGNORE" Card.

Field 1: "IGNORE"

Fields 2-4: Ignored.

Subroutines Called: None.

Use: All subsequent observation cards are treated as "ERROR" cards, until a "NOTICE" card is encountered. The"IGNORE" and "NOTICE" cards could be used to bracket a group of observations that were in error because of a sample-changer malfunction.

13. The "NOTICE" Card.

Field 1: "NOTICE"

Fields 2-4: Ignored.

Subroutines Called: None.

Use: The "NOTICE" card is used to cancel the effect of a previous "IGNORE" card.

14. The "RESET" Card.

Field 1: "RESET "

Fields 2-4: Ignored.

Subroutines Called: None.

Use: All previous observations in the run are erased. The elapsed-time counter is not affected. A "RESET" card could be used to delete observations which contained a short-lived component which could not be separated by a Frantic analysis.

Information Cards for Printed Output.

Note: The following cards should precede the "PRINT" or "ANALYZ" card to which they refer.

15. The "BKGD" (Background) Card.

Field 1: "BKGD "

Field 2: The number of the background sample if one is used. If no background sample is used, Field 2 should be blank.

Field 3: If Field 2 is blank, Field 3 contains an average background count rate. Otherwise it is not used.

Field 4: Not used.

Subroutines Called: None.

Use: The "BKGD" card is used to transmit the average background count rate of the counter, or to identify the number of an empty planchet as a background sample. If a background sample is used, a later call to STDCAL causes computation of the background rates $B(T_i)$, and the variance in the background rate $(\delta B(T_i))^2$. A later call to NOISE places $B(t)$ and $(\delta B(t))^2$ in storage locations BKGD and BERR, respectively. Here t is the time of a sample observation, which is transmitted to NOISE as an argument. $B(t)$ and $(\delta B(t))^2$ are determined by linear interpolation.

The appearance of a "BKGD" card with a blank Field 2 erases any reference to a background sample. If no "BKGD" card appears in the deck, it is assumed that BKGD = BERR = 0 for all observations.

16. The "STD" (Standard) Card.

Field 1: "STD "

Field 2: Number of standard sample.

Field 3: Normal count rate R_o for standard sample, to be used to compute the normalization factor. If Field 3 is left blank, the average value of the standard-sample count rates is used as the normal rate.

Field 4: Label to be used for output.

Subroutines Called: None.

Use: A long-lived sample may be used to correct for slow variations in the sensitivity of the counter with time. If a standard sample is used, a later call to the subroutine STDCAL causes computation of the factors $F(T_i)$, where T_i is the starting time for each standard-sample observation:

$$F(T_i) = R_o/R(T_i),$$

where $R(T_i)$ is the count rate of the standard-sample observation which began at T_i. A vector of the variances in $F(T_i) = (\delta F(T_i))^2$ is also computed. A later call to the subroutine NORMAL causes the value of $F(t)$ and $(\delta F(t))^2$ to be placed in the storage locations F and FERR. Here t is the starting time of an observation which is given to the NORMAL routine as an argument. $F(t)$ and $(\delta F(t))^2$ are determined from the vectors $F(T_i)$, T_i and $(\delta F(T_i))^2$, T_i by linear interpolation.

Reference to a standard sample may be deleted by use of a "NORM" card. If no "NORM" or "STD" card appears in the deck, it is assumed that $F = 1.0$ and $\delta F = 0$ for all observations.

17. The "NORM" (Normalization) Card.

Field 1: "NORM "

Field 2: Not used.

Field 3: Value of normalization factor F.

Field 4: Not used.

Subroutines Called: None.

Use: All count rates are multiplied by the number in Field 3. Any reference to a standard sample is deleted.

18. The"HEDING" Card.

Field 1: "HEDING"

Fields 2-4: Ignored.

Subroutines Called: None.

Use: The normal input format is suspended; the 80 columns of the following card are used as a heading for printed and punched output.

19. The "LABEL" Card.

Field 1: "LABEL "

Field 2: Sample number

Field 3: Frantic identification number(an integer between 1.0 - 6.0).

Field 4: A label for printed and punched output.

Subroutines Called: None.

Use: The"LABEL" card is used to transmit a label for each sample for output. The Frantic identification number must be the same as a number read from field 2 of a "FRANIC" card.

Program Control Cards:

20. The "PRINT" Control Card.

Field 1: "PRINT "

Field 2: The number of the first sample to be printed. If Field 2 is left blank, all samples will be printed.

Field 3: If Field 2 is blank, Field 3 is ignored. If Field 2 contains a number and Field 3 contains a higher number, the number in Field 3 is that of the last sample to be printed. If Field 2 is not blank, but Field 3 is, then only the sample whose number appears in Field 2 will be punched.

Field 4: Not used.

Subroutines Called: TAPOUT, CHANGE, STDCAL, LINE, BKPNT, STDPNT, and Service Routines.

Use: (MAIN) transfers control to TAPOUT, which a) moves any sample observation data waiting in bottom common storage to "saved tape" common storage; b) calls STDCAL to compute the rates for background and standard samples (if any); c) prints a summary of the data taken for each sample, using subroutine LINE. BKPNT and STDPNT are used to print the summary of the background and standard samples.

The following data are printed for each observation: a) The clock time at the beginning of the observation, b) the number of minutes elapsed from the beginning of the counting run to the start of the observation (the value of the elapsed-time counter), c) the length of the observation, d) the number of counts accumulated during the observation, the count rate (corrected for standard and background),

and the standard deviation in the count rate. The observations are grouped by sample number.

In order to make comparisons, it is possible to place several "PRINT" cards after the deck of observation cards, and to change background and normalization parameters using "NORM","STD", and "BKGD" cards before each new "PRINT" card.

If observation cards follow a "PRINT" card, their data are added to the data which were printed, unless the previous data is erased by a "RESET" card, or a new run is signaled by a "START" card.

21. The "ANALYZ" Control Card.

Field 1: "ANALYZ"

Fields 2-3: The same as fields 2-3 of the "PRINT" control card, except that the data of the indicated samples are analyzed by the Frantic routines instead of printed.

Field 4: The number of a sample whose saturation activity per unit flux will be used for comparison. This number is converted by COUNTR, and therefore must be left-adjusted to column 25.

Subroutines Called: CHANGE, STDCAL, FRANIC and associated routines, Service Routines, ZPRINT

Use: (MAIN) transfers control to the FRANIC routine, which fits the observation data of the specified samples to the sum of one or more exponential curves. The program flow of the FRANIC routine is described starting on p. 240 . After plotting the curves for each of the samples, control is transferred to ZPRINT, which makes one of several possible comparisons.

22. The "COMPAR" Control Card.

Field 1: "COMPAR"

Fields 2-3: Not Used.

Field 4: The same as field 4.of the "ANALYZ" card.

Subroutine Called: ZPRINT

Use: The "COMPAR" card may be inserted after an "ANALYZ" card to make comparisons among the samples, other than the comparisons which were set up at the time the "ANALYZ" card was read. The following cards may be inserted between an "ANALYZ" card and a "COMPAR" card, or between successive "COMPAR" cards: "HEDING", "LABEL", "NODOSE", "OLDOSE" , and "FRANST". Note that if a "LABEL" card is used before a "COMPAR" card, the sample number - Frantic identification number relation should be the same as it was at the time of the preceding "ANALYZ" card.

23. The "QUIT" Control Card.

Field 1: "QUIT "

Fields 2-4: Ignored.

Subroutine Called: EXITM, from the system library tape.

Use: The "QUIT" card is the last card in the data deck. It is used to terminate the program and skip any following post-mortem request cards which were inserted in the deck in case of an error.

24. The "BEAM" Control Card.

Field 1: "BEAM "

Fields 2-4: Ignored.

Subroutines Called: CHANGE, BEAM, and associated subroutines. Service Routines.

Use: (MAIN) transfers control to the BEAM subroutine to compute the effective doses given each sample during irradiation. Control is returned to (MAIN) by the appearance of a "RETURN" control card in the Beam data deck. All cards which appear between the"BEAM" and "RETURN" cards must be Beam data or control cards. Note especially that the control mnemonics "START", "HEDING", and "DOSE", as well as the observation cards (all blanks in columns 1-6) have the same initial format, but are interpreted differently by the two programs.

Data Cards for the Frantic Analysis Routines.

The cards which follow are used to supply data for the Frantic Analyses, which are initiated by "ANALYZ" cards. These cards are read by the SAMTAPE main program, and may be inserted anywhere in the SAMTAPE data deck before the "ANALYZ" card to which they refer. Data from the following cards are also used in the Frantic analyses: "BKGD", "STD", "NORM", "HEDING" , and "LABEL".

Data Cards for the Frantic Analysis Routines (continued).

25. The "FRANIC" Card.

Field 1: "FRANIC"

Field 2: Frantic identification number (1-6).

Field 3: Number of sample which is to be used for comparison if no effective-dose information is available (punched as a floating-point integer----such as "2.0").

Field 4: Not used.

Subroutine Called: READIN.

Use: A "FRANIC" card and associated data cards must appear in the data deck before the "ANALYZ" card which uses them. The data for up to 6 different analyses may be stored in the computer at one time (in "saved Frantic" common storage). The Frantic identification number on the "FRANIC" and "LABEL" cards tells the FRANIC subroutine which of the data sets is to be used for each sample.

The normal SAMTAPE input format is suspended for the following data cards, which are almost identical with the header card, control card, and estimate cards described by P. C. Rogers.[1] If the input format on the following cards is different from his format, it is flagged with a "$\frac{1}{4}$" in the left margin.

A. The header card contains 80 columns of identification information which is used as a subtitle for the printed output of the Frantic analysis of each sample.

B. The contents of the control card, which follows the header card, are as follows:

Col. 1-4: An identification code which is used with the sample label for any intermediate output.

Col. 5-14: Ignored.

Columns 15-72 contain 29 fixed-point control numbers, which must be right-adjusted in their respective fields.

Col. 15-16: JMAX ($\leq$ 10), the number of half-lives which are to be fit to the experimental decay curve.

Col. 17-18: IC (= 1,2, or 3), the case number.

IC=1: The Frantic program attempts to guess the decay constants of each decay scheme, one at a time, until JMAX components have been guessed. No estimate (or "PG") cards are read. Experience has shown that this case should be used with care.

IC = 2: All half-lives (or λ's) are read from columns 1-12 of the "PG" cards, as well as any initial activities A_o which are to be held fixed. Any, all, or none of the half lives (or λ's) may be held fixed. Frantic will iterate to find any half-lives which are not held fixed.

IC = 3: All A_o and half-life (or λ) estimates are inserted on "PG" cards. None, any, or all may be held fixed. Frantic will iterate to find a better fit (unless all are held fixed).

NOTE: IC must be positive.

Col. 19-20: ID, (= 1, 2, or 3), the weight-function control number.

ID = 1: Each data point is weighted equally in fitting the curve.

ID = 2: Each data point is weighted by the inverse of its absolute variance.

ID = 3: Each data point is weighted by the inverse of its fractional variance.

NOTE: ID must be positive.

Col. 21-32: The "IS" control vector. IS(1) is in columns 21-22, IS(2) is in columns 23-25,...IS(6) is in columns 31-32. Each element in the vector is either zero or non-zero.

IS(1) $\neq$ 0 : Each new half-life guessed for IC = 1 is assumed to be 1/3 the smallest half-life from the previous guesses.

IS(1) = 0: Each new half-life for IC = 1 is assumed to be 1/10 the previous minimum. (Frantic iterates with each guess to find the right value).

IS(2) $\neq$ 0: The signs of the half-lives are allowed to vary during iterations, to allow for exponential growth, as well as decay, in case of a parent-daughter decay scheme.

IS(2) = 0. The signs are held fixed, either positive (IC = 1), for as read from the "FG" cards (IC = 2,3).

IS(3) $\neq$ 0: The results of each iteration are printed as intermediate output.

IS(3) = 0: Results are printed only after the iterations have converged.

IS(4) $\neq$ 0: The least-squares matrices are printed for each analysis.

IS(4) = 0: The least-squares matrices are not printed.

IS(5): Not used.

IS(6) $\neq$ 0: Columns 1-12 of the "PG" cards contain the half-life of that component. The decay constant λ is computed by the subroutine DATA.

IS(6) = 0: Columns 1-12 of the "PG" cards contain the decay constants λ.

Col. 33-72: The "IX" control vector. IX(1) is in columns 33-34, IX(2) is in columns 35-36,...IX(20) is in columns 71-72. Each element is either zero or non-zero.

IX(2J) $\neq$ 0: The half-life of the J-th component is fixed.

IX(2J) = 0: The half-life of the J-th component is allowed to vary. If any IX(2J) = 0, Frantic will iterate for IC = 2,3.

IX(2J-1) $\neq$ 0: The initial activity of the J-th component is read from columns 13-24 of the J-th "PG" card and is held fixed (IC = 2,3).

IX(2J-1) = 0: The initial activity of the J-th component is computed (IC = 2), or read from columns 13-24 of the J-th "PG" card; but in both cases it may vary.

NOTE: For IC = 1, all IX(J) are set = 0 by the GUESS routine.

C. The "PG" cards (or estimate cards) follow the control card for IC = 2,3. For IC = 1, no "PG" cards are used. The half-lives (or λ's) and initial activities for each component, one component per card, are entered in columns 1-12 and 13-24 respectively. If IC = 2, an unfixed initial activity may be omitted. The half-lives (or λ's) and initial activities are read in Fortran"E" Format; that is, a number 1.234×10^{5} would be punched 1.234 E 5, 4.321×10^{-5} is 4.321 E-5. Plus signs may be omitted, but minus signs may not. The decimal point should be punched. The number following the "E" must be right-adjusted, since blanks are treated as zeroes. If the number after the "E" would be zero, it and the "E" may be omitted.

$\ddagger$ In the original programs a data control card follows the "PG" cards. The present version omits this card. The data scale factor and the data normalization factor which were on the original data control card are set = 1.0. The other data is transmitted by one of the SAMTAPE data cards given below, and is the same for all analyses. The Fortran Format for the cards which follow the "FRANIC" card is (13A6,A2/A6, 8X 29 I2/(2 E12.7)).

26. The "TIMERR" Card.

Field 1: "TIMERR"

Field 2: Not used.

Field 3: δD, the average error in the length of an observation (in minutes).

Field 4: Not used.

Subroutines Called: None.

Use: A "TIMERR" card must appear in the data deck before the first "ANALYZ" card to which it applies. The quantity δD is used in computing the variance of each data point used in the Frantic analysis. If no "TIMERR" card appears, it is assumed that $\delta D = 0$.

27. The "TAUD" Card.

Field 1: "TAUD "

Field 2: Not used.

Field 3: τ, the dead-time for the counter (in microminutes).

Field 4: Not used.

Subroutines Called: None.

Use: A "TAUD" card must appear in the data deck before the first "ANALYZ" card to which it refers. The quantity τ is used to compute the corrected activity A and the variance $(\delta A)^2$ for each data point used in the Frantic analysis. If no card appears it is assumed $\tau = 0$.

28. The "DTAUD" Card.

Field 1: "DTAUD "

Field 2: Not used.

Field 3: $\delta\tau$, the error in the dead-time τ (in microminutes).

Field 4: Not used.

Subroutines Called: None.

Use: A "DTAUD" card must appear in the data deck before the first "ANALYZ" card to which it applies. The quantity $\delta\tau$ is used in the computation of the variance in each data point used in the Frantic analysis. If no card is read it is assumed that $\delta\tau = 0$.

29. The "MAXVAR" card.

Field 1: "MAXVAR"

Field 2: Not used.

Field 3: The maximum acceptable value of $(\delta A/A)^2$, the fractional variance in a data point, for the point to be used in a Frantic analysis. If the variance $(\delta A/A)^2$ is greater than this value, the point will not be used.

Subroutines Called: MXFRAC

Use: A "MAXVAR" card must appear before the first "ANALYZ" card to which it applies. If no card is read, points whose fractional variance exceeds 0.0625 will be rejected.

30. The "TAU" Card.

Field 1: "TAU "

Fields 2 and 4: Not used.

Field 3: Extrapolation time in minutes before (+) or after (-) the time on the previous "START" card.

Subroutines Called: None.

Use: Frantic computes the initial activity A_o for each component at the time on the previous "START" card. Frantic also computes the quantity A_o/λ, which may be extrapolated to a time bfore or after the time on the "START" card, using the extrapolation time read on the "TAU" card, computed from data on an "ENDRUN" card, or computed from the time of an effective dose. The "TAU" card must appear before the "ANALYZ" card to which it refers. If a "TAU" or "ENDRUN" card appear after an effective dose was computed by the Beam routines, reference to this dose is deleted, until it is reinstated by using an "OLDOSE" card.

31. The "ENDRUN" Card.

Field 1: "ENDRUN"

Field 2: Not used (see note A)

Field 3: Clock time to which the initial activity (divided by λ) for each component of each sample should be extrapolated.

Field 4: The date of the extrapolation (see note C)

Subroutines Called: Service Routines.

Use: This card is used in the same manner as a "TAU" card, except that the extrapolation time is computed from the time on the "ENDRUN" card to the time on the "START" card.

32. The "DOSE" Card.

Field 1: "DOSE "

Field 2: Number of half-lives to be read

Field 3: Time of the effective dose (see note B).

Field 4: Date of the effective dose (see note C).

Subroutines Called: Service Routines

Use: Normally the effective doses are computed by the Beam routines. However if the doses were computed during a previous run, and the results were punched on cards, it is possible to read these cards on subsequent computer runs, rather than to recompute the doses. The following cards must come immediately after the "DOSE" card:

A. A card with the total dose in Col. 1-20 (Fortran Format is E20.5)RE20.

B. N cards (where N is the number in field 2 of the "DOSE" card)

Each card contains:

1. A Frantic identification number in columns 1-2.

2. A dose label in columns 7-12.

3. The half-life in columns 13-24.

4. The decay constant in columns 25-36 (if it is omitted it will be computed by the program).

5. The effective dose in columns 37-42.

Except for item 1, these data are in the format in which they are punched by the Beam Routines. Items 3-5 are in Fortran "E" Format; that is, a number 1.2345×10^{6} would be punched 1.2345E6; 1.2345×10^{-6} becomes 1.2345E-6. The number following the "E" must be right-adjusted, since blanks are treated as zeroes. The Fortran Format for these cards is (I2, 4X A6, 3E12.3).

55. The "NODOSE" Card.

Field 1: "NODOSE"

Fields 2-4: Ignored.

Subroutines called: None.

Use: The "NODOSE" Card may be used before a "COMPAR" card to delete reference to effective dose calculations.

24. The "OLDOSE" Card.

Field 1: "OLDOSE"

Fields 2-4: Ignored.

Subroutines Called: None.

Use: The "OLDOSE" Card may be used before a "COMPAR" or "ANALYZ" card to reinstate reference to the previously computed effective doses (or doses previously read by use of a "DOSE" card), which reference was deleted by a "NODOSE", "TAU", or "ENDRUN" card.

Data Cards for the SAMTAPE Main Program (continued).

Notes:

A. In an earlier version of SAMTAPE, cards containing a date used Field 4 only for the month; the day of the month was in Field 2. Except for the "DOSE" card, the present version of SAMTAPE is compatable with this format.

B. Clock times are based on a 24-hour day; that is, 1:30 p.m. is punched as 1330. Thirty seconds later the time would be 1330.5.

C. Dates may be punched either in the form "MAR 11" or "3/11". In the first case the abbreviation of the month must include its first three letters: JAN, FEB, MAR, APR, MAY, JUN, JUL, AUG, SEP, OCT, NOV, or DEC. In the second case any non-numeric may be used to separate the month from the day. The dates are read in Fortran "A" format, and are converted to binary by the subroutine CALENS.

A.5 FRANTIC ROUTINES

The Frantic Routines were originally written as 8 Fortran-II subprograms by P. C. Rogers[48] to fit activation data to a sum of exponentials. Three of the routines – MATRIX, GUESS, and OUTPUT (the last with minor format changes) – are used in the SAMTAPE programs as they were originally written. The following modifications were made to the other routines.

1. DATA and INPUT were rewritten in FAP to use the activation data supplied by the SAMTAPE data-sorting routines.

2. The curve-fitting routine LESFIT was rewritten in FAP, and the matrix-inversion routine MATINV was made a skeleton routine to call the library matrix-inversion routine XSIMEQ, so that overflows occurring occasionally during iterations would be trapped internally, thereby causing FRANIC to terminate the present analysis, and to go on to the next sample. In the original versions an overflow was trapped by a library routine, which terminated the program completely.

3. Certain results of each analysis are saved for later comparisons with the ZPRINT routine.

Although the Frantic routines are designed to find the half-lives, as well as the initial activities, the following discussion deals mainly with the initial activities, since it is this feature of the program that was most useful in the reduction of the activation data from the blanket assemblies. Further details of the Frantic routines may be found in the original report.[48]

Theory: Curve for Multicomponent Radioactive Decay

The usual equation for describing multicomponent decay of a radioactive sample is

$$a_{\text{inst},n} = \sum_i A_{oi} \exp(-\lambda_i T_n), \tag{A.1}$$

where

A_{oi} is the initial activity of the i^{th} component,

λ_i is the decay constant ($= \log_e 2/T_{1/2}$),

T_n is the time of the n^{th} observation of the sample, and

$a_{\text{inst},n}$ is the computed activity.

The data supplied to the Frantic routines give the average rate A_n over an interval D_n:

$$A_n \doteq a_n = \sum_i A_{oi} \left[(1/D_n) \int_{T_n}^{T_n+D_n} \exp(-\lambda_i t)\, dt \right] = \sum_i A_{oi} \exp(-\lambda_i T_n) \frac{\exp(-\lambda_i D_n) - 1}{-\lambda_i D_n}$$

$$= \sum_i A_{oi} \exp(-\lambda_i T_n)\, \text{EXP1F}(-\lambda_i D_n) \tag{A.2}$$

$$A_n \doteq a_n \equiv \sum_i A_{oi} f_{in}. \tag{A.3}$$

In (A.2), EXP1 is the service routine described in Section A.6. In the following discussion the coefficients of the A_{oi} will be abbreviated as in (A.3).

Theory: Least-Squares Analysis

If the λ_i are all given, a unique least-squares analysis can be made to find the A_{oi}. They are chosen so that for the sum over all observations the variance of fit

$$\sum_n [A_n - a_n]^2 W_n = \sum_n \left[A_n - \sum_i A_{oi} f_{in} \right]^2 W_n \tag{A.4}$$

is a minimum, where W_n is the weight given to each observation. To satisfy the criterion (A.4) it is necessary that for each component j

$$\sum_n W_n (\partial / \partial A_{oi}) \left[A_n - \sum_i A_{oi} f_{in} \right]^2 = 0. \tag{A.5}$$

Expansion of (A.5) leads to the normal equations:

$$\begin{aligned}
A_{o1} g_{11} + A_{o2} g_{21} + \ldots + A_{oI} g_{I1} &= \sum_n W_n A_n f_{1n} \equiv \beta_1 \\
A_{o1} g_{12} + A_{o2} g_{22} + \ldots + A_{oI} g_{I2} &= \sum_n W_n A_n f_{2n} \equiv \beta_2 \\
\ldots\ldots\ldots\ldots\ldots\ldots\ldots\ldots & \quad \ldots\ldots\ldots\ldots \quad \ldots \\
A_{o1} g_{1I} + A_{o2} g_{2I} + \ldots + A_{oI} g_{II} &= \sum_n W_n A_n f_{In} \equiv \beta_I,
\end{aligned} \tag{A.6}$$

where

$$g_{ij} = \sum_n W_n f_{in} f_{jn}. \tag{A.7}$$

Equation A.6 can be written in matrix form:

$$\begin{bmatrix} g_{11} & g_{21} & \cdots & g_{I1} \\ g_{12} & g_{22} & \cdots & g_{I2} \\ \ldots\ldots & \ldots\ldots & \ldots\ldots & \ldots\ldots \\ g_{1I} & g_{2I} & \cdots & g_{II} \end{bmatrix} \begin{bmatrix} A_{o1} \\ A_{o2} \\ \ldots \\ A_{oI} \end{bmatrix} = \begin{bmatrix} \beta_1 \\ \beta_2 \\ \ldots \\ \beta_I \end{bmatrix}. \tag{A.8}$$

Here the matrix $[g_{ij}]$ is called the least-squares matrix, and the vector $\{\beta_j\}$ is called the transformation vector. The A_{oi} are found by inverting the least-squares matrix:

$$\{A_{oi}\} = [g_{ij}]^{-1}\{\beta_j\}. \tag{A. 9}$$

b. Iterative Least-Squares Method

A unique least-squares analysis cannot be used to find the λ_i because the resulting equations are nonlinear. Therefore the difference between the actual activities A_n and the computed activities from an initial guess or previous (ℓ^{th}) iteration a_n^ℓ is expanded in a first-order Taylor series:

$$A_n - a_n^\ell \doteq \sum_i \left(\partial a_n^\ell / \partial A_{oi}\right) \Delta A_{oi} + \sum_i \left(\partial a_n^\ell / \partial \lambda_i\right) \Delta \lambda_i. \tag{A. 10}$$

Equation A. 10 and the resulting normal equations are linear in the ΔA_{oi} and $\Delta\lambda_i$, so these quantities, if not the original λ_i, can be computed by a least-squares analysis. The $\left(\partial a_n^\ell / \partial A_{oi}\right)$ are just the f_{in} of (A. 2). The $\left(\partial a_n^\ell / \partial \lambda_i\right)$ are computed by the MATRIX routine. The $\Delta\lambda_i$ and ΔA_{oi}, which are found from the unique least-squares analysis based on (A. 10), are added to the previous estimates of λ_i and A_{oi}. The new estimates are used to compute the $a_n^{\ell+1}$. The iterations continue until 25 iterations have been made, or until the variance of fit (the left side of Eq. A. 4) and the A_{oi} and λ_i remain constant to one part in 10^6.

We found that sometimes the iterative method would diverge, ending with an overflow in the computations. The reasons for this divergence are not clear. Since the iterative feature of the Frantic routines was not essential to finding the initial activities, no attempt was made to find the cause of the overflow.

c. Program Flow

When an "ANALYZ" card is read, (MAIN) transfers control to FRANIC, the governing program for the Frantic analyses. The operations performed by FRANIC are the following.

1. Before analyzing the first sample, the subroutine CHANGE is called to move any data that are waiting in bottom common to the "saved tape" common storage area. STDCAL is called to compute the rates from the background sample observations, and/or the normalization factors from the standard sample observations, if these samples were identified on "BKGD" and/or "STD" cards.

2. The Frantic control data (read following a previous "FRANIC" card) which correspond to the Frantic identification number in Field 3 of the "LABEL" card for the sample are transferred to bottom common, which will now be used by the Frantic routines, by the subprogram INPUT. If either the identification number or the control data corresponding to that number is missing, an error comment is printed, and this step is

repeated for the next sample.

3. The DATA subroutine is then called to compute the activation rates from the raw data for each observation (the counts C, and the observation length D), as well as the dead time τ. The normalization factor F and the background rate B are determined by the NORMAL and NOISE routines, which use the starting time of the observation T. The raw count rate R is computed from the equation

$$R = FC/D. \tag{A.11}$$

The corrected activity A is computed by using the equations

$$X \equiv R/(1-R\tau), \tag{A.12}$$

$$A = X - B. \tag{A.13}$$

The fractional variance of each point $(\delta A/A)^2$ is computed from the equations:

$$(\delta R/R)^2 = (\delta F/F)^2 + (\delta C/C)^2 + (\delta D/D)^2;$$

$$= (\delta F/F)^2 + 1/C + (\delta D/D)^2; \tag{A.14}$$

$$(\delta X/X)^2 = (\delta R/R)^2 + (X\delta\tau)^2 + X^2\tau^2(\delta R/R)^2; \tag{A.15}$$

and finally

$$(\delta A/A)^2 = [(\delta X)^2+(\delta B)^2]/A^2. \tag{A.16}$$

4. If there are minus flags on the observation length or the counts (transferred from the sample number by TAPE), or if $(\delta A/A)^2$ computed from (A.16) exceeds 0.0625 (or the value read from a previous "MAXVAR" card), the observation is deleted from the analysis. If A from (A.13) is negative, DATA assumes that the activity of this sample has decayed to the background level, so no more points are examined.

5. If no more than 2 · JMAX points have been accepted by DATA (where JMAX is the number of components for which the analysis is to be made), an error comment is printed, and DATA goes back to step 2 for the next sample.

6. The weight W of each point is computed according to the value of ID for this analysis:

If ID = 1, W = 1.

If ID = 2, $W = 1/(\delta A)^2$.

If ID = 3, $W = 1/(\delta A/A)^2$.

7. If IS(6) $\neq$ 0, the decay constants λ are computed from the half-lives which were read from columns 1-12 of the "PG" cards. If IS(6) = 0, the λ were read in directly.

8. DATA returns control to FRANIC, which calls GUESS to guess a λ if IC = 1. The first λ returned by GUESS is computed by the equation

$$\lambda = \log_e (A_1/A_N)/(T_N-T_1),$$

where A_1, T_1 and A_N, T_N are the activities and starting times of the first and last observations for the sample. On subsequent callings for the same analysis GUESS returns for the new λ a number which is 3 or 10 times the value of the largest λ from the previous iterations, the number depending on the value of IS(1) (nonzero or zero).

9. FRANIC then calls LESFIT to compute the least-squares curve. If one or more of the half-lives are not fixed (or if IC = 1), LESFIT uses the iterative least-squares method. Any partial derivatives with respect to the λ are evaluated by MATRIX. The least-squares matrices are inverted by MATINV, which uses the library matrix-inversion routine XSIMEQ. Any overflows occurring in the LESFIT, MATRIX, or MATINV (XSIMEQ) routines cause an error comment to be printed, and control to be transferred to the skeleton program AUSWEG. AUSWEG prints a breakpoint post mortem of the bottom common storage, and then calls A2SWEG, the secondary entry to FRANIC, which goes to step 2 with a new sample.

10. After the curve-fitting routine has been completed, FRANIC calls OUTPUT to print the results for that sample.

11. If IC = 1, and more half-lives (λ's) are to be guessed, the program goes to step 8. Otherwise FRANIC retrieves the values of $A(T')/\lambda$ and $\delta A(T')/\lambda$ for the component whose half-life (or λ) was on the first "PG" card for that Frantic control data. T' is the extrapolation time (see 30. The "TAU" card). These quantities will be used for comparisons. The next sample is then analyzed, starting with step 2.

12. When all samples have been analyzed, FRANIC calls ZPRINT to make any desired comparisons (see section A. 7). FRANIC then returns program control to (MAIN).

A.6 BEAM PROGRAMS

The Beam routines were written to compute the effective dose given to each sample from the neutron flux during the irradiation $\phi(t)$. If the irradiation time is much less than the half-lives of the daughter products of interest, the dose is just

$$\phi_{eff} = \int_0^{t_o} \phi(t)\, dt,$$

where t_o is the length of the irradiation. If the irradiation time is not much shorter than the half-lives of interest, but $\phi(t) = \phi_o = \text{const.}$, then the effective dose for each component (λ) is

$$\phi_{eff} = (\phi_o/\lambda)\left(1-e^{-\lambda t_o}\right),$$

where λ is the decay constant. If neither of these conditions is true, then a more complicated scheme must be used to compute the effective dose.

The differential equation describing the change in N, the number of daughter-product atoms per unit volume of sample, is

$$dN(t)/dt = \Sigma\phi(t) - \lambda N(t), \tag{A.17}$$

where Σ is the macroscopic cross section. If $N(0) = 0$, the number of daughter-product atoms at time t_o is given by

$$N(t_o)/\Sigma = \phi_{eff} = e^{-\lambda t_o} \int_0^{t_o} \phi(t)\, e^{\lambda t}\, dt. \tag{A.18}$$

In the Beam programs it is assumed that the flux varies linearly between times t_1 and t_2 at which the flux is observed from a strip chart recorder:

$$\phi(t) = \phi(t_1) + [\phi(t_2)-\phi(t_1)][(t-t_1)/(t_2-t_1)], \qquad (t_1 \leq t \leq t_2). \tag{A.19}$$

Substitution of (A.19) in (A.18) and considerable algebraic manipulation yield the algorithm used by the Beam programs:

$$\phi_{eff}(t_n) = \phi_{eff}(t_{n-1})\, e^x + \phi(t_{n-1})\,(t_n-t_{n-1})\left[\frac{e^x-1}{x}\right] + [\phi(t_n)-\phi(t_{n-1})]\,(t_n-t_{n-1})\left[\frac{e^x-1-x}{x^2}\right], \tag{A.20}$$

where

$$x = -\lambda(t_n-t_{n-1}), \tag{A.21}$$

and t_{n-1} and t_n are two successive observation times from the strip-chart recorder.

The functions of x in brackets in (A.20) are evaluated by two FAP-coded functions:

$$EXP1F(x) = (e^x - 1)/x \tag{A.22}$$

and

$$EXP1XF(x) = (e^x - 1 - x)/x^2. \tag{A.23}$$

If $|x| \geq 1$, these functions are evaluated directly, by using the library routine for e^x. If $|x| < 1$, these functions are evaluated more accurately by the power-series

$$EXP1F(x) = 1 + \frac{x}{2!} + \frac{x^2}{3!} + \frac{x^3}{4!} + \ldots \tag{A.24}$$

and

$$EXP1XF(x) = \frac{1}{2!} + \frac{x}{3!} + \frac{x^2}{4!} + \frac{x^3}{5!} \ldots . \tag{A.25}$$

In (A.24) and (A.25) up to 10 terms are used for an accuracy of at least one part in 10^7.

b. Program Flow

When a "BEAM" card is read by the SAMTAPE main program, (MAIN) transfers control to BEAM, the governing program for the effective dose calculations. The operations performed by BEAM are as follows:

1. Before processing the Beam data cards, the subroutine CHANGE is called to move any data from the sample-changer tape from bottom common to "saved tape" common, since the bottom common is also used for the Beam calculations.

2. The data from up to 200 Beam data cards are read and stored in the appropriate vectors in bottom common. When the 200^{th} card, a card with an illegal mnemonic in Field 1, a "CALC" card, or a "RETURN" card is encountered, the card-reading routine is terminated, and the cards are processed. This procedure reduces the computer time required by the programs, because of the organization of the input/output routines at the installations where these programs were run. The only exception to this procedure is the "FORMAT" card, which is processed as soon as it is read, since the following Beam data cards are read under the new format (see Data Card 44).

3. In processing the various Beam data cards, other routines are called. These routines are listed and described under the appropriate data card.

4. After the last card has been processed, BEAM returns control to (MAIN) if the last card read was a "RETURN" card. If it was the 200^{th} card read, or a "CALC" card, more Beam data cards are read as in step 2. If it contained an illegal mnemonic in Field 1, the programs are terminated with an error comment.

c. Interim Timer

Provision is made in the Beam programs to compute the total dose between two observation times. The use of this feature is described under the "Beam Observation Card."

d. Standard Input Format for the Beam Programs

Data cards for the Beam programs, like those for the SAMTAPE main program, are read, for the most part under a standard format. Only the "HEDING" and "FORMAT" cards temporarily suspend the standard format to read the next card under another format. The standard format for the Beam data cards consists of four fields:

Field 1: Columns 1-6 contain a control word of up to 6 characters, which must be left-adjusted to column 1. An improperly adjusted control word is treated as an illegal mnemonic.

Field 2: Columns 7-20 contain a floating-point number.

Field 3: Columns 21-30 contain a second floating-point number.

Field 4: Columns 31-36 contain a 6-character word, which is usually a comment, but may serve other purposes.

Columns 37-80 of the card are ignored. The cards are read under the Fortran Format (A6, E14.2, E10.5, A6); this format may be changed by using a "FORMAT" control card.

Floating-point numbers are punched in exponential form: 1.234×10^{5} becomes 1.234 E5; 1.235×10^{-4} becomes 1.235 E-4. Minus signs must be punched. If the exponent part of the number is zero, the exponent and the "E" may be omitted. The decimal point should be punched. The number following the E must be right-adjusted, since blanks are treated as zeros.

Blank cards, and cards with an asterisk in column 1 and blanks in columns 2-6, will be ignored.

e. Data Cards for the Beam Programs

The data cards which are read while the program is under control of the BEAM routine are described on the following pages. The same conventions are used that were used to describe data cards for the SAMTAPE main program. The card-numbering system is continued from the last SAMTAPE data card.

35. The Beam Observation Card.

Field 1: Must be left blank.

Field 2: The time of the observation. This is in the units on the time-scale of the strip-chart if the program is in the "CHART" mode (the normal mode of operation); the number of minutes which have elapsed since the last observation or "START" card if the program is in the "DT" mode; or the clock time (see note B) if the program has been changed to the "CLOCK" or "DATE" mode.

Field 3: The value of the flux $\phi(t)$ at the time of the observation. $\phi(t)$ is usually given as a fraction of full scale of the flux scale on the chart paper. The value of the full-scale flux is set by a "FLUX" card. The observation points should be chosen so that $\phi(t)$ between these points may be approximated as a straight line.

Field 4: Usually a 6-column comment, but may also contain the control words "ON ", "OFF" or "OFF*" for the interim timer (see below). If the program is in the "DATE" mode, Field 4 contains the date (see note C).

Subroutines Called: CHART, TIMDIV, Service Routines.

Use: The Beam observation cards are used to transmit the values of the flux and time of the observation points. Normally the program

is in the "CHART" mode, in which case the time is in the units of the time scale on the strip-chart. As written, the program assumes that the chart paper moves at the rate 5 minutes/inch, and that the numbers on the time scale (inches) repeat every 12 inches. The distance between the observation points must be less than the recycle length on the chart paper (12 inches). The values of the inverse speed of the chart paper and the recycle length may be changed from the set values of 5.0 and 12.0 by use of a "TSCALE" card. The mode of the program may be changed by a "MODE" card.

To process each Beam observation card, BEAM transfers control to CHART, which performs the following operations:

1. If the program is in the "CHART" mode, the clock time and the time which has elapsed since the last observation are computed using the TIMDIV routine. In the "DT" mode the clock time is computed using the service routines. In the "CLOCK" and "DATE" modes the elapsed time is computed. In the "DATE" mode the date is taken from Field 4 of the Beam observation card. In the "CLOCK" mode the date is assumed to be that on the preceding "START" card.

2. The total dose (computed from $\int\phi(t)dt$) and the effective dose (computed from Eq. A.20) for any half-lives which were read previously are brought up to date.

3. The clock times, the chart time (if the program is in the "CHART" mode), the current value of the flux $\phi(t)$, the current total dose $\int\phi(t)dt$, the contents of Field 4, and the effective dose for

each half life.

5. CHART then examines the first three characters of Field 4 for the word "ON ". If the word "ON " (there must be at least one blank following the "N"), the next three characters of the field are saved for a label, and the interim timer is started. On all future observation cards CHART looks for the word "OFF" in the first three columns of Field 4. When the word "OFF" is found, the interim timer is stopped, and an extra line including the times, the label, the elapsed time and total dose during the interim is printed. If an asterisk immediately follows the word "OFF" (= "OFF*"), the line of information is also punched.

The interim timer may be turned on and off as often as desired during the run. The interim timer should not be on when a "START" card is read. Note that the interim timer may not be used if the program is in the "DATE" mode.

6. After processing the interim timer requests in Field 4 (if any), CHART returns control to BEAM) to read a new Beam data card.

36. The Beam "START" Card.

Field 1:"START "

Field 2: The chart time when the run begins if the program is in the "CHART" mode; otherwise the clock time (see note B).

Field 3: The value of the flux at the beginning of the run (may be zero) as a fraction of full scale on the chart paper.

Field 4: The data (see note C) if the program is in the "CLOCK", "DT", or "DATE" modes. If the program is in the "CHART" mode, Field 4 is ignored.

Subroutines Called: START, BPRINT, TIMDIV ("CHART" mode only).

Use: The Beam "START" card must precede the first Beam observation card for the irradiation run. If the program is in the "CHART" mode, the chart time must have been set by a preceding "SETIME" card.

When a "START" card is read, BEAM transfers control to START, which resets the elapsed time, total dose, and effective dose registers, and calls BPRINT, a Fortran-coded subroutine, to print the page heading for a new run. Reference to a previous effective dose is deleted by a Beam "START" card. The Beam "START" card is not to be confused with the "START" card used by the SAMTAPE main program (card no. 2).

37. The "SETIME" Card.

Field 1: "SETIME"

Field 2: The chart time (as described for the Beam Observation Card, ---card no. 35).

Field 3: The clock time

Field 4: The date

Subroutines Called: SETDIV, Service Routines.

Use: The "SETIME" card is used to define the time at a point on the chart paper. It is only needed when the program is in the "CHART" mode. It usually appears before the first "START" card for each irradiation run, but may also be used during the run (when the recorder runs out of paper during a run, for example, and new paper must be installed, and the recorder restarted). BEAM converts the time and date to the internal formats using the service routines, and then calls SETDIV to set the chart time.

38. The "FLUX" Card.

Field 1: "FLUX "

Field 2: The base-line setting on the chart paper when the flux is zero. Field 2 is usually zero, but may be used to correct for zero-drift in the recorder.

Field 3: The value of the flux when the pointer on the recorder is at full scale.

Field 4: Not used.

Subroutines Called: FSCALE, FBASE

Use: The flux $\phi(t)$ reported on the line of print which is generated for each Beam observation card is computed from

$\phi(t)$ = [(Contents of Field 3 of the Beam obs. card) - FBASE]·FSCALE

where FBASE is from Field 2, and FSCALE is from Field 3 of the "FLUX" card. If no "FLUX" card is read, it is assumed that FBASE = 0.0, and FSCALE = 10^5. FBASE and FSCALE may be changed only by a "FLUX" card.

39. The "TSCALE" Card.

Field 1: "TSCALE"

Field 2: The inverse rate of travel of the chart paper in minutes per chart unit. (TSCALE)

Field 3: The number of chart units per cycle. (DELTAT)

Field 4: Not used.

Subroutines Called: TSCALE, DELTAT

Use: The "TSCALE" card may be used to reset the inverse rate of travel of the chart paper from its original value of 5 minutes/inch, and the cycle length from its original value of 12 inches.

40. The "JUMP" Card.

Field 1: "JUMP "

Field 2: Not used.

Field 3: The value of the flux (fraction of full scale) after a step change.

Field 4: Not used.

Subroutines Called: None.

Use: The "JUMP" card is used to indicate a step change in the flux.

41. The "HAFLIF" Card.

Field 1: "HAFLIF"

Field 2: The half-life in minutes.

Field 3: A Frantic identification number. The half life in Field 2 must be the same as the half-life (or corresponding λ) on the first "PG" card in the corresponding "FRANIC" control deck.

Field 4: A 6-column label which is used for output.

Subroutines Called: None.

Use: A "HAFLIF" card for each component for which an effective dose is to be computed must appear before the first Beam "START" card. Only 8 components may be entered at one time. After 8 "HAFLIF" cards have been read, succeeding "HAFLIF" cards will be ignored. In order to erase the half-lives presently being used, a "NOLIF" card, described below, should be inserted in the Beam data deck.

42. The "NOLIF" Card.

Field 1: "NOLIF "

Fields 2-4: Not used.

Subroutines Called: None.

Use: A "NOLIF" card is used to erase old values of the half-lives and labels, so that new ones may be read.

43. The Beam "HEDING" Card.

Field 1: "HEDING"

Fields 2-4: Ignored.

Subroutines Called: None.

Use: The normal Beam input format is suspended; the 80 columns of the following card are used as a page heading for the Beam program output. Note: This card should not be confused with the SAMTAPE "HEDING" card (card no. 18).

44. The Beam "FORMAT" Card.

Field 1: "FORMAT"

Fields 2-4: Ignored.

Subroutines Called: None.

Use: The normal Beam input format is suspended; columns 1-72 of the following card replace the format vector (A6,E14.2, E10.5,A6) under which the Beam data cards are usually read. The new format should be constructed so that the four fields on the Beam data cards are properly converted. It would be possible with a new Format to read in more than one observation point per card.

46. The Beam "DOSE" Card.

Field 1: "DOSE ", "DOSE* ". or "DOSEX "

Field 2: The clock time for which the effective dose rates are desired, if Field 4 contains the date; the number of minutes from the time of the last observation point, if Field 4 contains "DT "; or unused if Field 4 contains "NOW ".

Field 3: The total accumulated counts to be used for normalization; blank if no normalization is desired.

Field 4: The date of the effective dose, "DT " or "NOW ".

Subroutines Called: EFCONT, Service Routines.

Use: When a "DOSE" Card is read, BEAM transfers control to EFCONT. If Field 4 contains "NOW ", the effective doses, updated to the last observation point are removed from the erasable bottom common, to the "saved beam" common, for later use by the SAMTAPE program. If Field 4 contains "DT ", each effective dose is multiplied by $\exp(-\lambda\Delta t)$, where λ is the decay constant for that half-life, and Δt is the contents of Field 2. If Field 4 contains the date, Δt is computed from that date (and clock time in Field 2) and the time of the last observation point.

If Field 3 is neither zero nor blank, each effective dose is normalized by multiplication by the factor

(Contents of Field 3)/$\int\phi(t)dt$.

If Field 1 contains "DOSE " the effective doses are printed. If Field 1 contains "DOSE* ", the results are also punched. If Field 1 contains "DOSEX " no printing or punching takes place.

NOTE: The values of the effective doses which are stored in bottom common are not changed by a "DOSE" card. The numbers which are stored in "saved beam" common by the last "DOSE" card. are the

ones which will be used for comparisons with the results of the Frantic analyses (by the subroutine ZPRINT). If no SAMTAPE "TAU", "ENDRUN" or "NODOSE" card intervenes between the "DOSE" card and the "ANALYZ" card, the time of the effective dose will be used to determine the extrapolation time used by FRANIC. The BEAM "DOSE" card described here should not be confused with the SAMTAPE "DOSE" card (card no. 32).

46. The "MODE" Card.

Field 1: "MODE "

Fields 2-3: Not used.

Field 4: "CLOCK ", "DT ", "DATE ", or "CHART " .

Subroutines Called: None.

Use: A "MODE" card is used to change the interpretation of Field 2 and Field 4 of the Beam observation card and the Beam "START" Card.

47. The "CALC" Card.

Field 1: "CALC "

Fields 2-4: Ignored.

Subroutines Called: None.

Use: When a"CALC"card is read, the card-reading routine is terminated, and BEAM begins to process the cards already read. After the last card is processed, BEAM continues to read more cards.

48. The "RETURN" Card.

Field 1: "RETURN"

Fields 2-4: Ignored.

Subroutines Called: None.

Use: When a "RETURN" card is read, the card-reading routine is terminated, and BEAM begins to process the cards already read. After the last card has been processed, BEAM returns control to the SAMTAPE main program. The "RETURN" card should be the last card in the BEAM data deck.

A.7 ZPRINT COMPARISON ROUTINE

ZPRINT is called after a Frantic analysis, and may be recalled by using one or more "COMPAR" cards following the "ANALYZ" card. Its purpose is to provide a series of ratios which will be useful in evaluating the results of the foil activations. The main data inputs are the activities at the extrapolated time divided by the decay constants λ ... $A(T')/\lambda$, as well as the standard deviation in this quantity. Note that these ratios are labeled A(N) in the output (a sample output is shown in Table A.2). If effective dose information is available, a summary is printed, and each A(N), where N is the sample number, is divided by the appropriate dose. If in addition, Field 4 of the "ANALYZ" or "COMPAR" card contains the number of a successfully analyzed sample, each A'(N) is ratioed with the A' for that sample. Standard deviations are also given for all ratios.

If no effective dose information is available, the only meaningful ratios that can be made are among samples with the same decay schemes. So, all samples with a given Frantic identification number are ratioed with the sample whose number appeared in Field 3 of the "FRANIC" card for that Frantic identification number.

a. Arrangement of Cards in the Data Deck

The versatility of the SAMTAPE programs allows almost any card but an observation card or a control card such as an "ANALYZ" or "PRINT" card to be the first card in the data deck. To ensure that all numbers that will be needed to process an observation or control card are in the memory when that card is read, the following grouping of the cards is suggested.

Group 1: Cards that are used in every data set, including the data cards from the Frantic analysis, "HAFLIF" cards (preceded by a "BEAM" card and followed by a "RETURN" card).

Group 2: Data cards for the Beam programs (preceded by a "BEAM" card). The first card for each beam run should be a "HEDING" card to allow easy identification of the data cards for that run. The "DOSE" cards for each run should be the last cards in the Beam data deck before the "RETURN" card.

Group 3: Data cards for a sample-changer run. The first cards should include a "HEDING" card, a "START" card, a "BETWN" card, a "RECYC" card, "LABEL" cards, and "COUNT" cards. "STD", "NORM", and "BKGD" cards may be included. Then come the SAMTAPE observation cards, interspersed with any required "RESTAR", "PAUSE" or "COUNT" cards that may be required.

Group 4: Output cards, such as "PRINT", "ANALYZ", and "COMPAR". Note that any number of analyses, printouts, and comparisons may be made with the same observation data. Various parameters such as the number of the standard sample may be changed before each new analysis or print request. The changes that may be made before a "COMPAR" card are more restricted (see Card 22.).

Additional data decks containing the cards described in groups 2-4 may follow. Note

that groups 2 and 3 could be interchanged. The last card in the data deck should be a "QUIT" card to cause a normal termination of the programs. If the system library contains the required diagnostic routines, post mortem request cards (which are not a part of the data deck) may follow the "QUIT" card. These cards are not processed if the program terminates with the "QUIT" card; however, in case of an error stop the diagnostic routines scan the data deck for the post mortem cards, and dump the desired areas of the computer memory.

A sample input deck is shown in Table A. 1. The resultant output from the ZPRINT comparison routine is shown in Table A. 2.

TABLE A.1 SAMPLE INPUT DECK

```
*       DATA
TIMERR          .02
MAXSAM  25
FRANIC    1       5.
URANIUM ANALYSIS WITH TWO HALF-LIVES
U30.   U30.       2 2 3             99  99   99   99   99   99
425.
31.6
FRANIC    2         3.
ANALYSIS FOR SI-31  BACKGROUND SUBTRACTED
SI31-BSI31        1 2 3             99  99
157.2     E00   0.
FRANIC    3         2.
ANALYSIS FOR MN-56           BACKGROUND SUBTRACTED

MN-56B            1 2 3             99  99
154.6     E00     0.
FRANIC    5         4.
ANALYSIS FOR F-18         BACKGROUND SUBTRACTED
F18B              1 2 3             99  99
110.      E00
FRANIC    4         3.        IODINE
ANALYSIS FOR I-126     BACKGROUND SUBTRACTED
       I126       1 2 3             99  99  99
1.9520000E04      0.
STD       1        784.      BA*133
BEAM
HAFLIF    31.6                1.      U-1
HAFLIF   425.                   1.   U-2
HAFLIF   157.2               2.      P-SI31
HAFLIF   154.6              3.       FEMN56
HAFLIF         1.952E4               I-126
HAFLIF   110.           5.           F-18
HEDING
STANDARDS WITH NO BLANKET ON ALUMINUM CART
SETIME 4.00           1050.         03/26
FLUX     .02             3.E04
START  4.55              .05
       4.70              .054
       4.74              .385
       4.80              .35
       4.82              .40
       4.90              .70
       5.83              .698
       5.92              .65
       6.00              .68
       7.25              .615
       7.65              .57
       7.80              .66
```

TABLE A.1 SAMPLE INPUT DECK (CONT.)

```
        8.60                .64
        8.80                .648
        9.50                .572
       11.25                .576
         .70                .501
        2.75                .51
        7.50                .45
       11.00                .402
        2.38                .394
        3.75                .386
        4.10                .40
        7.00                .40
         11.                .354
        1.40                .36
        1.60                .05
DOSE*    1451.      2072.    E3  3/27     PUNCH RESULTS
DOSE                2.072 F06NOW        USE IN PROGRAM
RETURN
HEDING                                  MARCH 26,1964
TEST OF STANDARDS WITH NO BLANKET IN PLACE
LABEL    2        5       FC-S
LABEL    3        1       UT-S
LABEL    4        1       UB-S
LABEL    5        3       EA-S
LABEL    6        2       PA-S
START     1337.           MAR 26
BETWN           0.27
RECYC     1.38166667
*       SHIFT ELAPSED TIME COUNTER.
RESTAR     1357.17        MAR 26
COUNT          3000.       N
COUNT           900.       B
STD      1      980.       BA-133
BKGD            13.0
         1       101       B
         2       324       N
COUNT           300.       B
         3       128       B
         4       146       B
         5       103       N
         6       195       N
PAUSE           2.25
         1       314       N
         2       367       N
         3       202       B
         4       197       B
         5       107       N
         6       203       N
```

TABLE A.1 SAMPLE INPUT DECK (CONT.)

```
          4        241     B
          5        122     N
          6        221     N
          1        312     N
COUNT             300.    T
          2        389     N
          3        235     B

*        (SOME ACTUAL DATA CARDS WERE DELETED TO
*            SHORTEN THE TABLE.)

          1        324     N
          2       2017     T
          3       1009     B
          4       1146     B
          5       5672     N
          6        837     T
          1        319     N
          2       2064     T
          3       1035     B
          4       1310     B
          5        918     T
          6       1143     T
          1        316     N
          2       2279     T
          3       1238     B
          4       1250     B
          5       1072     T
          6       1125     T
          1        312     N
          2       2025     276     MANUAL COUNT STOP
PRINT
ANALYZ    2   6.           2
STD       1
ANALYZ    2   6.           2
HEDING
TEST OF STANDARDS WITH NO BLANKET IN PLACE     TAUD=4.E-6 MIN. ERROR=2
TAUD            4.
DTAUD             2.
ANALYZ    2   6.           2
NORM            1.
ANALYZ    2   6.           2
QUIT
FORTRAN PM  (/77461,/41250)  DUMP COMMON STORAGE IF ERROR
```

TABLE A.2 SAMPLE SUMMARY OF RESULTS

TEST OF STANDARDS WITH NO BLANKET IN PLACE

COUNTS STARTED 1337.00 ON MAR 26

EFFECTIVE DOSE AT 1338.00 ON MAR 26, TOTAL DOSE = 2.072E 06

M	LABEL	HALF-LIFE	LAMBDA	EFF. DOSE
1	U-1	3.160E 01	2.194E-02	4.709E 05
2	U-2	4.250E 02	1.631E-03	1.789E 06
3	P-SI31	1.572E 02	4.409E-03	1.413E 06
4	FEMN56	1.546E 02	4.483E-03	1.405E 06
5	I-126	1.952E 04	3.551E-05	2.065E 06
6	F-18	1.100E 02	6.301E-03	1.216E 06

A(N) = CPM/LAMBDA AT 1338.0 ON MAR 26 (1.0 MIN. AFTER COUNTS STARTED).

A'(N) = A(N)/DOSE(M).

R(N) = A'(N)/A'(2).

N	SAMPLE	A(N)	DA(N)	A'(N)	DA'(N)	M	R(N)	DR(N)	MAR 26
2	FC-S	1.69E 05	1.33E 03	1.39E-01	1.09E-03	6	1.00E 00	7.86E-03	MAR 26
3	UT-S	3.53E 04	3.19E 03	1.97E-02	1.78E-03	2	1.42E-01	1.29E-02	MAR 26
4	UB-S	3.57E 04	1.86E 03	2.00E-02	1.04E-03	2	1.43E-01	7.57E-03	MAR 26
5	EA-S	7.62E 05	2.74E 03	5.42E-01	1.95E-03	4	3.89E 00	3.37E-02	MAR 26
6	PA-S	4.14E 05	1.51E 03	2.93E-01	1.07E-03	3	2.10E 00	1.82E-02	MAR 26

RATES NORMALIZED TO SAMPLE 1 FOR A 'STD' RATE OF 980.00 CPM.

AVERAGE RATE = 940.661 STD. DEV. = 4.120

AVERAGE BACKGROUND = 13.00 CPM.

TABLE A.2 SAMPLE SUMMARY OF RESULTS (CONTINUED)

TEST OF STANDARDS WITH NO BLANKET IN PLACE

COUNTS STARTED 1337.00 ON MAR 26

EFFECTIVE DOSE AT 1338.00 ON MAR 26, TOTAL DOSE = 2.072E 06

M	LABEL	HALF-LIFE	LAMBDA	EFF. DOSE
1	U-1	3.160E 01	2.194E-02	4.709E 05
2	U-2	4.250E 02	1.631E-03	1.789E 06
3	P-SI31	1.572E 02	4.409E-03	1.413E 06
4	FEMN56	1.546E 02	4.483E-03	1.405E 06
5	I-126	1.952E 04	3.551E-05	2.065E 06
6	F-18	1.100E 02	6.301E-03	1.216E 06

A(N) = CPM/LAMBDA AT 1338.0 ON MAR 26 (1.0 MIN. AFTER COUNTS STARTED).

A'(N) = A(N)/DOSE(M).

R(N) = A'(N)/A'(2).

N	SAMPLE	A(N)	DA(N)	A'(N)	DA'(N)	M	R(N)	DR(N)	MAR 26
2	FC-S	1.62E 05	1.28E 03	1.34E-01	1.05E-03	6	1.00E 00	7.87E-03	MAR 26
3	UT-S	3.33E 04	3.07E 03	1.86E-02	1.72E-03	2	1.39E-01	1.29E-02	MAR 26
4	UB-S	3.38E 04	1.80E 03	1.89E-02	1.01E-03	2	1.42E-01	7.61E-03	MAR 26
5	EA-S	7.31E 05	2.62E 03	5.20E-01	1.87E-03	4	3.90E 00	3.37E-02	MAR 26
6	PA-S	3.97E 05	1.45E 03	2.81E-01	1.02E-03	3	2.10E 00	1.82E-02	MAR 26

RATES NORMALIZED TO SAMPLE 1 FOR A 'STD' RATE OF 940.66 CPM.

AVERAGE RATE = 940.661 STD. DEV. = 4.120

AVERAGE BACKGROUND = 13.00 CPM.

TABLE A.2 SAMPLE SUMMARY OF RESULTS (CONTINUED)

TEST OF STANDARDS WITH NO BLANKET IN PLACE TAUD=4.E-6 MIN. ERROR=2.E-6 MIN.

COUNTS STARTED 1337.00 ON MAR 26

EFFECTIVE DOSE AT 1338.00 ON MAR 26, TOTAL DOSE = 2.072E 06

M	LABEL	HALF-LIFE	LAMBDA	EFF. DOSE
1	U-1	3.160E 01	2.194E-02	4.709E 05
2	U-2	4.250E 02	1.631E-03	1.789E 06
3	P-SI31	1.572E 02	4.409E-03	1.413E 06
4	FEMN56	1.546E 02	4.483E-03	1.405E 06
5	I-126	1.952E 04	3.551E-05	2.065E 06
6	F-18	1.100E 02	6.301E-03	1.216E 06

A(N) = CPM/LAMBDA AT 1338.0 ON MAR 26 (1.0 MIN. AFTER COUNTS STARTED).

A'(N) = A(N)/DOSE(M).

R(N) = A'(N)/A'(2).

N	SAMPLE	A(N)	DA(N)	A'(N)	DA'(N)	M	R(N)	DR(N)	MAR 26
2	FC-S	1.63E 05	1.29E 03	1.34E-01	1.06E-03	6	1.00E 00	7.93E-03	MAR 26
3	UT-S	3.33E 04	3.08E 03	1.86E-02	1.72E-03	2	1.39E-01	1.29E-02	MAR 26
4	UB-S	3.38E 04	1.80E 03	1.89E-02	1.01E-03	2	1.41E-01	7.60E-03	MAR 26
5	EA-S	7.37E 05	2.59E 03	5.25E-01	1.85E-03	4	3.92E 00	3.40E-02	MAR 26
6	PA-S	3.99E 05	1.44E 03	2.82E-01	1.02E-03	3	2.11E 00	1.84E-02	MAR 26

RATES NORMALIZED TO SAMPLE 1 FOR A 'STD' RATE OF 940.66 CPM.

AVERAGE RATE = 940.661 STD. DEV. = 4.120

AVERAGE BACKGROUND = 13.00 CPM.

TABLE A.2 SAMPLE SUMMARY OF RESULTS (CONTINUED)

TEST OF STANDARDS WITH NO BLANKET IN PLACE TAUD=4.E-6 MIN. ERROR=2.E-6 MIN.

COUNTS STARTED 1337.00 ON MAR 26

EFFECTIVE DOSE AT 1338.00 ON MAR 26, TOTAL DOSE = 2.072E 06

M	LABEL	HALF-LIFE	LAMBDA	EFF. DOSE
1	U-1	3.160E 01	2.194E-02	4.709E 05
2	U-2	4.250E 02	1.631E-03	1.789E 06
3	P-SI31	1.572E 02	4.409E-03	1.413E 06
4	FEMN56	1.546E 02	4.483E-03	1.405E 06
5	I-126	1.952E 04	3.551E-05	2.065E 06
6	F-18	1.100E 02	6.301E-03	1.216E 06

A(N) = CPM/LAMBDA AT 1338.0 ON MAR 26 (1.0 MIN. AFTER COUNTS STARTED).

A'(N) = A(N)/DOSE(M).

R(N) = A'(N)/A'(2).

N	SAMPLE	A(N)	DA(N)	A'(N)	DA'(N)	M	R(N)	DR(N)	MAR 26
2	FC-S	1.64E 05	8.06E 02	1.35E-01	6.63E-04	6	1.00E 00	4.92E-03	MAR 26
3	UT-S	3.35E 04	2.68E 03	1.87E-02	1.50E-03	2	1.39E-01	1.12E-02	MAR 26
4	UB-S	3.40E 04	1.56E 03	1.90E-02	8.75E-04	2	1.41E-01	6.53E-03	MAR 26
5	EA-S	7.40E 05	2.63E 03	5.27E-01	1.87E-03	4	3.91E 00	2.37E-02	MAR 26
6	PA-S	4.01E 05	1.29E 03	2.84E-01	9.10E-04	3	2.11E 00	1.24E-02	MAR 26

ABOVE RATES WERE MULTIPLIED BY 1.0000

AVERAGE BACKGROUND = 13.00 CPM.

A.8 SERVICE ROUTINES

The following routines are used throughout the SAMTAPE programs for input/output conversions, and to perform various computations. Details of the calling sequences may be found on the first pages of the source-deck listing of each routine in Appendix B.

The Date Input/Output Routines: CALENS and BCDATE

CALENS converts a 6-character word containing the date in the format described in Notes: Data Cards for SAMTAPE to the internal format used by the computer (the day in bits 21-35, the number of the month in bits 3-17 of the binary word—bits 0-35). CALENS first converts the month, then the day of the month. If the month cannot be converted, a word of zeros is returned. If the day cannot be converted, bits 3-17 will contain the month number, but the rest of the word returned will be zeros.

BCDATE converts a date in the internal format to the format given above for output purposes. The form "MAR 11" will always be used. The day of the month will always be converted if the month can be converted. If the month cannot be converted, "NEVER" is returned.

The Time Input/Output Routines: MINUT and TINUM

MINUT converts the clock time in the format given above to the internal format, which is minutes past the preceding midnight. TINUM performs the reverse calculation. Both formats are floating-point numbers.

The Chart-Time Routines: TIMDIV, SETDIV, TSCALE, and DELTAT

TIMDIV is used by the Beam programs to compute the clock time and date from the chart time. TIMDIV computes the time from an initial chart time, clock time, and date which were transmitted to the SETDIV routine. The entries TSCALE and DELTAT may be used by FAP routines to reset parameters (see Cards 35 and 39).

Space-Allocation Routines: XINDEX and SETX

XINDEX computes the linear position of the data for the first observation of a given sample in the data-storage arrays. The number of samples which share storage is transmitted to the SETX routine (see the discussion of the "MAXSAM" card – Card 7).

The Exponential Routines: EXPP, EXP1, and EXP1X

EXP1 and EXP1X perform the computations shown in Eqs. A.22 and A.24, and Eqs. A.23 and A.25, respectively. To avoid frequent recomputation of e^x in the Beam programs, the entry EXPP is used. If the argument x is different from the argument at the previous calling, EXPP calls the library routine EXP to compute e^x. If the arguments are the same, EXPP returns the previous result.

The Chart-Flux Routines: FLUX, FSCALE, FBASE

FLUX computes $\phi(t)$ from the reading of the flux on the strip chart, using the parameters FSCALE and FBASE.

APPENDIX B

Spectral Analysis Programs

B. 1 INTRODUCTION

The operation and input formats for the computer programs to deduce the neutron spectrum from a set of threshold-detector data are described in this appendix. These programs use the methods outlined in Section VI. These programs are written in either the Fortran or FAP languages for the IBM 709/7090/7094 computers, and are compatible with the operating systems in use in the summer of 1964 at the Computation Center, M. I. T., and the Cooperative Computation Laboratory, M. I. T. As in Appendix A, input and output is via magnetic tape, although the words "read a card" and "print" are used. The Fortran and FAP nomenclature is used in this discussion. A description of the most important variables is given in Table B. 1, along with the corresponding nomenclature from Section VI.

B. 2 SPECTRUM OPERATIONS

The basic input parameters to the SPECTRUM programs are the cross sections, the weight function, the energy range, and the threshold reaction rates. SPECTRUM is designed so that various combinations of these parameters may be used to compute $\phi(E)$ from Eq. 31. Additional cross sections may be read in, and SPECTRUM will compute the reaction rates for these data when $\phi(E)$ has been determined.

The flow diagram of the SPECTRUM programs is shown in Fig. B-1. The main program, as far as the computer monitor system is concerned, is MAIN1, which is a skeleton program that prints a storage map of the routines in the memory, and calls MAIN, the governing program for the SPECTRUM calculations. After the parameter card and the cross sections have been read, program control is directed by 5 control cards: WEIGHT, SETUP, ACT, CALC, and QUIT. Three other cards, the DATE, FACTOR, and page-title ("*") cards are used to supply additional information for calculations or for identifying output.

WEIGHT Control Card

Columns 7-72 of the WEIGHT control card contain a number and a code word. The number is NPOLY (<10), which is the maximum number of orthogonal polynomials to be formed. The control word is used by the SETW routine to determine which of the weight functions in the program deck is to be used to form the orthogonal polynomials. Three weight functions are now available:

$$\text{WGAUSS}(E) = c_1 + c_2(E+c_3)^{c_4} + c_5 \exp\left\{-(E-c_6)^2/c_7^2\right\}, \tag{B. 1}$$

$$\text{WMAX}(E) = c_1 + c_2(E+c_3)\exp\{-(E+c_3)/c_4\} + c_5 \exp\left\{-(E-c_6)^2/c_7^2\right\}, \tag{B. 2}$$

Table B.1. Nomenclature for spectral analysis.

Variable Name		
In Appendices B and G.	In Chapter 6	Description
A(I,J)		Erasable matrix
AC(J)[a]	a_j	Coefficients in Eq. 31.
ACT(J)	T_j	Input activities
ALABEL(J)		Labels for input activities (6-column BCD-word.
AX(J)	T_j	Input activities that are used to compute spectrum.
B(I,J)	b_{ij}	Polynomial coefficients in Eq. 33.
BO(I)	B_i	Normalization coefficients for orthogonal polynomials.
C(I,J)		Erasable matrix.
DAO(J)	δa_j	Standard deviation in AO(J)
DACT(J)	δT_j	" " in ACT(J)
DAX(J)	δT_j	" " in AX(J)
DPHI(I)	$\delta\phi$(ENERGY(I))	" " in ϕ(ENERGY(I))
EMAX		Maximum energy of spectrum in Mev, should be an even 0.1 Mev.
EMIN		Minimum energy of spectrum in Mev, should be an even 0.1 Mev.
ENERGY(J)	E	Vector with values of the energy each 0.1 Mev between EMIN and EMAX. ENERGY(J) = 0.1 J.
EXTRA(J)[b] FAC		Normalization factors for activities, which are read following a "FACTOR" card.
FSIG(J,I)	τ_{JI}	Fourier coefficients for all σ(E) which are read in.
IMAX		Index, = 10 EMAX
IMAXS(J)		10 x maximum energy for which J^{th} cross section is tabulated.
IMIN		Index = 10 EMIN
IMINS(J)		10 x threshold energy for J^{th} cross section.
JSIG(J)		Vector containing cross section numbers, in the order in which they were read.

Table B. 1. (continued)

Variable Name In Appendices B and G.	In Chapter 6.	Description
JTAU(J)		Vector with I.D. numbers of reactions to be used to compute spectrum, in the order in which they appear on "SETUP" card.
NACT		Number of activities that are read in.
NPOLY		Maximum number of polynomials to be computed.
NSIG		Number of cross sections read in.
NTAU	N	Number of reactions to be used to determine spectrum (determined from the number of I.D. numbers which appear on "SETUP" card).
PHI(J)	ϕ(ENERGY(2J))	Vector with computed spectrum.
PHIM(J)		PHI(J) - DPHI(J)
PHIP(J)		PHI(J) + DPHI(J)
PNOM(J,I)	p_j(ENERGY(I))	Tabulation of values of orthogonal polynomials.
SCALE		Scale factor for graph . > 1 if |PHIP(J)| or |PHIM(J)| > |PHI(J)|; < 1 to bring out details of small values of variables plotted. MUST NOT BE ZERO.
S(J)	S_J	Integrals in Eq. 45.
SIG(I,J)	σ_J(ENERGY(I))	Read-in cross sections.
SLABEL(J)		6-Column BCD label for J^{th} cross section.
TAU(I,J)	τ_{ij}	Fourier coefficients that are to be used to determine spectrum.
TAUINV(I,J)	τ'_{ij}	Inverse of TAU(I,J) matrix.
VECTOR(J)		Erasable vector.
WEIGHS(J)	w(ENERGY(2J))	Vector with weight function for graph-routine.
WEIGHT(J)	w(ENERGY(J))	Vector with weight function for calculations.
XLABEL(J)		Labels of reactions that are used to compute spectrum.

Notes: a: "O" in this column is "zero."

b: "FAC" is the name of the vector in the "MAIN" subroutine, "EXTRA" is used in other routines.

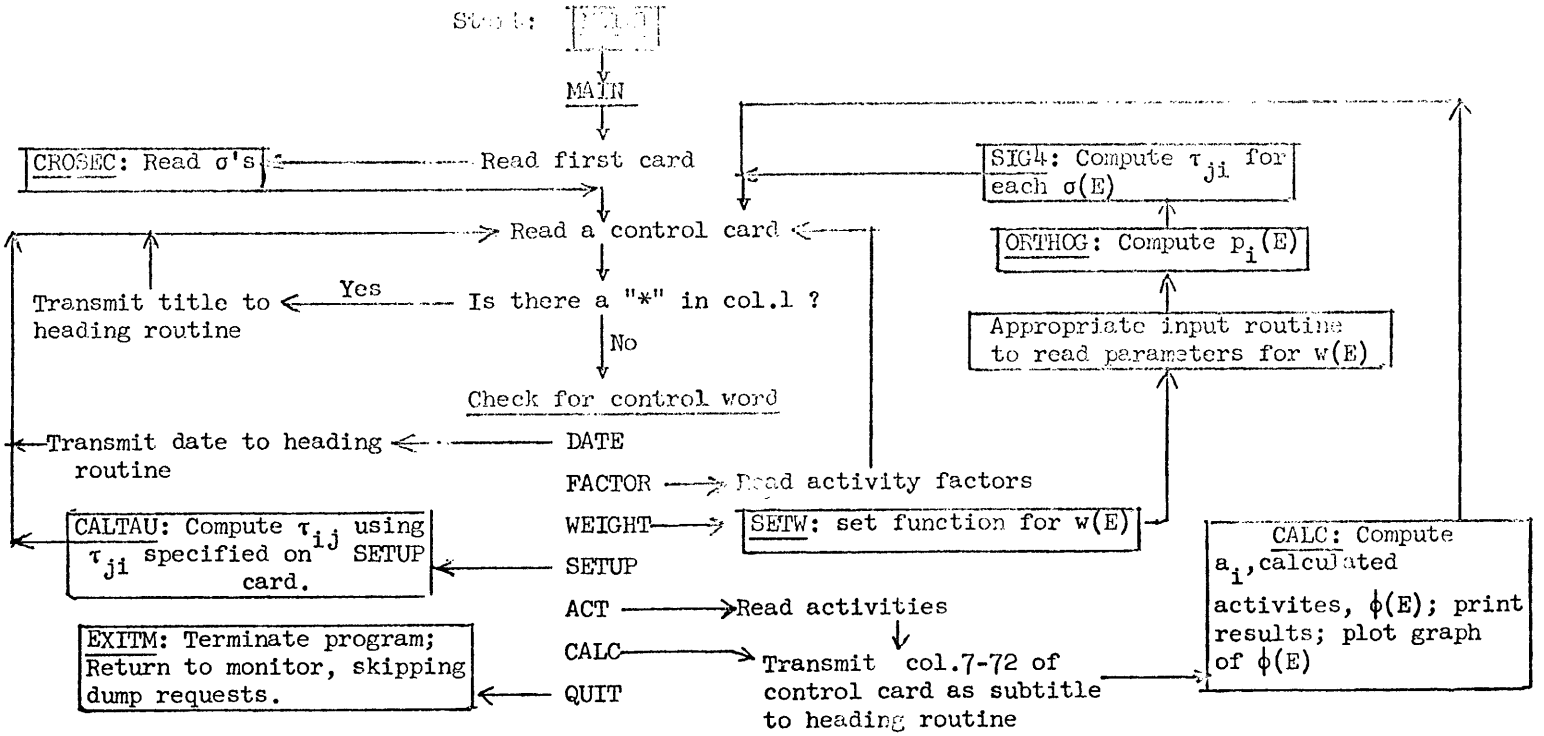

Fig. B-1. Flow diagram of spectrum routines.

$$\text{WDGUS(E)} = c_1 + c_2 \exp\left\{-(E-c_3)^2/c_4^2\right\} + c_5 \exp\left\{-(E-c_6)^2/c_7^2\right\}. \quad \text{(B. 3)}$$

The code words for these functions are GAUSS, MAXWEL, and DGAUSS, respectively.

The card(s) following the WEIGHT control card contain the input parameters for the chosen weight function. For the three functions above, only one card is required, containing the constants $c_1, \ldots, c_7$. If a weight function using the results of Impink's calculations were added, for example, the values of the flux for the various energy groups would be read at this point.

After the chosen weight function has been set up, control is transferred to ORTHOG, which reads a card containing EMIN and EMAX, and then computes the parameters for the orthogonal polynomials from Eqs. 43-46. To perform the numerical integrations in Eq. 45 and in the equation

$$\int w(E)\, p_i^2(E)\, dE = 1/B_i = 1/BO(I), \quad \text{(B. 4)}$$

the energy range EMIN-EMAX is divided into NPOINT subintervals, and Weddle's rule[38] is applied to each subinterval. Since the integrations are done on a compute-as-you-go basis, any number of subintervals may be used. A large number of subintervals unduly increases the running time for the program, and round-off errors prevent any additional accuracy. It is recommended that NPOINT = 25 in the cases of interest, where EMIN $\doteq$ 1 Mev, and EMAX = 14 Mev.

The Fourier coefficients for Eq. 34 are computed by the subroutine SIG4, which performs the integrations numerically with Simpson's rule,[38] and tabulated values of WEIGHT(I), PNOM(J, I), and SIG(I, K) at each 0. 1 Mev. Since Simpson's rule requires an odd number of points, the lowest energy point is dropped if the number of points is even.

SETUP Control Card

Columns 7-72 of the SETUP card contain 3-10 reaction I. D. numbers, each separated from the others by at least one blank space. These numbers specify which reactions are to be used to form the TAU and TAUINV matrices. The proper set of Fourier coefficients are selected from the FSIG matrix and stored in the TAU matrix, which is then inverted by the subroutine CALTAU, using the Computation Center, M. I. T. Library routine XSIMEQ.[49] A WEIGHT card (and associated data cards) must precede the first SETUP card.

ACT Control Card

Columns 5-6 of the ACT Control Card contain NACT, the number of reaction rates which is to be read. Columns 7-72 are used as a subtitle on each page of output. NACT cards follow, each with a reaction I. D. number, the reaction rate, the standard deviation in the reaction rate, and a 6-column label for that I. D. number. After the activity cards have been read, the activities that were selected by the previous SETUP card are used

with the TAUINV matrix to compute AO(J) for Eq. 32. Note that up to 20 different activities may be read; the additional activities are printed out for comparison with the activities for these reactions that are computed from Eq. 36.

After these computations are complete, four pages of output are generated, including tables with the AO(I), computed and input activities, and ϕ(E), each with the computed (and input) standard deviations (from Eqs. 39-41). A rough graph is plotted, including PHI(I), PHIP(I), PHIM(I), and WEIGHS(I). The scale of the graph is adjusted so that the quantity $[SCALE*(|PHI(I)|)_{max}]$ is at the top of the graph. The factor SCALE is read from the parameter card. Note that a WEIGHT card (and associated data cards) and a SETUP card must precede the first ACT card.

CALC Control Card

Columns 7-72 of the CALC card are used as a subtitle on each page of output. The CALC card initiates the same computations as does the ACT card, except that the previously read activities are used. For example, after an ACT card, a SETUP card and a CALC card could be used to determine the spectrum from a different combination of the previously read reaction rates.

FACTOR Control Card

Columns 7-72 of the FACTOR card contain NFAC ($\leq$20), the number of conversion factors to be read. The following NFAC cards each contain a code number, and a conversion factor by which future reaction rates and standard deviations with that code number will be multiplied as they are read in. Conversion factors that are not read are assumed to be 1.0.

For proper calculations, the activities must have the same dimensions as the cross sections. The use of the conversion factor allows activities to be read in other dimensions.

DATE Card

Columns 7-12 of the DATE card follow the page title on each page of output.

Page Title Card

Columns 2-72 of the page title card, which has an asterisk (*) in column 1, are used as the title of each page of output.

QUIT Card

The QUIT Card terminates the program. Its use is the same as that of the SAMTAPE QUIT card.

B.3 INPUT TO THE SPECTRUM PROGRAMS

The input formats for the Spectrum programs are described below. Data on control cards are in a free format, as described above. Other data are read by using Fortran Format Statements.[50]

Table B.2. Control card deck.

The contents of the control cards, and the input cards which follow the control cards (if any) are listed below. For a description of variables, see Table B.1 and the text.

Control Card			Following Cards (if any)	
Control[a] Word	Rest of Control Card Col.	Contents	Contents	Fortran Format
*	2-72	Page title	None	
DATE	7-12	Date	None	
FACTOR	7-72[b]	NFAC	NFAC cards, each with ID, FAC(ID)	(I2,E10.2)
WEIGHT	7-72[b]	NPOLY, Code word for wt. fn.	1. Input information for selected weight function. For the weight functions presently available (GAUSS, MAXWEL, DGAUSS) one card is necessary, which contains the constants $c_1,\ldots,c_7$.	(7E10.3)
			2. One card with EMIN, EMAX (integral multiples of 0.1 Mev).	(2F10.2)
SETUP	7-72[b]	Up to ten reaction ID numbers.	None	
ACT	5-6 7-72	NACT Subtitle	NACT cards, each with ID, ALABEL(ID), ACT(ID), DACT(ID)	(I2,1XA6,2E10.3)
CALC	7-72	Subtitle	None	
QUIT	Ignored		None (A QUIT card terminates the program.)	

Notes: a. Control word must be left-adjusted to column 1.
b. Fields (number(s) or control words) may be anywhere within specified columns of control card. At least one blank must separate fields.

TABLE B.3. SAMPLE INPUT DECK FOR 'SPECTRUM' PROGRAMS.

```
*     DATA
  7 25   1.25                    NSIG,NPOINT,SCALE(FOR GRAPH)
******* CROSS SECTION DECK GOES HERE (SEE APPENDIX D.)**************************
FACTOR   5
 1  186.                                URANIUM OF 8/28
 2  1.015                              PHOSPHORUS OF 8/28
 3  .831                       IRON OF  8/17
 4  8.75                        IODINE OF 8/17
 8  1.892                      RUSSIAN FLUORINE DATA
*INCREASED U AND P FACTORS, DGAUSSIAN WEIGHT FUNCTION
DATE  AUG 29
WEIGHT  4   DGAUSS
0.05       0.5       5.5       2.0       0.5        13.3      0.65
2.1         14.1
SETUP     1 3 4 8
ACT 5 GRAPHITE BLANKET - NO WALL.  'BEST' VALUES AT 5 CM
 1  UB 5  5.4        .5
 2  PB 5  103.       7.
 3 FEB 5  131.       5.
 4 IB 5   131.       10.
 8 FB 5   24.5       1.
ACT 5 GRAPHITE BLANKET - NO WALL  'BEST' VALUES AT 10 CM
 1 UB 10  4.3        1.
 2 PB 10  92.        5.
 3 FEB 10 107.       5.
 4 IB 10  97.        10.
 8 FB 10  17.6       .5
SETUP    1 2 3 4
CALC    TRY WITH NO FLUORINE DATA
QUIT
```

Parameter Card

The parameter card is the first card in the data deck. This card contains NSIG, NPOINT, and SCALE; it is read with the Format (2I3, E10.3).

Cross Sections

The cross section deck is shown in Appendix D. It is divided into NSIG subdecks. The first card of each subdeck is the cross-section header card, which contains the reaction ID number, SLABEL(ID), AMIN, and AMAX. Here AMIN and AMAX are the minimum and maximum energies (integral multiples of 0.1 Mev) for which the cross sections for that reaction are tabulated. The Format for the cross-section header card is (I2, 2XA6, 2F5.1). The values of $\sigma(E)$ are on the following cards (Format (10F7.1)). The cross-section values are arranged so that $\sigma(U-1.0+0.1)$ is in the first field (columns 1-7), $\sigma(U-1.0+0.2)$ is in the second field, ..., and $\sigma(U)$ is in the tenth field (columns 64-70). Here U is an integral multiple of 1 Mev. The first card after the header card contains $\sigma(AMIN)$, and the last card in each subdeck contains $\sigma(AMAX)$, each in its proper field.

Control Card Deck

The control card deck which follows the cross-section deck, contains control cards and associated data cards, as described in the operations section above. The formats for these cards are listed in Table B.2.

A sample input deck is shown in Table B.3. To save space, the presence of the cross-section deck is indicated by a row of asterisks.

B.4 OUTPUT FROM THE SPECTRUM PROGRAMS

Each ACT or CALC card generates four pages of printed output. In general this output is self-explanatory. In the graph of $\phi(E)$ negative numbers are reflected above the X-axis, and are plotted with a special set of symbols. A symbol key appears below each graph.

APPENDIX C

Toepler Pump Operation

C. 1 INSTALLATION

The Toepler pump should be well supported in an upright position in a large pan to catch the mercury if the pump should break. Wiring connections are made as shown in Fig. C-1. Care should be taken in sealing the ball-and-socket joints so that no undue stress is placed on the glass tubing. These joints should be opened before working on any part of the system, so that the stress of an accidental jerk will not be transmitted to the glass.

The lower chamber of the Toepler pump is filled with mercury through the side-arm connection to the safety reservoir. A funnel and care should be used to avoid mercury spills. Small mercury drops may be sponged up with a copper-wire brush wetted in dilute nitric acid. Gold is an even better sponge, so be careful of gold rings, watches, and so forth. Inaccessible drops should be covered with flowers of sulfur; the toxic mercury and (less toxic) sulfur combine to form the inert compound HgS.

Note: The control circuit shown in Fig. C-1 was designed for the author by a technician. The circuit works, but the author makes no claims for its reasonableness.

C. 2 OPERATION PROCEDURES

Before start-up the mercury level should be below the point Q; the by-pass stopcock, the valve to the pressure line, and the stopcock between the upper and lower chambers should be closed. The common contact should be shorted first to the upper contact and then to the lower one to be sure that the automatic system is operating. The vacuum pump for the vacuum line should be running. This pump should be an old one; the large volumes of gas which are pumped during the operation of the Toepler pump will soon ruin a good vacuum pump. The stopcock between the upper and lower chambers should be opened carefully to allow the residual gas in the safety reservoir to force the mercury into the upper chamber. If the mercury rises too fast it will hammer against the upper chamber and break it. When the mercury rise ceases, the pressure valve is opened just enough so that the mercury will continue to rise to open float valve A, and close the circuit between the upper and common contacts, activating the solenoid valve to connect the vacuum to the lower chamber. Be ready to close the stopcock between the two chambers if the solenoid valve does not operate. If it does, the vacuum will pull the mercury into the lower chamber. The pump will now cycle automatically. The furnace in Fig. 31 is evacuated when the mercury descends at the same levels in arms I and II.

To halt the operation, close the stopcock between the two chambers when the mercury is in the lower chamber but the circuit between the lower and common contacts is open. The batteries should be disconnected, and the pressure valve should be closed.

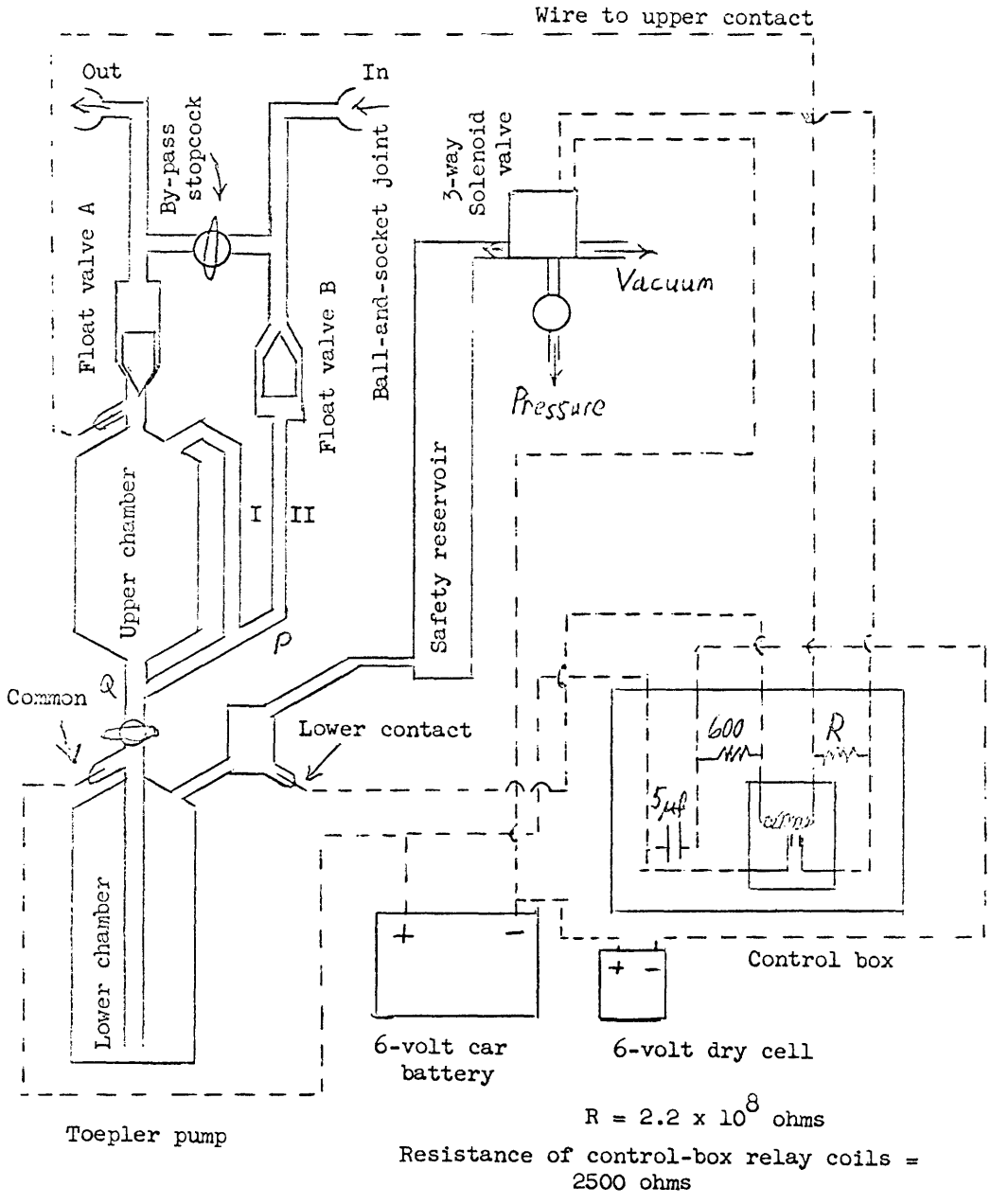

Fig. C-1. Schematic diagram of the Toepler pump and control circuitry.

APPENDIX D

Listing of Threshold Detector Cross Sections as They Appear in the 'SPECTRUM' Cross-Section Deck

APPENDIX D. LISTING OF THRESHOLD DETECTOR CROSS SECTIONS AS THEY APPEAR IN THE 'SPECTRUM' CROSS SECTION DECK.

THIS IS A LISTING OF THE CARDS AS THEY APPEAR IN THE CROSS SECTION DECK FOR THE 'SPECTRUM' PROGRAMS. THE NUMBER UNDER 'UNIT' IS THE CROSS SECTION IN MILLIBARNS AT THE ENERGY (IN MEV) IN THE LAST COLUMN. CROSS SECTIONS TO THE LEFT ARE FOR ENERGIES THAT ARE 0.1,0.2,ETC. MEV LESS.
THE CARD AT THE HEAD OF EACH REACTION IS THE CROSS-SECTION HEADER CARD DESCRIBED ON PAGE 283.

.1	.2	.3	.4	.5	.6	.7	.8	.9	UNIT		
1	U-238	1.1	17.0	CROSS SECTIONS FOR URANIUM-238 FISSION							
25.	40.7	50.	116.	300.	382.	435.	495.	540.	570.	U238	02
582.	582.	582.	582.	582.	581.	580.	579.	577.	575.	U238	03
572.	570.	568.	568.	568.	568.	568.	567.	566.	566.	U238	04
565.	565.	565.	565.	565.	565.	565.	567.	568.	569.	U238	05
571.	572.	575.	577.	579.	583.	586.	588.	600.	610.	U238	06
650.	684.	731.	750.	800.	835.	860.	895.	925.	960.	U238	07
980.	990.	995.	1020.	1025.	1025.	1025.	1025.	1025.	1025.	U238	08
1025.	1025.	1024.	1024.	1023.	1023.	1022.	1021.	1020.	1020.	U238	09
1020.	1019.	1018.	1017.	1016.	1015.	1014.	1013.	1012.	1011.	U238	10
1010.	1010.	1010.	1010.	1010.	1010.	1010.	1010.	1010.	1010.	U238	11
1010.	1010.	1010.	1010.	1010.	1010.	1010.	1010.	1010.	1010.	U238	12
1012.	1014.	1016.	1018.	1020.	1023.	1027.	1033.	1039.	1045.	U238	13
1052.	1064.	1076.	1088.	1100.	1112.	1124.	1136.	1148.	1160.	U238	14

APPENDIX D. LISTING OF THRESHOLD DETECTOR CROSS SECTIONS
AS THEY APPEAR IN THE 'SPECTRUM' CROSS SECTION DECK.

```
.1      .2      .3      .4      .5      .6      .7      .8      .9      UNIT

1170.   1180.   1190.   1200.   1220.   1240.   1260.   1275.   1290.   1300.    U238   15
1310.   1320.   1330.   1340.   1350.   1352.   1354.   1356.   1358.   1360.    U238   16
1360.   1360.   1360.   1360.   1360.   1360.   1360.   1360.   1360.   1360.    U238   17
 2  P-N,P  1.6 17.0 CROSS SECTIONS FOR P-31(N,P) SI-31
0.      0.      0.      0.      0.      1.      1.8     2.3     3.5     10.      P-N,P  2
25.     36.     46.5    55.     59.     80.     67.     89.     59.     70.      P-N,P 03
115.    80.     66.     80.     79.5    79.     139.    120.    100.    99.1     P-N,P 04
92.     90.     113.    118.    130.    136.    127.    137.    120.    108.     P-N,P 05
130.    135.5   136.6   137.8   139.5   140.3   141.    141.7   142.1   142.7    P-N,P 06
142.7   142.7   142.6   142.5   142.3   142.2   142.1   142.1   142.    142.     P-N,P 07
142.    142.    142.    142.    141.9   141.9   141.8   141.8   141.7   141.7    P-N,P 08
141.6   141.5   141.5   141.4   141.2   141.2   141.1   141.1   141.    141.     P-N,P 09
141.    141.    140.9   140.9   140.9   140.8   140.8   140.7   140.6   140.2    P-N,P 10
139.5   138.3   137.4   136.6   135.5   134.7   133.5   132.5   131.3   130.     P-N,P 11
129.2   128.    126.8   125.5   124.3   123.1   121.8   120.5   119.4   118.     P-N,P 12
116.7   115.5   114.    112.6   111.3   109.9   108.5   107.    105.5   104.     P-N,P 13
102.3   100.7   99.4    97.5    96.     94.3    92.6    90.8    89.     87.      P-N,P 14
86.     85.3    84.     82.5    81.     79.5    78.5    77.     76.     75.      P-N,P 15
73.5    72.5    71.7    69.8    68.5    67.5    67.     66.3    65.2    64.5     P-N,P 16
64.     63.     62.     61.     59.5    58.7    58.     57.     56.     55.      P-N,P 17
 3  FE-56 4.5  15.0    CROSS SECTIONS FOR FE-56(N,P)MN-56
```

APPENDIX D. LISTING OF THRESHOLD DETECTOR CROSS SECTIONS
AS THEY APPEAR IN THE 'SPECTRUM' CROSS SECTION,DECK.

```
.1      .2      .3      .4      .5      .6      .7      .8      .9      UNIT

0.      0.      0.      0.      0.2     0.4     0.8     0.9     1.3     1.9     FE-N,P05
2.3     3.1     3.8     4.8     5.5     7.1     8.5     11.2    13.1    15.     FE-N,P06
16.7    18.2    20.1    21.8    23.2    24.6    26.     27.6    29.3    30.7    FE-N,P07
32.1    33.8    35.5    37.     38.6    40.2    42.     43.5    45.2    47.     FE-N,P08
48.7    50.5    52.5    54.6    56.7    58.3    60.8    62.7    64.9    67.     FE-N,P09
69.     71.     73.1    75.2    77.2    79.3    81.     83.     85.2    87.     FE-N,P10
88.8    90.7    92.6    94.5    96.4    98.3    100.    101.8   103.7   105.5   FE-N,P11
107.3   109.2   111.    112.5   114.4   116.    117.5   119.5   121.    122.8   FE-N,P12
124.2   126.    127.5   129.    130.7   132.2   133.6   135.    136.8   138.2   FE-N,P13
139.5   141.    142.    142.3   142.8   142.6   142.1   141.4   140.2   139.    FE-N,P14
137.8   136.5   135.    133.7   132.2   131.    129.6   128.    126.2   124.8   FE-N,P15
 4  I-N,2N 9.5  15.0  CROSS SECTIONS FOR I-127(N,2N)I-126
0.      0.      0.      0.      3.      11.     25.     42.     64.     110.    I-N,2N10
135.    171.    210.    250.    289.    333.    365.    404.    438.    472.    I-N,2N11
505.    540.    562.    594.    624.    655.    687.    719.    753.    782.    I-N,2N12
814.    842.    878.    913.    942.    980.    1014.   1050.   1090.   1123.   I-N,2N13
1150.   1168.   1195.   1210.   1224.   1233.   1244.   1253.   1262.   1270.   I-N,2N14
1275.   1276.   1275.   1273.   1272.   1272.   1272.   1271.   1268.   1260.   I-N,2N15
 7  LI7-NT 2.7  17.0  CROSS SECTIONS FOR LI-7(N,TN)HE-4
0.      0.      0.      0.      0.      0.      1.      3.5     5.      7.      I-7   03
10.     13.     19.5    31.6    34.     45.4    54.5    65.     79.     89.     I-7   04
```

APPENDIX D. LISTING OF THRESHOLD DETECTOR CROSS SECTIONS
AS THEY APPEAR IN THE 'SPECTRUM' CROSS SECTION DECK.

```
.1      .2      .3      .4      .5      .6      .7      .8      .9      UNIT

100.5   113.3   126.4   146.    156.6   173.    187.    207.4   224.7   243.2    I-7    05
261.6   277.7   298.    317.7   331.8   339.8   353.5   367.5   375.    382.2    I-7    06
388.5   396.2   405.    414.    421.    427.5   433.    437.    442.    447.     I-7    07
452.    455.    459.    464.5   467.    471.    474.    477.    478.    480.5    I-7    08
483.    484.3   486.    488.    488.    488.1   488.    487.    486.    485.     I-7    09
484.5   484.3   483.5   483.    480.    476.    474.    470.    466.5   465.     I-7    10
463.    461.    457.6   454.    441.5   450.6   443.    441.    439.    433.     I-7    11
429.    422.    419.    411.    410.    407.    404.    400.    396.    392.     I-7    12
388.    384.    380.    376.5   373.    369.    366.    362.    358.    355.     I-7    13
351.    348.5   345.    342.    338.5   335.5   332.6   329.6   326.7   323.7    I-7    14
320.8   317.9   315.4   312.9   310.    307.5   304.5   302.1   300.    297.2    I-7    15
294.7   292.2   290.    287.5   285.4   283.2   280.6   278.6   276.5   274.5    I-7    16
272.5   270.    268.1   266.2   264.2   261.8   259.9   258.1   256.3   254.4    I-7    17
 8  F19RUS 11.1  15.       RUSSIAN CROSS SECTIONS FOR F-19(N,2N)F-18
.8      1.2     2.0     2.8     3.8     4.9     6.2     7.5     9.2     11.5     F-19RU12
13.6    16.     18.8    21.5    24.2    26.9    29.5    32.2    35.0    37.6     F-19RU13
40.     42.5    45.     47.6    50.2    52.6    55.2    57.8    60.4    62.9     F-19RU14
65.2    68.     70.5    73.0    75.4    77.7    80.0    82.6    85.0    87.5     F-19RU15
 9  F19FRN 11.1 15.0  FRENCH CROSS SECTIONS FOR REACTION F-19(N,2N)F-18F-19FR
3.2     5.0     6.7     8.3     9.9     11.5    13.1    14.8    16.3    18.0     F-19FR12
19.5    21.2    23.0    25.8    26.8    28.5    30.0    31.9    33.4    35.0     F-19FR13
```

APPENDIX D. LISTING OF THRESHOLD DETECTOR CROSS SECTIONS AS THEY APPEAR IN THE 'SPECTRUM' CROSS SECTION DECK.

.1	.2	.3	.4	.5	.6	.7	.8	.9	UNIT	
37.7	38.1	39.7	41.1	42.8	44.2	45.8	47.3	48.8	50.1	F-19FR14
51.6	52.9	54.3	55.7	56.9	58.1	59.5	60.7	61.9	63.0	F-19FR15

Omitted Appendices (See Preface)

APPENDIX E

Threshold Detector Data

(Explanation of Tables)

APPENDIX F

Listing of SAMTAPE Source Programs

APPENDIX G

Listing of SPECTRUM Source Programs

Acknowledgment

The author is indebted to many people and organizations for aid and guidance in the conception, execution, and evaluation of these experiments, for making available the necessary materials and equipment, and for financial support. In particular, he would like to express his gratitude to Professor David J. Rose, Professor N. C. Rasmussen, Leon E. Beghian, L. M. Petrie, Jr., C. Robertson, R. Rydin, A. J. Impink, Jr., W. G. Homeyer, K. Soosaar, M. Driscoll, and K. Papadopoulos.

Among the many laboratories and organizations thanks go especially to the following:

The Solid State Chemistry Branch of the U. S. Air Force Cambridge Research Laboratories, especially to E. Burke, P. Cali, M. Deane, L. Lowe, H. DeAngelis, C. Jimenez;

The Radiation Protection Committee at the Massachusetts Institute of Technology, especially S. Levin and F. Massee;

The Wing Radiological Hazards Committee at AFCRL, especially M. Wilson;

The Reactor Chemistry Division of Oak Ridge National Laboratory, especially Dr. R. A. Strehlow;

The Research Laboratory of Electronics, M. I. T., especially R. A. Sayers, J. B. Keefe, and R. V. Keyes, Jr.; and

The Cooperative Computation Laboratory, M. I. T.

The author was supported in part by a U. S. AEC Special Fellowship in Nuclear Science and Engineering, during the period September 1960 to September 1963.

The development of the computer codes was done in part at the Computation Center, M. I. T.

References

1. D. J. Rose, W. G. Homeyer, A. J. Impink, Jr., and P. S. Spangler, "Engineering Calculations for Barely Conceivable Fusion Reactors" (unpublished memorandum, 1962).
2. L. Spitzer, Jr., D. J. Grove, W. E. Johnson, L. Tonks, and W. F. Westendorp, "Problems of the Stellarator as a Useful Power Source," Report NYO-6047, Princeton University, New Jersey, August 1954.
3. A. J. Impink, Jr., "Neutron Economy in Fusion Reactor Blanket Assemblies," Ph. D. Thesis, Department of Nuclear Engineering, M. I. T., January 1963.
4. W. G. Homeyer, "Thermal and Chemical Aspects of the Thermonuclear Blanket Problem," Sc. D. Thesis, Department of Nuclear Engineering, M. I. T., December 1962.
5. L. N. Lontai (see Technical Report 436, Research Laboratory of Electronics, M. I. T., Cambridge, Mass., July 6, 1965).
6. L. Petrie, Sc. D. Thesis, Department of Nuclear Engineering, M. I. T., 1964; see also Technical Report 438, Research Laboratory of Electronics, M. I. T., Cambridge, Mass., July 20, 1965.
7. D. J. Rose and M. Clark, Jr., Plasmas and Controlled Fusion (The M. I. T. Press, Cambridge, Mass., and John Wiley and Sons, New York, 1961).
8. K. O. Hinterman and R. Wideröe, "Tritium Production and Cycling in a Fusion Reactor with a Lithium Blanket," Proceedings of the Second United Nations Conference on the Peaceful Uses of Atomic Energy, Geneva, 1958, Vol. 32, p. 440 (United Nations Publication, 1958). (Paper P/1471).
9. P. S. Spangler, "Fusion Reactor Blanket Experiment," Quarterly Progress Report No. 69, Research Laboratory of Electronics, M. I. T., Cambridge, Mass., April 15, 1963, pp. 81-88.
10. P. S. Spangler, "Fusion Reactor Blanket Experiment: Neutron-Energy Spectrum from a Tritium-Gas Target," Quarterly Progress Report No. 71, Research Laboratory of Electronics, M. I. T., Cambridge, Mass., October 15, 1963, pp. 137-146.
11. P. S. Spangler, "Fusion Reactor Blanket Experiment," Quarterly Progress Report No. 73, Research Laboratory of Electronics, M. I. T., Cambridge, Mass., April 15, 1964, pp. 87-98.
12. C. H. Johnson and H. E. Banta, Rev. Sci. Instr. 27, 132 (1956).
13. P. S. Spangler, "Proposal for a 30-Curie Tritium Gas Target for Use with the 1-3 Mev Van de Graaff Accelerator at the Air Force Cambridge Research Laboratory, Bedford, Massachusetts" (unpublished report, March 13, 1963). (A copy of this report has been deposited in the Document Room of the Research Laboratory of Electronics, M. I. T.)
14. A. E. Profio, "Methods of Investigating Neutron Moderation and Absorption Using a Pulsed Source," Ph. D. Thesis, Department of Nuclear Engineering, M. I. T., November 1962, Appendix B.
15. N. Jarmie and J. D. Seagrave (eds.), "Charged Particle Cross Sections," AEC Report No. LA-2014, Los Alamos Scientific Laboratory, University of California, Los Alamos, New Mexico, March 1956, p. 41.
16. R. D. Evans, The Atomic Nucleus (McGraw-Hill Book Company, New York, 1955), pp. 408-421; 828-836.
17. BNL-325, Brookhaven National Laboratory, Upton, New York, Second Edition, 1958; Supplement, 1960.
18. P. Cuzzorrea, G. Pappalardo, and R. Ricamo, Nuovo cimento 16, 450 (1960).

19. J. Kantele and D. G. Gardner, Nuclear Phys. 35, 353 (1962).

20. J. Depraz, G. Legros, and R. Salin, J. Phys. Radium 21, 377 (1960).

21. S. Yasumi, J. Phys. Soc. Japan 12, 443 (1957).

22. B. D. Kern, W. E. Thompson, and J. M. Ferguson, Nuclear Phys. 10, 233 (1959).

23. D. M. Chittenden II, D. G. Gardner, and R. W. Fink, Phys. Rev. 122, 860 (1961).

24. M. Bormann, S. Cierjaks, R. Langkau, and H. Neuert, Z. Phys. 166, 477 (1962).

25. E. B. Paul and R. L. Clark, Can. J. Phys. 31, 267 (1953).

26. C. W. Williamson and J. Picard, J. Phys. Radium 22, 651 (1961); J. Phys. (Paris) 24, 813 (1963).

27. O. D. Brill', N. A. Vlasov, S. P. Katinin, and S. L. Sokolov, Dokl. Akad. Nauk S. S. S. R. 136, 55 (1961).

28. L. A. Rayburn, Bull. Am. Phys. Soc., Ser. II 3, 377 (1958).

29. V. J. Ashby, H. C. Catron, L. L. Newkink, and C. J. Taylor, Phys. Rev. 111, 616 (1958).

30. L. H. Weinberg, R. P. Schuman, and B. A. Gottschalk, KAPL-1283, Knolls Atomic Power Laboratory, 1955.

31. V. M. Pankratov, N. A. Vlasov, and B. V. Rybakov, Atomnaya Energia 9, 399 (1960).

32. H. W. Schmitt, R. B. Murray, and J. J. Manning, ORNL-2842, p. 240; Phys. Rev. 116, 1575 (1959).

33. R. G. Jung, H. M. Epstein, and J. W. Chastain, Jr., BMI-1486, Batelle Memorial Institute (1960).

34. J. Moteff, "Neutron Flux and Spectrum Measurement with Radioactivants," Nucleonics 20, No. 12, 56-60 (December 1962).

35. W. D. Lanning and K. W. Brown, WAPD-T-1380, Bettis Atomic Power Laboratory, Pittsburgh, Pennsylvania, 1961; see also Trans. Am. Nuclear Soc. 4, 267 (1961).

36. P. S. Spangler, "Fusion Reactor Blanket Experiment," Quarterly Progress Report No. 70, Research Laboratory of Electronics, M. I. T., Cambridge, Mass., July 15, 1963, pp. 145-150.

37. A. J. Impink, Jr. (Private communication, November 1962).

38. G. A. Korn and T. M. Korn (eds.), Mathematical Handbook for Scientists and Engineers (McGraw-Hill Book Co., New York, 1961).

39. R. A. Rydin (Private communication, November 1962).

40. D. R. Christman, Nucleonics 19, No. 5, 51 (May 1961).

41. A. J. Impink, Jr., "Neutron Economy in Fusion Reactor Blanket Assemblies," Ph. D. Thesis, op. cit., Chapter 3.

42. M. Driscoll (Private communication, August 1964).

43. A. J. Impink, Jr., Ph. D. Thesis, op. cit., Chapter 8.

44. L. N. Lontai (in preparation).

45. R. A. Strehlow (Private communication, September 1964).

46. L. Petrie, Sc. D. Thesis, Department of Nuclear Engineering, M. I. T.; (see also Technical Report 438).

47. L. N. Lontai, S. M. Thesis, Department of Nuclear Engineering, M. I. T., June 1963; (see also Technical Report 436).

48. P. C. Rogers, "FRANTIC Program for Analysis of Exponential Growth and Decay Curves," Technical Report No. 76, Laboratory of Nuclear Science, M. I. T., June 1962.

49. A. M. Niell, Bulletin CC-174-3, Computation Center, M. I. T., Cambridge, Mass., October 1963 (unpublished).

50. "709/7090 Fortran Programming System," Reference Manual, International Business Machines Corporation, New York, 1961.

JOINT SERVICES DISTRIBUTION LIST

Department of Defense

Defense Documentation Center
Attn: TISIA
Cameron Station, Bldg. 5
Alexandria, Virginia 22314

Director, National Security Agency
Attn: C3/TDL
Fort George G. Meade, Maryland 20755

Mr. Charles Yost, Director
For Materials Sciences
Advanced Research Projects Agency, DOD
Washington, D.C. 20301

Director
Advanced Research Projects Agency
Department of Defense
Washington, D.C. 20301

Dr. James A. Ward
Office of Deputy Director (Research and Information Rm. 3D1037) DOD
The Pentagon
Washington, D.C. 20301

Dr. Edward M. Reilley
Asst. Director (Research)
Ofc of Defense Res. & Eng., DOD
Washington, D.C. 20301

Department of the Army

Librarian PTA130
United States Military Academy
West Point, New York 10996

Director
U.S. Army Electronics Laboratories
Fort Monmouth, New Jersey 07703
Attn: AMSEL-RD-ADT

DR	NR	SR
FU#1	PE	SS
GF	PF	X
NE	PR	XC
NO	SA	XE
		XS

Commanding General
U.S. Army Electronics Command
Attn: AMSEL-SC
Fort Monmouth, New Jersey 07703

C.O., Harry Diamond Laboratories
Attn: Mr. Berthold Altman
Connecticut Ave. & Van Ness St. N.W.
Washington, D.C. 20438

The Walter Reed Institute of Research
Walter Reed Army Medical Center
Washington, D.C. 20012

Director
U.S. Army Electronics Laboratories
Attn: Mr. Robert O. Parker, Executive Secretary, JSTAC (AMSEL-RD-X)
Fort Monmouth, New Jersey 07703

Director
U.S. Army Electronics Laboratories
Attn: Dr. S. Benedict Levin, Director Institute of Exploratory Research
Fort Monmouth, New Jersey 07703

Commanding Officer
U.S. Army Research Office (Durham)
Attn: CRD-AA-IP (Richard O. Ulsh)
P.O. Box CM, Duke Station
Durham, North Carolina 27706

Commanding Officer
U.S. Army Medical Research Laboratory
Fort Knox, Kentucky

Commanding Officer
U.S. Army Personnel Research Office
Washington, D.C.

Dr. H. Robl, Deputy Director
U.S. Army Research Office (Durham)
P.O. Box CM, Duke Station
Durham, North Carolina 27706

Commandant
U.S. Command and General Staff College
Attn: Secretary
Fort Leavenworth, Kansas 66207

Director
U.S. Army Eng. Geodesy, Intell. and Mapping
Research & Development Agcy.
Fort Belvoir, Virginia 22060

Commanding Officer
Human Engineering Laboratories
Aberdeen Proving Ground, Maryland 21005

Commanding Officer
U.S. Limited War Laboratory
Attn: Technical Director
Aberdeen Proving Ground, Maryland 21005

Commanding Officer
U.S. Army Security Agency
Arlington Hall, Arlington, Virginia 22212

C.O., Harry Diamond Laboratories
Attn: Dr. R. T. Young, Elec. Tubes Div.
Connecticut Ave. & Van Ness St., N.W.
Washington, D.C. 20438

U.S. Army Munitions Command
Attn: Technical Information Branch
Picatinney Arsenal
Dover, New Jersey 07801

Commanding General
Frankford Arsenal
Attn: SMUFA-1310 (Dr. Sidney Ross)
Philadelphia, Pennsylvania 19137

Commanding General
U.S. Army Missile Command
Attn: Technical Library
Redstone Arsenal, Alabama 35809

Commandant
U.S. Army Air Defense School
Attn: Missile Sciences Division, C&S Dept.
P.O. Box 9390
Fort Bliss, Texas 79916

Commanding Officer
U.S. Army Ballistics Research Lab.
Attn: V.W. Richards
Aberdeen Proving Ground
Aberdeen, Maryland 21005

Commanding Officer
U.S. Army Materials Research Agency
Watertown Arsenal
Watertown, Massachusetts 02172

Commanding General
U.S. Army Strategic Communications
Command
Washington, D.C. 20315

Commanding General
U.S. Army Materiel Command
Attn: AMCRD-RS-PE-E
Washington, D.C. 20315

Commanding Officer
Foreign Service & Technology Center
Arlington Hall
Arlington, Virginia

Research Plans Office
U.S. Army Research Office
3045 Columbia Pike
Arlington, Virginia 22204

Chief of Research and Development
Headquarters, Department of the Army
Attn: Physical Sciences Division P&E
Washington, D.C. 20310

Director
Human Resources Research Office
The George Washington University
300 N. Washington Street
Alexandria, Virginia 22314

Commanding Officer
U.S. Army Electronics R&D Activity
White Sands Missile Range
New Mexico 88002

Commanding Officer
U.S. Army Engineers R&D Laboratory
Attn: STINFO Branch
Fort Belvoir, Virginia 22060

Commanding Officer
U.S. Army Electronics R&D Activity
Fort Huachuca, Arizona 85163

Mr. Alvin D. Bedrosian
Room 26-131
Massachusetts Institute of Technology
Cambridge, Massachusetts 02139

Department of the Air Force

Battelle Memorial Inst.
Technical Library
505 King Avenue
Columbus, Ohio 43201

Goddard Space Flight Center
NASA
Greenbelt, Maryland 20771

Research and Tech. Div. (AFAPL)
Attn: APIE-2, Mr. Robert F. Cooper
Wright-Patterson AFB, Ohio 45433

Technical Library
White Sands Missile Range
New Mexico 88002

AFSC (Tech Library)
Andrews AFB
Washington, D.C. 20031

AUL-3T-9663
Maxwell AFB
Alabama 36112

DDR&E (Tech Library)
Rm. 3C 128
The Pentagon
Washington, D.C. 20301

Systems Engineering Group
Deputy for Systems Eng'g., SEPRR
Directorate of Tech. Pubs. & Specs.
Wright-Patterson AFB, Ohio 45433

APGC (PGBAP-1)
Eglin AFB
Florida 32542

RTD (Tech Library)
Bolling AFB
District of Columbia 20332

BSD (Tech Library)
Norton AFB
California 92409

ASD (Tech Library)
Wright-Patterson AFB
Ohio 45433

Industrial College of the Armed Forces
Attn: Library
Washington, D. C.

Southwest Research Institute
Library
8500 Culebra Road
San Antonio, Texas

Stanford Research Institute
Library
820 Mission St.
South Pasadena, Calif. 91030

Library
National Science Foundation
Washington 25, D.C.

Linda Hall Library
5109 Cherry St.
Kansas City, Mo.

Dr. H. Harrison
NASA (Code RRE)
Fourth and Independence Sts.
Washington, D.C. 20546

Mr. James Tippett
National Security Agency
Fort Meade, Maryland

Brig. Gen. J. T. Stewart
Director of Science & Technology
Deputy Chief of Staff (R&D)
USAF
Washington 25, D.C.

Dr. R. L. Sproull, Director
Advanced Research Projects Agency
Washington 25, D.C.

Lt. Col. Edwin M. Myers
Headquarters USAF (AFRDR)
Washington 25, D.C.

Dr. John M. Ide
Div. Director for Eng'g.
National Science Foundation
Washington 25, D.C.

Dr. Zohrab Kaprielian
University of Southern California
University Park
Los Angeles 7, California

Dr. Lowell M. Hollingsworth
AFCRL
L. G. Hanscom Field
Bedford, Massachusetts

Professor Nicholas George
California Institute of Technology
EE Department
Pasadena, California

Hon. Alexander H. Flax
Asst. Secretary of the Air Force
Office of the Secretary of the Air Force
(R&D)
Washington 25, D.C.

Prof. Arwin Dougal
University of Texas
EE Department
Austin, Texas

Mr. Roland Chase
National Aeronautics & Space Admin.
1512 H Street, N.W.
Washington 25, D.C.

AFAL (AVTE)
Wright-Patterson AFB
Ohio 45433

Systems Engineering Group (RTD)
Attn: SEPIR
Wright-Patterson AFB
Ohio 45433

JOINT SERVICES DISTRIBUTION LIST (continued)

AFAPL (APIE-2, Lt. Barthelmey)
Wright-Patterson AFB, Ohio.45433

Rome Air Dev. Center (RAWL, H. Webb)
Griffiss Air Force Base, New York 13442

S. H. Sternick
Aerospace Com - Attn: ESNC
Waltham Federal Center
424 Trapelo Road
Waltham, Massachusetts 02154

AFCRL (CRFE-Dr. Nicholas Yannoni)
L. G. Hanscom Field
Bedford, Massachusetts

Mr. Rocco H. Urbano, Chief
AFCRL, Appl Math. Branch
Data Sciences Laboratory
Laurence G. Hanscom Field
Bedford, Massachusetts

AFCRL
Office of Aerospace Res., USAF
Bedford, Mass.
Attn: CRDA

Dr. Louis C. Block
AFCRL (CROO)
Laurence G. Hanscom Field
Bedford, Massachusetts 01731

Commander, AFCRL
Attn: C. P. Smith (CRBS)
L. G. Hanscom Field
Bedford, Massachusetts

AFETR (Tech Library MU-135)
Patrick AFB, Florida 32925

Mr. C. N. Hasert
Scientific Advisory Board
Hq. USAF
Washington 25, D. C.

Dr. Harvey E. Savely, SRL
Air Force Office of Sci. Res.
Office Aerospace Research, USAF
Washington 25, D. C.

Department of the Air Force
Headquarters, United States Air Force
Washington 25, D. C.
Attn: AFTAC/TD-1

John Crerar Library
35 West 33rd St.
Chicago, Ill.

LOOAR (Library)
AF Unit Post Office
Los Angeles, Calif. 90045

Office of Research Analyses
Library
Holloman AFB, New Mexico 88330

Office of Research Analyses
Attn: Col. K. W. Gallup
Holloman AFB, New Mexico 88330

ARL (ARD/Col. R. E. Fontana)
Wright-Patterson AFB
Ohio 45433

Brig. Gen. B. G. Holzman, USAF (Ret.)
National Aeronautics and Space Admin.
Code RS
Washington, D. C. 20546

AFRST (SC/EN)
Lt. Col. L. Stone
Room 4C 341
The Pentagon
Washington, D. C. 20301

Commander
Rome Air Development Center
AFSC
Office of the Scientific Director
Griffiss AFB, Rome, New York

Commander
Research & Technology Division (AFSC)
Office of the Scientific Director
Bolling AFB 25, D. C.

Commander
Air Force Systems Command
Office of the Chief Scientist
Andrews AFB, Maryland

Commander
Air Force Cambridge Research Lab.
Office of the Scientific Director
L. G. Hanscom Field
Bedford, Massachusetts

Commander
Aerospace Research Laboratories (OAR)
Office of the Scientific Director
Wright-Patterson AFB, Ohio

Commander, Aerospace Systems Division
AFSC
Office of the Scientific Director
Wright-Patterson AFB, Ohio

JOINT SERVICES DISTRIBUTION LIST (Continued)

Commander
Space Systems Division (AFSC)
Office of the Scientific Director
Inglewood, California

Dr. G. E. Knausenberger
c/o Hq Co. Munich Post
APO 09407, New York, N.Y.

AVCO Research Lab, Library
2385 Revere Beach Parkway
Everett, Mass. 02149

California Institute of Technology
Aeronautics Library
1201 East California St.
Pasadena 4, Calif. 91102

Carnegie Institute of Technology
Science & Engineering Hunt Library
Schenley Park
Pittsburgh, Pa. 15213

Rand Corporation
1700 Main St.
Santa Monica, Calif. 90401

Aerospace Corp. (Tech Library)
P.O. Box 95085
Los Angeles, Calif. 90045

Lewis Research Center (NASA)
Technical Library
21000 Brookpark Road
Cleveland, Ohio

George C. Marshall Space Flight Center
(NASA)
Redstone Arsenal, Ala. 35808

High Speed Flight Center (NASA)
Technical Library
Edwards AFB, Calif. 93523

Ames Rsch. Center (NASA)
Technical Library
Moffett Field, Calif. 94035

CIA OCR/LY/IAS
IH 129 HQ
Washington, D.C. 20505

RADC (Tech Library)
Griffiss AFB, N.Y. 13442

AEDC (Tech Library)
Arnold AFS
Tennessee 37389

APGC (Tech Library)
Eglin AFB
Florida 32542

AFWL (WLIL, Technical Library)
Kirtland Air Force Base
New Mexico 87117

AFMDC (Tech Library)
Holloman AFB
New Mexico 88330

AFFTC (Tech Library)
Edwards AFB
California 93523

Space Systems Division
Los Angeles Air Force Station
Air Force Unit Post Office
Los Angeles, California 90045
Attn: SSSD

Churchill Research Range
Library
Fort Churchill
Manitoba, Canada

National Defense Library
Headquarters
Ottawa, Ontario, Canada

Director
National Aeronautical Establishment
Ottawa, Ontario, Canada

EDS (ESTI)
Laurence G. Hanscom Field
Bedford, Massachusetts 01731

Johns Hopkins University
Applied Physics Lab., Library
White Oak, Silver Spring, Maryland 20919

Los Alamos Scientific Lab
Attn: Technical Library
Los Alamos, New Mexico 87544

ARL (AROL)
Wright-Patterson AFB
Ohio 45433

Frank J. Seiler Rsch. Lab.
Library
USAF Academy, Colo. 80840

U.S. Atomic Energy Commission
Library
Gaithersburg, Maryland 20760

JOINT SERVICES DISTRIBUTION LIST (continued)

AFAL
AVR(L)
Wright-Patterson AFB
Ohio 45433

Air Force Cambridge Res. Lab.
L.G. Hanscom Field
Bedford, Massachusetts 01731
Attn: CRDM, Mr. Herskovitz

Commander
Air Force Office of Scientific Research
Washington 25, D.C.
Attn: SREE

Director
Air University Library
Maxwell A.F. Base, Alabama

NASA/AFSS/1 FOB6
Tech Library, Rm. 60084
Washington, D.C. 20546

USAFA (DLIB)
U.S. Air Force Academy
Colorado

ARPA
Tech Info Office
The Pentagon
Washington, D.C. 20301

AFCRL(CRXL)
L.G. Hanscom Field
Bedford, Mass. 01731

U.S. Regional Sci. Office (LAOAR)
U.S. Embassy
APO 676, New York, N.Y.

AEC
Div. of Tech Info. Ext.
P.O. Box 62
Oak Ridge, Tennessee

Dr. Hermann H. Kurzweg
Director of Research - OART
NASA
Washington, D.C. 20546

AFIT (MCLI)
Tech Library
Wright-Patterson AFB, Ohio 45433

Prof. W. H. Radford
Lincoln Laboratory, A-183
244 Wood Street
Lexington, Massachusetts

Department of the Navy

Chief of Naval Operations
Pentagon OP 07T
Washington, D.C.

Commanding Officer
Office of Naval Research Branch Office
Navy 100, Fleet P.O. Box 39
New York, New York

Library
U.S. Navy Electronics Lab.
San Diego, California 92152

Commander
U.S. Naval Air Development Center
Johnsville, Pennsylvania
Attn: NADC Library

Commanding Officer
Office of Naval Research Branch Office
495 Summer Street
Boston, Massachusetts 02110

Commanding Officer
U.S. Navy Underwater Sound Laboratory
Ft. Trumbull, New London, Connecticut

U.S. Navy Post Graduate School
Monterey, California
Attn: Electrical Engineering Department

Commander, Naval Ordnance Laboratory
White Oak, Maryland
Attn: Technical Library

Chief, Bureau of Ships, Attn: Code 680
Department of the Navy
Washington, D.C. 20360

Chief, Bureau of Weapons
Department of the Navy
Washington, D.C. 20360

Dr. Arnold Shostak, Code 427
Head, Electronics Branch
Physical Sciences Division
Office of Naval Research
Washington, D.C. 20360

Chief of Naval Research, Code 427
Department of the Navy
Washington, D.C. 20360

Director
Naval Research Laboratory
Washington, D.C. 20390